VILNIUS UNIVERSITY
CENTER FOR PHYSICAL SCIENCES AND TECHNOLOGY

Rasa Platakytė

Study of biologically active molecule structure, photodynamics and interactions with water by the means of vibrational spectroscopy

DOCTORAL DISSERTATION

Natural Sciences,
Physics (N 002)

VILNIUS 2022

The dissertation was prepared between 2017 and 2021 at the Institute of Chemical Physics, Vilnius University.

Academic supervisor –
Dr. Justinas Čeponkus (Vilnius University, Natural sciences, Physics – N 002).

This doctoral dissertation will be defended in a public meeting of the Dissertation Defence Panel:

Chairman – **Prof. Habil. Dr. Vidmantas Gulbinas** (Center for Physical Sciences and Technology, Natural Sciences, Physics – N 002).
Members:
Dr. Kęstutis Aidas (Vilnius University, Natural Sciences, Physics – N 002),
Prof. Dr. Liutauras Marcinauskas (Kaunas University of Technology, Natural Sciences, Physics – N 002),
Dr. Ieva Matulaitienė (Center for Physical Sciences and Technology, Natural Sciences, Chemistry – N 003),
Dr. George Pitsevich (Belarusian State University, Natural Sciences, Physics – N 002).

The dissertation shall be defended at a public meeting of the Dissertation Defence Panel at 11:00 on 4th July 2022 in Room A101 of the National Center for Physical Sciences and Technology.
Address: Saulėtekio av. 3, NFTMC, Room A101, Vilnius, Lithuania
Tel. +370 5 264 8884; e-mail: office@ftmc.lt

The text of this dissertation can be accessed at the Vilnius University Library, as well as on the website of Vilnius University:
www.vu.lt/lt/naujienos/ivykiu-kalendorius

VILNIAUS UNIVERSITETAS
FIZINIŲ IR TECHNOLOGIJOS MOKSLŲ CENTRAS

Rasa Platakytė

Biologiškai aktyvių molekulių struktūros, vidinės fotodinamikos ir sąveikos su vandens molekulėmis tyrimas virpesinės spektrometrijos metodais

DAKTARO DISERTACIJA

Gamtos mokslai,
Fizika (N 002)

VILNIUS 2022

Disertacija rengta 2017-2021 metais Vilniaus universiteto Cheminės fizikos institute.

Mokslinis vadovas – **dr. Justinas Čeponkus** (Vilniaus universitetas, gamtos mokslai, fizika – N 002).

Gynimo taryba:
Pirmininkas – **prof. habil. dr. Vidmantas Gulbinas** (Fizinių ir technologijos mokslų centras, gamtos mokslai, fizika – N 002).
Nariai:
Dr. Kęstutis Aidas (Vilniaus universitetas, gamtos mokslai, fizika – N 002),
Prof. dr. Liutauras Marcinauskas (Kauno technologijos universitetas, gamtos mokslai, fizika – N 002),
Dr. Ieva Matulaitienė (Fizinių ir technologijos mokslų centras, gamtos mokslai, chemija – N 003),
Dr. George Pitsevich (Baltarusijos universitetas, gamtos mokslai, fizika – N 002).

Disertacija ginama viešame Gynimo tarybos posėdyje 2022 m. liepos mėn. 4 d. 11:00 val. Nacionalinio Fizinių ir technologijos mokslų centro A101 auditorijoje. Adresas: Saulėtekio al. 3, NFTMC, A101 audit., Vilnius, Lietuva tel. +370 5 264 8884; el. paštas office@ftmc.lt

Disertaciją galima peržiūrėti Vilniaus universiteto bibliotekoje ir VU interneto svetainėje adresu:
https://www.vu.lt/naujienos/ivykiu-kalendorius

ACKNOWLEDGEMENTS

The research and the writing of this thesis in particular were done during what could be called "interesting times". And although the times are never easy and neither is anything that is really worth doing, during the course of these doctoral studies, I felt how much the support of scientific community, of colleagues, of family and friends, really means. So now that the work of several years has been distilled into a couple hundred pages, I would be remiss not to express my gratitude for everyone who had a hand in it.

First of all, I would like to thank my supervisor, Dr. Justinas Čeponkus who first welcomed me to the laboratories of this institute and without whose guidance and support none of this would have been possible. I'd like to mention other colleagues from the Institute of Chemical Physics as well – Professor Valdas Šablinskas, Kęstutis Aidas, Vidita Urbonienė for helping me along on this journey. I would also like to express my gratitude to everyone on the French team – Claudine Crépin, Alejandro Gutiérrez-Quintanilla, Michèle Chevalier, and others. I had the pleasure of spending several months working with them on the studies I am presenting in this thesis and the collaboration of our laboratories continues and – I hope – will continue far into the future.

I want to thank my young colleagues in Vilnius as well. Your presence means everything. Martynas, Dovilė, Sonata, Rimantė, Gerda, now Jogilė and Morta too – you inspired me everyday and I don't think a paragraph can cover how grateful I am for the chance to spend time with you. I'm also thankful to all the students who taught me a lot by requiring me to teach them.

Finally, I would like to extend my gratitude beyond the halls of academia and thank my parents for taking care of me, encouraging me and teaching me how to deal with my insecurities. I'd like to thank my friends as well. You constantly remind me how much there is to do, to see and to enjoy in this world. I can't help by give a shout out to my dog as well. You will not understand any of what is written here but I don't think it will matter much at all.

TABLE OF CONTENTS

LIST OF ABBREVIATIONS

AA – acetic acid

AcAc – acetylacetone

AcAcF3 – trifluoroacetylacetone

AcAcF2Cl – chlorodifluoroacetylacetone

AcAcF6 – hexafluoroacetylacetone

ASA – acetylsalicylic acid

dAcAc – deuterated acetylacetone

DFT – density functional theory

FT – Fourier transform

HB – hydrogen bond

IHB – intramolecular hydrogen bond

IR – infrared

FTIR – Fourier transform infrared spectroscopy

MA – malondialdehyde

MACl – chloromalondialdehyde

MI – matrix isolation

pH_2 – parahydrogen

RAHB – resonance assisted hydrogen bond

SA – salicylic acid

INTRODUCTION

Hydrogen bond (HB) plays an essential part in the myriad of biological systems and processes that happen in the world every day. One of the early definitions of the hydrogen bond describes it as a system where "the hydrogen nucleus held between 2 octets constitutes a weak bond", with ammonium hydroxide as the main example of such bond [1]. Many later definitions offer descriptions of hydrogen bond as A-H…B system with electronegative A and B atoms – oxygen, nitrogen, halogens [2, 3]. The IUPAC recommended definition formulated by many authors states that "the hydrogen bond is an attractive interaction between a hydrogen atom from a molecule or a molecular fragment X–H in which X is more electronegative than H, and an atom or a group of atoms in the same or a different molecule, in which there is evidence of bond formation" [4]. What follows is a list of criteria, first of which states that the hydrogen bond can be formed due to electrostatic interaction, be a partial covalent bond or occur because of dispersion. The strength of the bond can be described by the H…Y distance. Historically, the X to Y distance was used as an indicator of how strong hydrogen bond was since it was impossible to detect hydrogen atoms with early X-ray techniques [6].

However, it has been known early on that hydrogen bond was important in many biological structures and systems – in water first of all, but also in amino acids, carbohydrates, pyrimidines, purines. The range of hydrogen bond strength now is usually given to be from around 1 kJ/mol to 150 kJ/mol [5, 7]. The former can be observed in C-H…C systems although there is still debate whether this type of interaction can be called hydrogen bond since carbon is not an electronegative atom. The strongest bonds occur when hydrogen is bonded to fluorine (in F-H…F systems) due to high electronegativity of fluorine atoms – these bonds are comparable in strength to weak covalent bonds [8]. Both the relative weakness and this concurrent wide strength range means that the hydrogen bond is very adaptable and can be broken and rearranged even in room temperatures. This quality is essential when it comes to biological structures which are dynamic and ever adjusting to changing circumstances, and processes such as unzipping of DNA which precedes replication or the hydration of biomolecules in water solutions [9 – 13]. Hydrogen bonds formed on the molecular level result in large systems with many unique qualities that help life not only to exist but to flourish.

The hydrogen bonding between water molecules is perhaps best known and well-explored type of hydrogen bonding since water plays such an important role in almost every aspect of our lives. One water molecule can form up to four hydrogen bonds, and the intermolecular hydrogen bond strength in a water dimer is around 20 kJ/mol [14 – 16]. Forming a hydrogen bond in large networks of water molecules can mean that strength is increased or decreased significantly. This specific quality of hydrogen bonding is called cooperative and competitive (or anti-cooperative) effect. Cooperativity effect means that acceptance of hydrogen bond increases the possibility of giving away the hydrogen that is participating in a covalent bond (meaning, being an acceptor strengthens the molecule as a donor) [17-25].

Quantum chemistry calculations for different water molecule clusters showed that hydrogen bond strength can change up to 90 % from extreme case of anti-cooperativity to the extreme case of cooperativity. In the latter case, the bond is strengthened by approximately 3 kJ/mol, and bond length is reduced by 0.03 Angstrom [26, 27]. Chains connected by hydrogen bonds (O-H...O-H...O) are cooperative – breaking of the first hydrogen bond requires the largest amount of energy, the second bond is easier to break and so on. This is important in such systems as DNA, which was already mentioned above, where two strands are connected by hydrogen bonds. In a double helix, the hydrogen bonds strengthen each other and stabilize the system, and when DNA needs to be copied – in the case of DNA unzipping, each successive bond is easier to break [28]. The cooperativity effect is important in protein and amide structures and other systems, such as in relative hydration properties for salt solutions that are responsible for swelling and deswelling behavior for hydrophilic polymeric gels [29-35].

The molecular structure and both intramolecular and intermolecular hydrogen bonds are mutually dependent. For example, in molecules with aromatic rings, the π electrons become delocalized and instead of having a few single and a few double bonds, they become sort of halfway bonds. If this charge distribution is favorable towards hydrogen bonding – that is to say that the partial charge on the bond acceptor becomes more negative, or the charge on donor – more positive, the hydrogen bond strength increases [36-44]. Molecular vibrations are undeniably tied into these processes as well. Since all atoms in molecules are constantly vibrating, their movements inevitably change the structure and charge distribution in a way that affects hydrogen bond [37]. If molecular structure changes, for example, via atom substitution, hydrogen bond is also affected [45, 46]. All in all, the mentioned π electron

delocalization in molecules with intramolecular hydrogen bonds formed in the aromatic ring structure, strengthens the HB. This is called resonance assisted hydrogen bond (RAHB), resonance referring to the fact that for these molecules, two structures are made possible by proton tunneling from donor to acceptor (from one electronegative atom towards another), and the mix of these two states results in more symmetric system with complete electron delocalization [47-50].

Molecules of β-diketone family exhibit this sort of hydrogen bond [51, 52]. These molecules can exist as two (enol and keto) tautomers. The keto form is more polar and therefore is mostly observed in polar solutions [53-56]. In other environments, the enolic form is observed more often as it is stabilized by the resonance assisted intramolecular hydrogen bond. Another class of molecules with intramolecular hydrogen bonds and even simpler structure are the aldehydes [48]. These relatively simple systems can be used to explore proton tunneling between two oxygen atoms. Proton transfer is a process that influences the complex structures and interactions of the molecular-level universe with consequences that can be clearly felt in the everyday macroscopic world. One of the most important reactions that involves such charge transfer is photosynthesis, without which the evolution of life as we know it would not have been possible. It is crucial to understand how these transfers happen and what conditions are needed to support them. However, by their very nature, these processes are very rapid and therefore hard to observe [57-60]. Ideally, one would want to have a system of a single molecule, inert and isolated, with functional groups that allow to model proton transfer on it.

The molecules of dialdehyde and β-diketone family can be used as model systems to explore the proton transfer and hydrogen bonding strength but they are also important in biological systems themselves. Malondialdehyde is often used as a marker of oxidative damage. It is produced by lipid peroxidation of polyunsaturated fatty acids and can easily interact with functional groups of proteins, lipoproteins, DNA, and RNA. Malondialdehyde is highly reactive and potentially mutagenic [61, 62]. Acetylacetone is not as biologically relevant as malondialdehyde but it has been used as an intermediate, in particular for the synthesis of heterocyclic substances for biologically active compounds and drugs. Another application of acetylacetone is for the purification of metal-containing wastewater and for corrosion protection [63, 64].

Apart from these molecules, acetylsalicylic acid and salicylic acid were also studied in this work. These molecules are present non-steroidal anti-inflammatory drugs that can be fairly easily obtained, which means it is important to detect even small amounts in human body or the environment where a large concentration can harm the ecosystem [65].

The information about molecular structure could be obtained by several methods. The issue with most of the spectroscopic methods are broad, non-specific bands that do not provide information when the subject is as fast as a proton transfer or change as small as rotation of one functional group in the molecule. The structural information such as the conformational variety of the molecule is usually obtained by studying molecular vibrations by the means of infrared absorption spectroscopy [66, 67]. This spectroscopic method yields better results when it is combined with low temperature matrix isolation, and can be used to both further explore known compounds and characterize new ones [68-78]. The molecules under study are isolated in a solid inert gas matrix where they do not interact with each other or their surroundings. This and the low temperature environment ensures that registered spectra are fairly easy to analyze. What is more, matrix isolation also provides a medium where irradiation leads to photoisomerization instead of dissociation. The method of low temperature matrix isolation has been used in many experiments, including ones studying acetylacetone, malondialdehyde, their derivatives and conformational variety [78-83]. The main requirement for matrix gases is weak interaction between the sample and matrix molecules. Inert noble gases are a good fit, and are usually used for these sort of experiments. In order to have the least perturbing environment, parahydrogen can be used. The spectral bands of molecules, isolated in this matrix, are usually very narrow and show practically no site effects but the experiments require more resources and longer preparation than the ones with noble gases [56, 68, 69, 84-87].

GOAL AND TASKS OF THESIS

In order to understand hydrogen bonding of complex biological molecules in detail, some model systems have to be studied first. So to explore the molecular structure in regards to the intramolecular and intermolecular hydrogen bonds, proton transfer and higher energy conformers specifically, the main goal set for this thesis was the application of low temperature matrix isolation method in combination with vibrational spectroscopy for the analysis of molecules possessing intramolecular hydrogen bond – malondialdehyde and acetylacetone derivatives, as well as acetylsalicylic and salicylic acids. Matrix isolation allows the observation of processes that are too fast to be observed under normal conditions but the dynamics of these processes are important for the understanding of hydrogen bond. To achieve this goal, specific tasks were formulated:

1. Measure vibrational spectra of chloromalondialdehyde molecules isolated in low temperature matrix environments in order to observe the effects of proton tunneling.

2. Produce open enol isomers of chloromalondialdehyde isolated in low temperature matrix environment through molecule photoexcitation.

3. Apply low temperature vibrational spectroscopy methods to fluorinated acetylacetone derivatives to obtain information about strength of intramolecular hydrogen bond and intermolecular hydrogen bond formed in associates with water.

4. Measure vibrational spectra of an asymmetric acetylacetone derivative – trifluoroacetylacetone – in different matrix environments in order to study the presence of higher energy isomer AcAcF3(OH).

5. Apply low temperature vibrational spectroscopy methods to the low vapor pressure samples of acetylsalicylic acid and salicylic acid in order to analyze their conformational properties.

STATEMENTS OF THE THESIS

1. Proton tunneling was observed for the first time in chloromalondialdehyde molecule isolated in parahydrogen matrix at very low temperatures (3 K).

2. Four out of eight theoretically predicted isomers of chloromalondialdehyde can be selectively produced in low temperature matrices by choosing a specific irradiation wavelength.

3. Intermolecular hydrogen bond in acetylacetone-water complex has little influence on the intramolecular hydrogen bond strength of acetylacetone molecule.

4. Coexistence of two isomers of trifluoroacetylacetone was confirmed in all analyzed matrices (neon, argon, parahydrogen, xenon, nitrogen, carbon monoxide). The ratio of isolated isomers depends on the matrix environment.

5. Optimal temperature for heating the ASA and SA samples was found (50 °C) in order to obtain a sample with little to no thermal dissociation products. One salicylic acid and two acetylsalicylic acid isomers are observed in low temperature argon matrix.

6. Only one salicylic acid and water complex structure can be stabilized in low temperature matrix environment.

PUBLICATIONS INCLUDED IN THE THESIS

1. Justinas Čeponkus, Rasa Platakytė, Valdas Šablinskas, Alejandro Gutiérrez-Quintanilla, FTIR study of acetylacetone, D2-acetylacetone and hexafluoroacetylacetone - water complexes in argon and nitrogen matrices, Chemija, 29(1), p. 1–16, 2018.

2. Alejandro Gutiérrez-Quintanilla, Michèle Chevalier, Rasa Platakytė, Justinas Čeponkus, Germán A. Rojas-Lorenzo, Claudine Crépin, 2-Chloromalonaldehyde, a Model System of Resonance-Assisted Hydrogen Bonding: Vibrational Investigation, Physical Chemistry Chemical Physics, 20(18), p. 12888 – 12897, 2018.

3. Alejandro Gutiérrez-Quintanilla, Michèle Chevalier, Rasa Platakytė, Justinas Čeponkus, Claudine Crépin, Selective photoisomerisation of 2-

chloromalonaldehyde, Journal of Chemical Physics, 150(3), 034305, p. 1 – 11, 2019.

4. Rasa Platakytė, Alejandro Gutiérrez-Quintanilla, Valdas Šablinskas, Justinas Čeponkus, Influence of environment and association with water to internal structure of trifluoroacetylacetone. Matrix isolation FTIR study, Low Temperature Physics, 45(6), p. 722-735, 2019.

5. Alejandro Gutiérrez-Quintanilla, Michèle Chevalier, Rasa Platakytė, Justinas Čeponkus, Claudine Crépin, Intramolecular hydrogen tunneling in 2-chloromalondialdehyde trapped in solid para-hydrogen, Physical Chemistry Chemical Physics, 22(11), p. 6115-6121, 2020.

6. Alejandro Gutiérrez-Quintanilla, Rasa Platakytė, Michèle Chevalier, Claudine Crépin, Justinas Čeponkus, Hidden Isomer of Trifluoroacetylacetone Revealed by Matrix Isolation Infrared and Raman Spectroscopy, The Journal of Physical Chemistry A, 125(11), p. 2249-2266, 2021.

PUBLICATIONS NOT INCLUDED IN THE THESIS

1. Yevhenii Vaskivskyi, Yelyzaveta Chernolevska, Antonina Vasylieva, Valeriy Pogorelov, Rasa Platakyte, Joana Stocka, Iryna Doroshenkoa, 1-Hexanol isomers in a nitrogen matrix: FTIR study and high-level abinitio calculations, Journal of Molecular Liquids, 278, p. 356 – 362, 2019.

2. Vilma Jonauskė, Rimantas Ramanauskas, Rasa Platakytė, Gediminas Niaura, Lina Mikoliūnaitė, Kunio Ishikawa, Aivaras Kareiva, Formation of 2D calcium hydroxyapatite on stainless steel modified with a TiN sublayer, Mendeleev Communications, 30(4), p. 512-515, 2020.

3. Thomas M. C. McFadden, Rasa Platakytė, Joanna Stocka, Justinas Čeponkus, Valdemaras Aleksa, T. Carrigan-Broda, Valdas Šablinskas, Paweł Rodziewicz, Gamil A. Guirgis, Experimental (Raman and IR) and computational (DFT, MP2) studies of conformational diversity of 1-chloromethyl-1- fluorosilacyclohexane, Journal of Molecular Structure, 1221, p. 1-10, 2020.

4. Joanna Stocka, Rasa Platakytė, Thomas M. C. McFadden, Justinas Čeponkus, Valdemaras Aleksa, A. G. Hanna, Valdas Šablinskas, Paweł Rodziewiczc, Gamil A. Guirgis, Conformational diversity of 1-chloro-1-chloromethylsilacyclohexane with experimental (Raman and IR) and

computational (DFT, MP2) methods, Journal of Molecular Structure, 1249, 2022.

CONFERENCE ABSTRACTS

1. Justinas Čeponkus, Rasa Platakytė, Claudine Crepin-Gilbert, Alejandro Gutierrez, Michèle Chevalier, Valdas Šablinskas, Vandens ir acetilacetono asociatų struktūros tyrimas matricinės izoliacijos infraraudonosios sugerties spektriniu metodu, LNFK, Vilnius, 2015.

2. Rasa Platakytė, Justinas Čeponkus, Valdas Šablinskas, Study of water-acetylacetone complexes by the means of matrix isolation infrared spectroscopy, Chemistry and Physics at low temperatures, Biarritz, Prancūzija, 2016.

3. Joanna Lach, Rasa Platakytė, Justinas Čeponkus, Valdas Šablinskas, Conformational analysis of tetrahydrofurean by means of FT-IR matrix isolation spectra - hot nozzle experiment, Open Readings, Vilnius, 2016.

4. Rasa Platakytė, Joanna Lach, Justinas Čeponkus, Claudine Crepin-Gilbert, Alejandro Gutierrez, Michele Chevalier, Valdas Šablinskas, Study of water-acetylacetone complexes by the means of matrix isolation infrared absorption spectroscopy, Open Readings, Vilnius, 2016.

5. Rasa Platakytė, Justinas Čeponkus, Claudine Crepin-Gilbert, Valdas Šablinskas, Fluoruotų acetilacetono darinių struktūros ir sąveikos su vandens molekulėmis tyrimas, LNFK, Vilnius, 2017.

6. Rasa Platakytė, Justinas Čeponkus, Study of Acetylsalicylic Acid by the Means of Matrix Isolation, EUCMOS, Coimbra, Portugalija, 2018.

7. Rasa Platakytė, Justinas Čeponkus, Valdas Šablinskas, Study of 3-methyl-acetylacetone structure and interaction with water, Open Readings, Vilnius, Lietuva, 2018.

8. Rimantė Bandzevičiūtė, Rasa Platakytė, Sonata Adomavičiūtė, Martynas Velička, Justinas Čeponkus, Vidita Urbonienė, Feliksas Jankevičius, Valdas Šablinskas, Optical fiber based spectroscopic device for in vivo detection of pathological tissue areas, Life Science Baltics, Vilnius, Lietuva, 2018.

9. Rasa Platakytė, Justinas Čeponkus, Conformational analysis of butanol and its complexes with water in low temperatures, Horizons in Hydrogen Bond Research, Amsterdamas, Nyderlandai, 2019.

10. Rasa Platakytė, Justinas Čeponkus, Valdas Šablinskas, Gamil A. Guirgis, Conformational analysis of 1-fluoro-1-chlormethylsilacyclohexane by vibrational spectroscopy, LNFK, Kaunas, 2019.

11. Morta Stadulytė, Rasa Platakytė, Justinas Čeponkus, Vaidas Pudžaitis, Library of red pigment Raman spectra and pigment identification in painted works of art, Open Readings, 2021.

12. Joanna Stocka, Rasa Platakytė, Justinas Čeponkus, Valdas Šablinskas, Gamil A. Guirgis, Paweł Rodziewiczc, Computational and experimental vibrational study of 1-chloromethyl-1-fluorosilacyclohexane conformations and its rearrangements, Open Readings, 2021.

13. Rasa Platakytė, Justinas Čeponkus, Claudine Crepin-Gilbert, Wutharath Chin, Julien Berthomier, Structural analysis of acetylsalicylic acid and its thermal dissociation products by low-temperature vibrational spectroscopy, LNFK, Vilnius 2021.

SCIENTIFIC NOVELTY

In this work, matrix isolation vibrational spectroscopy was used for the first time to experimentally characterize 2-chloromalondialdehyde molecule. The experimental results provided evidence of proton tunneling in chloromalondialdehyde in low temperature matrix environment. The conformational variety of chloromalondialdehyde was analyzed, proving that chloromalondialdehyde is the first member of the β-aldehyde and β-diketone families which has stable open enol isomers at the room temperature. The conformations which can be stabilized in photoisomerization experiments by ultraviolet irradiation were identified as well.

Trifluoroacetylacetone, a molecule with assymetric double well potential, was explored by low temperature IR and Raman spectroscopic methods and for the first time, it was shown that higher energy AcAcF3(OH) isomer exists in matrix isolation experiments. The dependence of its concentration on the environment was quantitatively evaluated.

Acetylsalicylic acid was isolated in low temperature matrices for the first time, and its conformational variety was analyzed by infrared spectroscopy and photoisomerization experiments. Raman spectroscopy method was applied to study salicylic acid molecules, isolated in nitrogen matrix.

A new method for analysis was created from the combination of low temperature matrix isolation and Raman spectroscopy. These measurements are much more complicated than IR since the sample has to be much more concentrated to produce spectra with good signal to noise ratio. The method was applied in the analysis of acetylacetone and salicylic acid.

AUTHOR'S CONTRIBUTION

The experimental work discussed in this thesis was performed in two laboratories – in the Institute of Chemical Physics, Vilnius University, Lithuania, and *Institut des Sciences Moléculaires d'Orsay* (ISMO) in *Université Paris-Sud*, France. Experiments in low temperature parahydrogen matrix environments were carried out exclusively in ISMO laboratories. Photochemistry experiments with malondialdehyde, chloromalondialdehyde, acetylacetone derivatives and salicylic acid were performed there as well. Large part of these experiments were performed by the author alone, during the rest, author was supervised and aided by Justinas Čeponkus, Claudine Crépin, Alejandro Gutiérrez-Quintanilla, Michèle Chevalier and Wutharath Chin. The related publications were written by author in collaboration with the mentioned people.

The experiments pertaining to acetylacetone derivative and water associate formation were done in Vilnius, Lithuania. The experimental work ant the analysis of the results was performed by the author, as were the vibrational assignments and part of the publication writing. The author also carried out the experiments of low temperature Raman spectroscopy, all done in Vilnius. All of experiments with salicylic acid and acetylsalicylic acid were carried out by author mostly in Vilnius, with some experiments done in parahydrogen and with photochemical excitation in France as well. The vibrational assignment of salicylic acid was done by Austėja Narvilaitė, supervised by the author. Theoretical calculations at B3LYP level were performed by the author, additional calculations at MP2 and M06 levels of theory which were relevant during trifluoroacetylacetone result analysis, were performed by Alejandro Gutiérrez-Quintanilla.

CHAPTER 1. MOLECULES WITH INTRAMOLECULAR HYDROGEN BOND

1.1. Hydrogen bond

Hydrogen bonding is an important interaction that governs many different biological and chemical processes in nature. It determines molecular structure and dynamics in both organic and inorganic compounds [88, 89]. These bonds can be formed both inside a molecule (intramolecular hydrogen bond, IHB) and between molecules (intermolecular hydrogen bonds) with widely varying strengths [90-94]. Since many organic molecules contain such atoms as nitrogen, oxygen and fluorine, there are countless possibilities to observe intramolecular hydrogen bonds. The strength of hydrogen bonds is also closely related to important biological processes that happen on molecular level, such as proton transfer reactions.
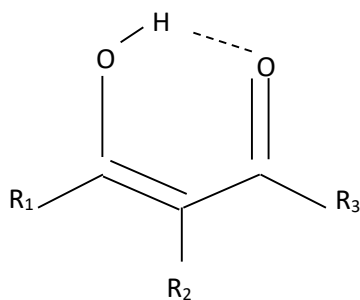

Figure 1. β-dicarbonyl molecule.

The molecules studied in this work can be classified as β-dicarbonyl (figure 1) type of molecules. The R_1 and R_3 can represent functional groups such as hydrogen atom (for aldehydes) or methyl group (for β-diketones). In this particular study, the R_2 group represented either hydrogen or chlorine atom. A molecule of β-diketone type can have two tautomeric forms. It is possible for the hydrogen atom to be bonded to oxygen in carbonyl group C=O in the molecule, in which case the molecule assumes enol form. If the hydrogen atom is attached to a carbon atom along with the R_2 group, the molecule is said to be in the keto form. In solutions, the enol-keto ratio depends on the polarity

of the solvent. Keto form is more polar than enolic and so it is more stable and more frequently observed in polar solvents [55, 56].

The enolic form is otherwise preferred because of the intramolecular hydrogen bond. As previously mentioned, those molecules possess something called resonance assisted hydrogen bond (RAHB). In molecules with such a bond, the proton donor and proton acceptor are linked by a chain of π-conjugated bonds [36, 40]. Usually, this interaction can be explained chemically through the alignment of the lengths of the conjugated bonds. The chemical interpretation of this interaction does not contradict the idea that the existence of two resonant forms stabilizes the molecular system. However, it is still not entirely clear what interactions affect this bond, and how electron delocalization and bond energy are linked, but such cooperative relationships are important in many systems such as DNA and secondary protein structures [28-30]. It has been calculated that for acetylacetone molecule stabilizing energy of this resonance assisted intramolecular hydrogen bond is 12.5 kcal/mol (52.3 kJ/mol), much bigger than in the case of hydrogen bond between water molecules [52, 95]. The resonant structure also enables proton transfer or tunneling between two potential minimums near oxygen atoms.

As electron delocalization increases, so does the symmetry of the molecule. This is one of the most important parameters that a molecule can be described by. In the example of β-dicarbonyls, if the proton is situated in the middle of two oxygen atoms, the molecule has three symmetry elements (axis C_2 and two symmetry planes σ_v) and thus is placed in C_{2v} symmetry group. C_s group structure has only one symmetry element (planar), because hydrogen is closer to one of the oxygen atoms. Studies have shown that C_{2v} form is unstable and corresponds to a saddle point instead of a real minimum [96]. In the stable C_s form, the calculated distance between oxygen atoms is 2.5 Å in the case of acetylacetone [52]. C_{2v} can be described as a transition state in the tunneling process. For the acetylacetone molecules, the symmetry can be different depending on what is the most stable position of the methyl groups in regards to each other.

Proton tunneling is a quantum phenomenon which has been studied extensively, especially by theoretical means. From experimental perspective, the techniques need to be very fast and precise in order to study this process. Matrix isolation is one of such techniques where the observation of measurable reaction rates at typical low temperatures (3-20 K) for reactions described by a small but thermally insurmountable barriers provides information about tunneling processes [97]. For a truncated parabolic barrier,

the possibility of tunneling for the molecule at a certain energy E depends on many parameters, such as barrier width w, barrier height V_0 and the mass m of the tunneling particle:

$$P(E) = \frac{1}{1 + \exp\left[\frac{\pi^2 w}{h} 2m(\sqrt{V_0 - E})\right]}.$$ (1)

Here h is Planck's constant, equal to $6.62607015 \times 10^{-34}$ m^2·kg/s. If a molecule can be described by a double well potential such as is the case of the molecules analyzed here (with proton being localized near either oxygen atom in either potential well), then the proton tunneling can cause vibrational levels to split. The tunneling splitting can be described through wavefunctions and its frequency depends on the potential barrier height. This value, in turn, depends on the molecular structure and differs significantly for acetylacetone and its derivatives [60]. For example, the potential barrier for hydrogen tunneling in acetylacetone molecule is calculated to be 9.62 kcal/mol (40.25 kJ/mol) and the tunneling frequency is 66 cm^{-1}. After deuteration of the molecule, the frequency decreases. In contrast, in the case of chloroacetylacetone, the tunneling frequency increases. This cannot be said for all the halogenated molecules such as chloromalondialdehyde. It can be concluded that tunneling is a complex process which depends on many things and there have been rules formulated to help estimate the value of the splitting in certain energy levels. These rules are necessary since different vibrational modes can either increase or decrease tunneling splitting. In other words, putting energy inside a potential well does not always mean it is easier for the molecule to cross the potential barrier. Some rules have been derived taking malondialdehyde – a planar, symmetric molecule – as an example. These rules state that excitation of either the tunneling mode itself, or a symmetric mode, increases the tunneling splitting, while the excitation of an antisymmetric mode (other than the tunneling mode) decreases this value. In addition, if any mode that is coupled to any other mode during the tunneling process, such that their combination is antisymmetric, is excited, the tunneling splitting decreases [98].
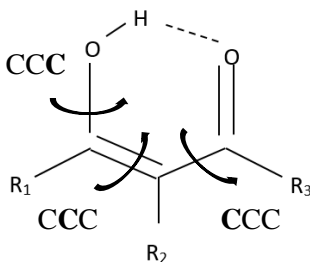
Figure 2. CCC isomer of a β-dicarbonyl molecule with the typical rotations around bonds during photoisomerization visualized.

Most complex molecules, including the β-dicarbonyls described here, can exist as several different isomers. Their relative energies and thus abundances depend on their structure, and one isomer can be transformed into another through rotation around certain bonds. If the barrier for rotation is small enough, the energy difference between the isomers $\varDelta E$ defines the ratio of higher energy isomers (N_1) to the most stable isomers (N_0) through Boltzmann distribution:

$$\frac{N_1}{N_0} = \mathrm{e}^{-\varDelta E/\mathrm{k}T}. \tag{2}$$

Here k is Boltzmann's constant, equal to 1.38×10^{-23} J/K, T is the temperature (room temperature for further calculations is taken as 298.19 K), and $\varDelta E$ is expressed in Joules. If the energy difference is large enough, the most stable isomer dominates in the sample and is the only one that can be observed in experimental spectra.

The most common isomerization is cis-trans, during which molecule (or atomic groups, more specifically) rotates around specific bonds. As discussed before, π electrons are delocalized in the chelated ring in the β-dicarbonyl molecules. For a rotation around a bond to become possible, the π bonds need to be broken. Therefore, a photoexcitation is necessasary to induce π-π* electronic transition in order to produce higher energy isomers through intermolecular rotations. This can be achieved by irradiating the sample with laser, usually at wavelengths of ultraviolet range. In the gas phase this usually leads to the fragmentation of the molecule. However, one of the benefits of cryogenic matrices used in these experiments is the ability to avoid such processes. When analyte is isolated in a matrix, the low temperatures and

surrounding matrix host molecules create an environment where the excited molecule loses energy through fast vibrational relaxation. Therefore, the molecule does not dissociate but instead can relax into a higher energy isomeric state. The exact isomeric form that can be achieved through photoexcitation experiments depends on the intersection between the potential energy surfaces of the ground and excited states of the molecule.

During photoisomerization process and the molecular rotations, the changing structure and charge interactions can change the energy as well. For the molecules analyzed during this study, it was especially interesting to see the energy difference arising from the intramolecular hydrogen bond breaking and possibly a weaker bond forming between the same hydrogen and fluorine or chlorine atoms in malondialdehyde and acetylacetone derivatives. Photosiomerization for acetylacetone (malondialdehyde) happens when OH, CH_3CO (HCO), and CH_3COH (HCOH) groups rotate around C-C, C=C, and C-O bonds in the enolic molecule (figure 2). Seven different isomers can be formed, each with its own local potential energy minimum [79]. That is confirmed by photoisomerization experiments with molecules isolated in nitrogen and rare gases matrices [81, 82]. The isomers are less stable than the enolic structure with IHB and can only be observed in gaseous or aqueous phases if their energy is low enough.
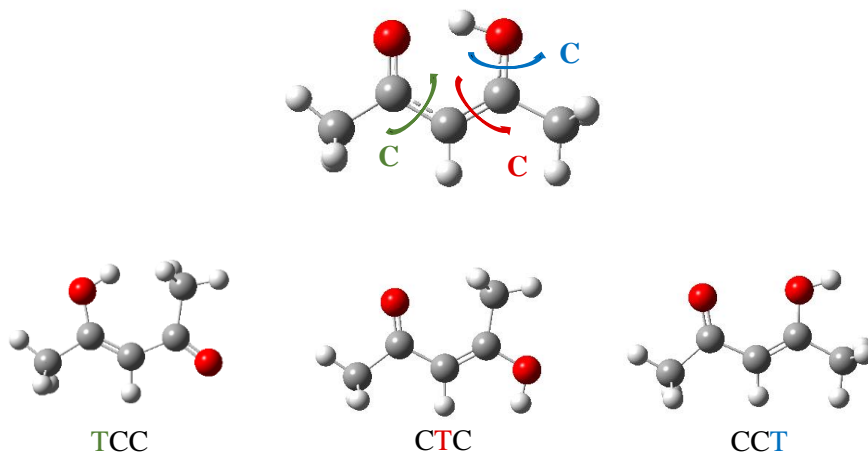

Figure 3. The most stable – CCC – and some of the higher energy isomers of acetylacetone. Arrows indicate the rotation around specific bonds necessary to produce these higher energy isomers.

The lowest energy or the unchanged enolic isomer is called CCC where C stands for *cis* (Latin for "on the same side") and the order of letters defines the position of the groups in relation to C-C, C=C, and C-O bonds, respectively (figure 3). If the groups change positions by rotating around one of the bonds, such position is denoted by the letter T for *trans* (Latin for "on the opposite side"). Therefore, acetylacetone CTC isomer is defined by OH group and CH_3 group exchanging places with respect to C=C bond and TTC isomer will exhibit the same exchange in addition to the C=O and CH_3 group rotation around C-C bond. In all of these cases, the intramolecular hydrogen bond is broken – the chelated ring is "opened" and these isomers are called open enol isomers.

1.1.1. Evaluating hydrogen bond strength

Hydrogen bond strength is closely related to molecular structure and can be determined from geometrical parameters, obtained from either theoretical or experimental studies. In the case of theoretical studies, different methods can be used in order to gather information about specific molecular parameters, such as bond lengths and angles that can be used to evaluate hydrogen bond strength. In a X-H…Y bond, the longer distances between H…Y and X…Y are coupled with shorter X-H length and mean weaker hydrogen bond. Other parameters are quite specific to the type of molecules analyzed in this work, such as malondialdehyde and acetylacetone derivatives. For example, another possible way to determine IHB strength is to calculate the energy difference between lowest energy isomer and an open isomer which differs from the first one only by the rotation of the OH group. That means only the severing of intramolecular hydrogen bond should contribute to the energy difference between those two isomers. In reality, however, other structural parameters are rearranged upon OH group rotation and the changed geometry or electron distribution can add to overall energy difference.

In addition to hydrogen bond strength, in systems with RAHB, it is necessary to evaluate the electron delocalization in the chelated ring. For this reason, a coupling parameter was defined by Gilli et al. [36]:

$$\lambda = \frac{\left(1 - \frac{Q}{0.32}\right)}{2},\tag{3}$$

where Q is the coordinate of π bond delocalization which can be expressed as $Q = d_{C-O} - d_{C=O} + d_{C-C} - d_{C=C}$. The value 0.32 represents fully localized system. Since Q decreases with decreasing difference between bond lengths in the chelated ring, the closer Q is to 0 (that is to say, the closer λ is to 0.5), the stronger is the delocalization. The coupling parameter λ and the coordinate of π bond delocalization Q are geometrical parameters that depend on bond lengths and are both measured in Angstroms.

In order to evaluate the hydrogen bond strength from the experimental vibrational spectra, it is necessary to separate which bands belong to vibrational modes involving only the OH group. As a rule, it is best to compare band positions for out-of-plane OH deformational vibration since the OH stretching band is too broad due to proton tunneling and the in-plane deformational vibrations are coupled to other modes [83, 99]. Stronger HBs are correlated with higher wavenumbers and broader bands but comparing bandwidths in different spectra can be tricky, even if molecules are isolated in a very similar environment.

As for the level of π electron delocalization, the C=C and C=O stretching mode vibrational bands can give a clue to how strong it truly is. Since the double bonds should be longer in systems with stronger π electron delocalization, the vibrational frequencies (and wavenumbers) should shift to the lower energy part of the spectrum.

In addition to intramolecular hydrogen bond, the intermolecular hydrogen bond formed between analyte molecules and water, can be evaluated by band shifts as well. In this case, what is most important is the νOH band shift from a free water molecule to a molecule bound in a complex. In the region of OH stretching modes, only water molecule modes are observed since the β-dicarbonyl OH stretching modes are still too delocalized for their vibrational bands to be detectable. Water monomers have several vibrational-rotational bands in the region from 3800 to 3600 cm^{-1}. When water molecule forms intermolecular hydrogen bond with another water molecule (case of water dimer), the νOH band shifts to approximately 3570 cm^{-1}. These values are given from experiments in argon matrix, since precise positions can depend on the environment. For example, nitrogen environment can prohibit molecule from rotating thus giving rise to a "non-rotating water" band at 3725 cm^{-1}. Similarly, bigger complexes will stop water molecules from rotating as well. There are several sites where a water can bond to molecule such as malondialdehyde or acetylacetone. When, for example, hydrogen in water bonds to oxygen in the C=O group of β-dicarbonyl molecule, the water

exhibits two shifted OH stretching bands. One is shifted less, and usually does not depend on the structure of the molecule water is bonded to, since this OH group points away from it. This vibration can be called free OH vibration, and the other one – bound OH vibration – is the one that depends on the structure of the molecule which forms a hydrogen bond with water. The position of the vibrational band of the latter mode is the one needed to evaluate intermolecular hydrogen bond strength.

1.2. Vibrational spectroscopy of biologically active molecules

1.2.1. Chloromalondialdehyde

Malondialdehyde is one of the simplest molecules that has a resonance assisted hydrogen bond. Due to this fact, the molecule and its derivatives are great model systems for analysis of proton tunneling processes. In this work, one of the derivatives was analyzed more thoroughly: chloromalondialdehyde, which is obtained by replacing olefinic hydrogen in MA with a chlorine atom. Properties of both malondialdehyde and chloromalondialdehyde have been extensively studied by various theoretical methods [100-105], most of these studies being focused on the proton tunneling.

This proton tunneling manifests as splitting of the energy levels. The value of splitting (the energy difference between two levels) is closely related to hydrogen bond strength [106]. Malondialdehyde molecule was analyzed in context of tunneling splitting by such methods as microwave spectroscopy [107] and jet experiments [108-112]. Some of these studies also explore the dependence of the tunneling splitting on the vibrational level and the comparison between theoretically calculated and experimentally obtained splitting values [113-115].

The two minima of the double well potential correspond to two energetically identical forms of malondialdehyde (and chloromalondialdehyde). The barrier height depends on the strength of hydrogen bond and determines whether or not the proton tunneling is possible between the two energetically identical forms. The transition state is the molecule of C_{2v} symmetry where the hydrogen atom is shared between two oxygen atoms. Because of quantum tunneling, the lowest energy vibrational state splits into two, and the same happens with higher energy states. Therefore, more than one transition from ground to excited state is possible (figure 4).
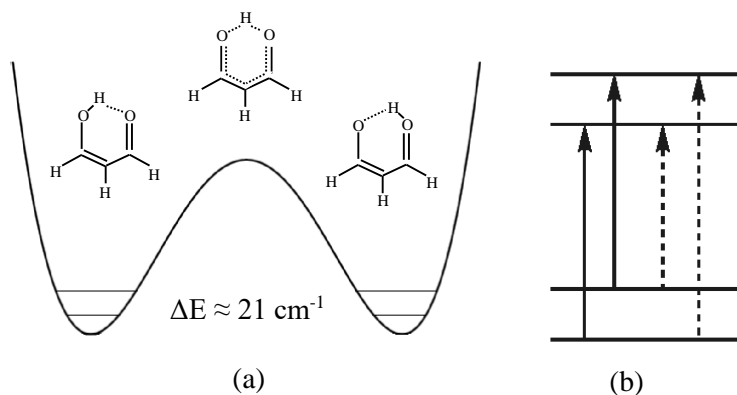
Figure 4. (a) Potential energy surface with split ground level for malondialdehyde molecule and (b) allowed transitions between ground and excited levels.

Malondialdehyde was also studied experimentally by the method of matrix isolation [81]. This study compared hydrogen bond in acetylacetone and malondialdehyde and found it was stronger in the former due to the electron release induced by the methyl groups. The energy difference between CCC and CCT isomers was also evaluated and overall hydrogen bond energy difference between malondialdehyde and acetylacetone molecules was found to be around 7.1 kJ/mol. The study also showed that unlike in the gas phase, UV excitation in nitrogen matrix environment can produce isomers. Different isomers are observed for acetylacetone and malondialdehyde molecules, with only some out of seven seen overall. As for proton tunneling, it was not observed for malondialdehyde molecule in this study or others [116, 117], unlike for chloromalondialdehyde as it will be discussed later on in this work.

Chloromalondialdehyde was mostly explored by theoretical methods [48, 118, 119]. It has a similar double well potential as malondialdehyde (figure 4). According to the study performed by Rios et al [120], the splitting value is around 22 cm^{-1} for malondialdehyde and 12 cm^{-1} for chloromalondialdehyde. The differences between chloromalondialdehyde and malondialdehyde stem mostly from the electronegative nature of chlorine atom. Since it is too far away from hydrogen atoms of CH groups, chlorine cannot form hydrogen bonds with them nor does it influence molecular geometry through the steric effect. The higher electronegativity of chlorine means it shifts the electrons

slightly towards itself thus weakening the intramolecular hydrogen bond. These differences mean that the observed open enol isomers will be different for chloromalondialdehyde in comparison to malondialdehyde, as well. During the course of this work, most attention was paid to proton tunneling observed in chloromalondialdehyde isolated in different matrix environments, a process which has not been experimentally explored for this molecule before.

1.2.2. Acetylacetone derivatives

Another one of the simple molecules with resonance assisted hydrogen bond is acetylacetone (noted hereafter as AcAc). Its enol (Z-4-hydroxy-3-penten-2-one) form is stabilized by the intramolecular hydrogen bond and is dominant in gas phase while the keto form exists in smaller concentrations in gas and liquid phases and for molecules isolated in the low-temperature cryogenic matrices. As previously stated, keto concentration in solutions increases together with solvent polarity. The structure and symmetry of acetylacetone molecule has been thoroughly analyzed [51-56, 60, 78-83, 95, 96, 121-124]. The conclusion most of the theoretical and experimental methods come to is that the two resonant forms of AcAc have C_s symmetry with hydrogen localized near one of the oxygen atoms and π electrons partially delocalized in the chelated ring [56]. Proton tunneling between two stable sites near oxygen takes place. The tunneling is highly coupled with two another large amplitude motions in acetylacetone, namely CH_3 torsional vibrations [125]. In the experimental spectra tunneling effects result in OH stretching mode being too broad to be observable, the out-of-plane and in-plane OH deformation modes are also affected to some degree [56, 80, 83]. Isotopically modified and halogenated [83, 126–128] derivatives of AcAc have also been studied using experimental and theoretical methods. One of the particularly interesting cases from halogenated derivatives is trifluoroacetylacetone (noted hereafter as AcAcF3). The major difference of this molecule compared to the parent AcAc molecule is the broken pseudo symmetry of the ring which is obtained by replacing one of the CH_3 group with a CF_3 group. The result of this symmetry breaking is that the potential energy surface for the hydrogen tunneling coordinate becomes asymmetric (figure 5).
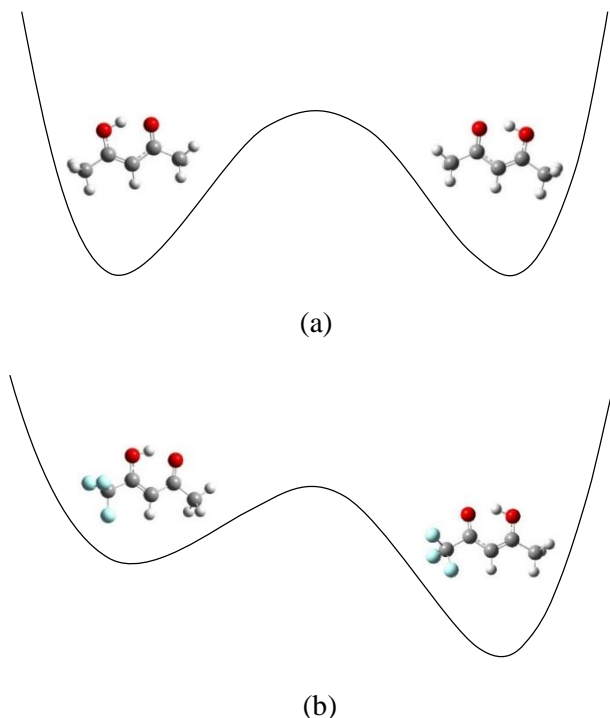
(a)

(b)

Figure 5. Schematic potential functions of hydrogen tunneling for (a) acetylacetone and (b) trifluoroacetylacetone.

As a result, trifluoroacetylacetone can exist as two distinguishable isomers: one where CF_3 group is on the same side of the molecule as -C=O group (AcAcF3(CO)) and another where CF_3 group on the same side of the molecule as -C-O-H group (AcAcF3(OH)). These structures are depicted in figure 5, and the schematic diagram already shows that in most calculations, AcAcF3(CO) is the more stable of the isomers. However, the exact value of the energy difference between these isomers highly depends on the method used. For examples, in the studies where MP2/6-31++G(d,p) method was used, the difference was calculated to be 0.7 kJ/mol, while MP2/6-311++G(d,p) calculations predict this value to be 2.2 kJ/mol [128]. The highest value of energy difference is 7.15 kJ/mol, obtained by B3LYP/6-311++G** level of theory [129]. The large distribution of the calculated energy differences means that both isomers could only be observed if the real energy difference is closer to the lower values in this range.

AcAcF3 has been studied by experimental and theoretical methods but to a lesser extent compared to its parent molecule, acetylacetone [83, 127, 128-130]. The theoretical studies focus on the structure and isomers of trifluoroacetylacetone and the competition between π electron delocalization and intramolecular hydrogen bond which is especially interesting in this asymmetric molecule. It has been found that while the AcAcF3(CO) isomer is more stable, AcAcF3(OH) exhibits a stronger intramolecular hydrogen bond which means that HB is not the most important parameter when talking about conformational preference [128].

Trifluoroacetylacetone was studied experimentally by electron diffraction, NMR, microwave, infrared and Raman spectroscopies. Electron diffraction was one of the first methods employed in the study of AcAcF3 structure but it was performed on the assumption that the hydrogen atom is symmetrically placed between two oxygen atoms [131]. NMR studies showed that AcAcF3(CO) isomer is more stable than AcAcF3(OH) but that they both exist at room temperatures with 0.4:1 ratio (for (OH):(CO)) [132]. One of the first vibrational spectroscopy studies involving trifluoroacetylacetone, used $\nu_{as}OH$ and $\nu C=O$ vibrational mode frequency values to determine hydrogen bond strength in acetylacetone and various derivatives. They found that the IHB in hexafluoroacetylacetone is the weakest, followed by trifluoroacetylacetone and then simple acetylacetone molecules. Other derivatives, such as chloro-acetylacetone were determined to have stronger intramolecular hydrogen bonds than their parent acetylacetone molecule. However, this study did not delve into the possible coexistence of two isomeric forms of AcAcF3. Several studies performed later on [129, 130] analyzed the molecule by both theoretical and experimental means and discarded the possibility of observing the less stable isomer in the experimental spectra. The first of the mentioned studies [129] calculated the isomer energy difference to be somewhere between 4 to 7 kJ/mol. In the second study [130], the authors also carried out calculations and experimental measurements with sample in gas and liquid phases. Comparing the results of these studies, they concluded that the most stable isomer dominates in the sample. Another study of trifluoroacetylacetone was carried out using microwave spectroscopy [133]. The rotational spectra showed that AcAcF3 exists as an enol form molecule with C_s symmetry and exhibits internal rotations of the CH_3 and CF_3 groups. It was concluded that internal rotation potential barriers are 379 cm^{-1} and 30.8 cm^{-1} for these respective groups. In addition, calculations yielded the isomer energy difference value of 2.1 kJ/mol. However, the second isomer was not

identified in the spectra. Fast relaxation to most stable isomers via proton tunneling was given as one of the possible reasons for this.

Matrix isolation is a useful method in case such as this where two species having very similar vibrational spectra have to be experimentally detected. However, the presence of the second AcAcF3 isomer was still in doubt even with the results of matrix isolation studies [127]. The authors concluded that they observe only one isomer in the experimental spectra and that any of the additional bands are due to matrix effects and Fermi resonance. There were studies carried out in parahydrogen matrix as well, with the spectral bands exhibiting fairly complex structure [83].

In conclusion, it can be said that trifluoroacetylacetone is a complex molecule with unclear abundance of second isomer, no complete assignment of vibrational bands and theoretical values highly dependent on the chosen method. The system becomes even more complicated if water molecule with the ability to form intermolecular hydrogen bond is added to it. There is one recent study of acetylacetone-water and hexafluoroacetylacetone (AcAcF6)-water complexes [134]. In the systems of AcAc–water and AcAcF6–water, the water molecule is bound to AcAc C=O group, but water orientation with the respect to AcAc and AcAcF6 is different. The broken symmetry of AcAcF3 molecule opens more possibilities for the formation of AcAcF3–water complexes therefore the identification of the possible AcAcF3–water complexes from experimental data is important. In this work, main focus is on trifluoroacetylacetone isomer distribution in different environments and the influence of water. The obtained results are compared with the similar studies of acetylacetone and hexafluoroacetylacetone.

1.2.3. Salicylic acid and acetylsalicylic acid

Salicylic acid (SA, $C_7H_6O_3$) is an aromatic compound with carboxy and hydroxy groups at the ortho positions (figure 6). The molecule is able to form an intramolecular hydrogen bond between neighboring hydroxyl and carboxyl groups. Salicylic acid can be found naturally in some plants (such as willow leaves or mint) and was used in ancient times in this form. It was later synthesized and widely used until the end of 19th century when a way to obtain acetylsalicylic acid (commonly known as aspirin) from it was developed in Germany [135]. Other drugs with similar anti-inflammatory, antipyretic and analgesic effects, such as acetaminophen (paracetamol), phenylbutazone, and

phenacetin, were soon discovered. Together, they are often grouped as "non-steroidal anti-inflammatory drugs" [136]. Aspirin and other drugs in this group relieve pain peripherally rather than through the central nervous system like morphine does. As these drugs have not only the same therapeutic properties but also side effects (indigestion, liver or kidney damage), it can be said that the effects of the drugs are based on biochemical intervention [137].
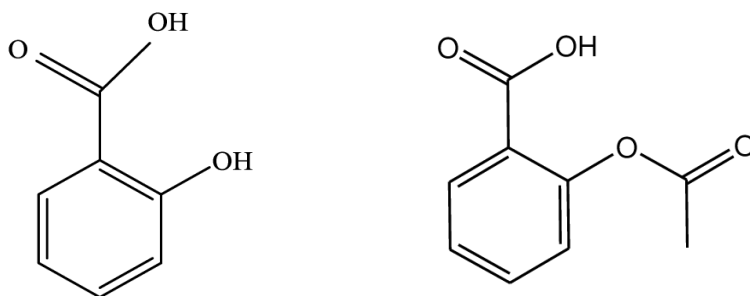

Figure 6. Salicylic acid and acetylsalicylic acid molecules.

The structure of salicylic acid monomers and dimers were analyzed by infrared absorption spectroscopy using jet-cooling method [138]. Two rotational isomers were identified for SA monomer by comparing vibrational spectra and theoretical calculations performed by the authors. Through exploring ground and first electronic excited states, authors noted that OH stretching vibrations drastically change upon molecule excitation which is consistent with distortion of the chelate ring. There was no evidence for proton tunneling between molecules in SA dimer, in either ground or excited state. A later study of jet-cooled salicylic acid derivative 5-methoxysalicylic showed that although electronic absorption-emission spectra show properties characteristic of internal proton transfer suppression, the infrared absorption spectra has evidence of elongated O-H bond and strengthened intramolecular hydrogen bond in the excited state [139]. Excited state of salicylic acid was further explored by theoretical methods. A study using time-dependent density functional theory (TDDFT) was carried out in order to calculate excited-state potential-energy surface for the molecule [140]. Results prove that intramolecular hydrogen bond is shortened by 0.322 Å in the excited state of the molecule.

Experiments with salicylic acid isolated in matrix environments have only been done once before [141]. This study was focused on photoreaction pathways of SA molecule, using low temperature infrared absorption

spectroscopy and density functional theory calculations. These calculations predict eight stable isomers of SA, with only one observed experimentally. Two higher energy isomers (second and fourth according to their energies) can be produced by UV irradiation ($\lambda > 290$ nm) of the sample. The third isomer is immediately transformed back to the most stable form. Apart from these isomers, ketoketene molecule and specifically ketoketene-water complexes were identified in the spectra (figure 7). Ketoketene is a molecule which forms when H and OH dissociate from one of the SA molecule isomers during a long period of UV irradiation).
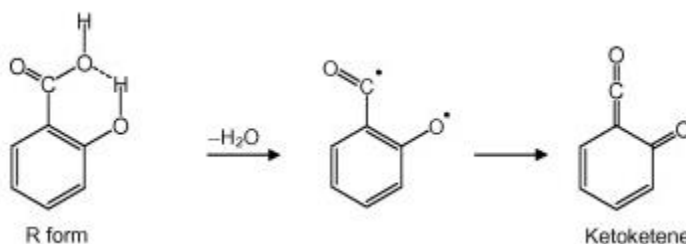

Figure 7. Ketoketene molecule formation from salicylic acid isomer.

Acetylsalicylic acid ($C_9H_8O_4$) can be synthesized from salicylic acid and acetic anhydride in the presence of acidic catalyst. Most of the research on these molecules is understandably biochemical and biomedical in nature. Spectroscopy is often used to characterize aspirin tablets and powder [142-148]. Upon drug's administration to human organism, it is quickly hydrolyzed to salicylic acid by spontaneous pH-dependent autolysis [149]. When heated to over 100 ºC, the mass loss occurs by elimination of acetic acid and evaporation of both SA and ASA [150]. The vapor pressure of ASA is lower than that of SA (3.3 mPa and 10.9 mPa, respectively).

Acetylsalicylic acid structure was thoroughly studied by theoretical methods at the RHF/6-31G* and B3LYP/6-31G* levels for potential energy surfaces and up to B3LYP/ 6-311G** level for single-point calculations [151]. The study identified nine aspirin isomers and detailed their structural properties, the thermochemical functions, relative energies and free enthalpies. The results of this study suggest that there is an overall repulsion beween the the carboxylic acid and the ester groups in all aspirin isomers, including the one where intramolecular hydrogen bonds are formed. This repulsion value can be quantitatively expressed as being at least 11.3 kJ/mol, and it can be as big as 25 kJ/mol at the higher limit.

33

A gas-phase experimental study was performed for acetylsalicylic acid [152]. The authors compared their results with ab initio calculations for different rotamers of ASA and concluded that they can see two different rotational isomers in the experimental spectra. Acetylsalicylic acid molecule has never been studied by matrix isolation methods.

CHAPTER 2. VIBRATIONAL SPECTROSCOPY METHODS FOR MOLECULAR STRUCTURE ANALYSIS

2.1. Matrix isolation

The term matrix isolation is usually applied when talking about a method where a small amount of analyte (or guest molecule) is mixed with larger amount of matrix gas (or host gas) and deposited on a surface cold enough so that the mixture is condensed into a solid. The technique was pioneered by Pimentel and Porter in 1945 and has been incredibly useful in the spectroscopic characterization of different molecules and processes happening on the molecular level ever since [154 - 157].

In experimental spectrometry the analyte is usually a large system where each molecule is influenced by different local environment, varying bond strengths, significant thermal motion and molecular complex formation. For this reason, measured spectra can become very complicated to analyze and possible overlap between bands means significant loss of information. The analysis of the internal structure of the molecule requires experimental method which could bring the spectra closer to that of a 'single molecule' by eliminating as many unnecessary interactions as possible. Low temperature matrix isolation accomplishes that as it places the analyte molecules in an environment where they are surrounded by matrix gas molecules with which they have limited interactions. In addition to that, the temperature of the solid is usually too low for the molecules to diffuse through the matrix [68, 70, 155].

Molecular processes such as isomerization, dissociation or proton transfer, happen so fast that they were virtually impossible to observe for quite some time [157]. Charge transfer is essential in order to understand such processes as photosynthesis or rhodopsin isomerization which is important in our vision. However, low temperature vibrational spectroscopy offers a way to study these interactions by controlling the sample temperatures and diffusion through the matrix.

If at the very beginning of matrix isolation studies, the lowest reached temperature was 66 K for xenon matrix, the closed-cycle cryostats of nowadays can bring the temperature down to 2 K [68]. However, the technical development necessary for better molecular studies is not limited to the minimal temperature cryostats can achieve. The advances in the area of spectroscopy, especially vibrational spectroscopy from which a lot

information about molecular structure can be gleaned, together with the developing field of matrix isolation meant obtaining new information about molecules previously thought to be thoroughly analyzed.

The main advantage of matrix isolation spectroscopy is the already mentioned weakened intermolecular interactions. As the molecules are trapped in a solid matrix, their rotation is severely hindered, and the spectra of larger molecules no longer have rovibrational bands. The smaller molecules, such as water, can still rotate although the number of observable rovibrational bands depends on the matrix temperature. In addition, at high temperatures the Boltzmann distribution allows population of higher vibrational levels and there is a possibility to observe transitions from these, also known as 'hot bands'. After lowering sample temperature, the excited levels are depleted and the 'hot bands' disappear from the spectra. The risk of overlap for the bands belonging to different vibrational modes is also much smaller since all the other bands become narrower. Overall, the bandwidth in matrix isolation is usually below 5 cm^{-1}, and the specific value depends on the molecular parameters and the choice of matrix [68, 155].

And even though in an ideal matrix isolation experiment, the molecules are completely isolated from each other, by increasing the temperature in small steps, the slow diffusion of sample molecules can be controlled. If the spectra are registered after each such step, the conclusions about various reactions, their partial products and molecular complexes that are forming in the matrix can be made. Another advantage is the possibility to study unstable compounds. In fact, one of the first historical usages of matrix isolation was analysis of free radicals [153, 155].

The many qualities mentioned in the above section do not mean that matrix isolation method does not have any flaws. Apart from fairly long experiments that are an inevitable part of operating at such low temperatures, there are a few other things that have to be kept in mind while both performing the experiments and analyzing the obtained results.

One of these things is the choice of the analyte. The final sample which is deposited on the cryostat-cooled spectral window or, more generally speaking, a very cold surface, has to be in the gas phase. This means that samples that are gaseous in room temperature and liquids with high vapor pressure do not pose any problems [68, 70, 71]. However, there are plenty of interesting solid analytes for which the transfer from the sample container to the matrix becomes so much more complicated.

Of course, there are several methods that can be employed to vaporize the materials in question, from simple heating of the sample to more complex methods that are used in other fields that require vapor in order to make desired structures such as thin and neat layers. Still, all of these methods pose similar dangers - first of which is molecular dissociation. Biological molecules are usually of most interest in scientific experiments and even the smaller ones are still fairly large and prone to dissociation. After heating them, or using methods such as laser ablation in which a laser beam is focused onto a sample in order to remove material from the chosen zone, during the sample preparation phase, it is likely for large concentrations of dissociation products to be observed in the deposited sample spectra. And even if the molecule does not dissociate in the gas stage, it can bring an excess of energy with it to the matrix and then use it for diffusion, isomerization or other processes that would complicate analysis of the results. So even though these methods are useful, they have to be employed in a very controlled way. There are other methods of preparing the sample that are worth mentioning – molecules can be synthesized by in situ diffusion method, through controlled chemical reactions, or photolysis.

It should also be mentioned that polar molecules are prone to forming dimers or higher level complexes even before the sample is mixed with the host gas. One of the possible solutions is to pass the evaporated sample through a heated tube and give the molecule complexes enough energy to dissociate. If the undesirable complex formation is observed in the matrix, the best approach is to increase the ratio of matrix gas and sample volumes. Additional electromagnetic irradiation may be utilized during the preparation or after the deposition of the matrix in order to cause photochemical reactions such as fragmentation, ionization or isomerization.

Another possible drawback has to do with the matrix environment and is perhaps not as much a disadvantage, as a specific characteristic of the technique that can be both disadvantageous and useful. There is a shift between the bands of the spectra in gas phase and in a cryogenic matrix [155, 158-160]. This shift is called matrix effect and is caused by van der Waals interactions between the sample and the matrix molecules. The direction of the shift depends on the type of vibration and the matrix, in which the analyte is isolated. Usually, the shift to the red end of the spectrum is observed but for some non-stretching vibrations the matrix can have the opposite effect, especially for neon matrices. Another way the environment can influence the molecular structure and thus the spectra are site (or cage) effects [68]. In order

to make place for analyte molecules in the matrix, several host atoms have to be removed. These sites can differ across the matrix and as a consequence, the analyte molecule can interact with its environment in different ways. This usually results in splitting of the bands in the vibrational spectra – because of this, such effect is also sometimes called the matrix splitting effect.

2.1.1. Matrix gases

Matrix isolation experiment requires inert environments, gaseous at room temperature and solid at the temperatures that can be achieved by experimental set-up. These requirements for matrix gases are fulfilled by nitrogen, hydrogen, the noble gases and a few other compounds. Atomic and homonuclear gases do not absorb radiation in the infrared and visible regions and at the same time, they allow obtaining a good spectral resolution [68, 155, 158].

In a typical matrix isolation experiment, sample is prepared by evaporating a small amount of it in a vacuumed system and then mixing it through with a much larger volume of host matrix gas. The mixture is then deposited on a low temperature surface (spectral window through which infrared light could pass unimpeded). The chosen temperature of this surface during the deposition depends on the chosen matrix gas – it can be in the range of 3 K to 20 K. The higher limit is decided by the gas diffusion temperature (which is more or less half of the melting temperature). Above this limit, molecular movement in the matrix allows the formation of big molecular complexes.

Argon and nitrogen are fairly often used as matrix gases. They are sufficiently inert, have no absorption spectra which could overlap with that of the isolated samples. They are also relatively easily obtained via partial distillation of liquid air. It is worth to mention that even though both of these gases are inert, nitrogen molecules exhibit stronger physical interaction with the analyte molecule in the low temperature environment due to their quadruple moment [66-68]. These type of interactions can be seen in the difference between water spectra in a noble gas matrix and nitrogen matrix. Since nitrogen atoms interact more with the guest molecule, the bands of water OH stretching vibrations are shifted. In nitrogen matrix spectra, they are called non-rotating water bands since the stronger interactions inhibit the rotation that the small water molecule can still display in other low temperature matrices such as argon or neon. Another one of the possible effects of nitrogen

matrix is that modes which were degenerated in argon matrix, separate in nitrogen.

Apart from argon, which forms quite a firm matrix (lattice), other noble gases such as neon, krypton and xenon, are used. In neon, the observed shifts from gas phase spectra are lower than for other matrices. Noble gases are also very poor heat sinks. Some of the other gases that are worth mentioning are carbon monoxide which creates an environment quite similar to nitrogen. Carbon monoxide absorbs infrared radiation but it does not interact with analyte molecules much more than nitrogen and so it can also be utilized. Many metal carbonyl compounds have been detected after experiments in the carbon monoxide matrix isolation experiments. Methane and other alkanes have been used because of their low chemical reactivity which is due to strong bonds and low polarity. Alkanes with chains containing five to eight carbon atoms were utilized in organic matrix isolation experiments since they freeze around 77 K temperature which makes liquid nitrogen a convenient cooling agent. Even rarer were the usages of O_2 (used to study oxidation reactions), F_2, Cl_2 and CO_2, SF_6 and CCl_4 compounds which served the need for higher temperature matrices [155, 158].

Quantum solids such as hydrogen and especially parahydrogen matrices have many advantages although they also require lower temperatures than the others (lower than 4 K). Parahydrogen is one of the most interesting environments, forming a very soft matrix that allows large amplitude motions of the host molecule [84-86, 161].

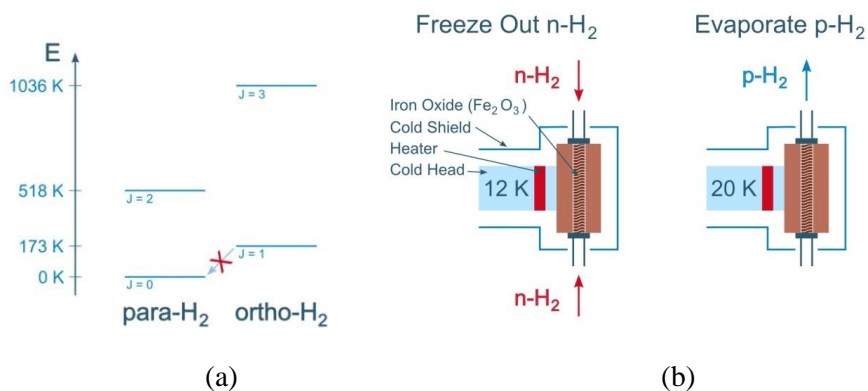(a)   (b)

Figure 8. Energy levels of ortho and parahydrogen and scheme of ortho-para conversion system.

Parahydrogen offers a lot of advantages in the matrix isolation experiments. *Para* in this case refers to nuclear spin of the molecule. The total nuclear spin moment for hydrogen molecule can be equal to $I = 0, 1$. Molecules assuming the lower value are given the prefix '*para*' and the ones assuming the higher value are called '*ortho*' (figure 8). At low temperatures, parahydrogen is the more stable of the two but at normal temperatures, the ratio is $n_o : n_p = 3 : 1$, the value corresponding to the three times degenerate ortho state (three projection values $M_I = 0, \pm 1$ for $I = 1$). The main advantages parahydrogen holds over other matrices are closely-packed structure and very weak interactions due to the zero value of the angular momentum [155].

A conversion system is required to obtain parahydrogen [162, 163]. The ortho-para conversion is performed at low temperatures (below 20 K) by placing condensed hydrogen in a conversion cell with a paramagnetic catalyst material (such as Fe_2O_3 or rare earth metals). The low temperatures ensure population only for the ground rotational level of parahydrogen and the catalyst allows spin flip from ortho to parahydrogen.

Freeze-out method for conversion is depicted in figure 8(b). In this method, normal hydrogen is let into the low temperature system from a storage bottle. After the desired amount of hydrogen is trapped in the conversion box, the temperature is slowly raised to around 18 K. This way, hydrogen evaporates from the catalyst as parahydrogen.

Overall, in matrix isolation infrared absorption experiments there can be several reasons for band structure, that is to say the presence of more bands than there are normal vibrational modes. They can be attributed to site effects, Fermi or combination bands, molecular complex formation in the matrix. Parahydrogen exhibits less band splitting due to site effects but the presence of ortho hydrogen and the coexistence of fcc and hcp ordering in the lattice can result in doublets in the experimental spectra [164, 165].

2.1.2. The experiment

Low temperatures are usually achieved by using closed cycle cryostats (figure 9). Two cycle cryostats can bring the temperature down to 7–8 K, and the new generation of three cycle cryostats can achieve even lower 2-3 K temperatures. Cryostat consists of a compressor and expander, connected via two high pressure steel tubes. Helium is used to achieve the low temperatures

– the coldest point (for three cycle cryostats) is at the end of the third expansion zone. Here, by using special materials, it is possible to get the temperature down to 6 K [68, 158].

Resistance heater next to the cold part is necessary during annealing experiments or during the deposition of the sample if there is a need to do it at a higher temperature than the lowest achievable. The heating element is controlled through an outside device – as the desired temperature is chosen, an electric current starts to run through the element. Along with the heater, there is also a temperature-measuring element such as thermocouple or silicone diode inside the cryostat. These elements can measure the temperature directly in the sample and provide information about the temperature of the cold point which is always a little lower.
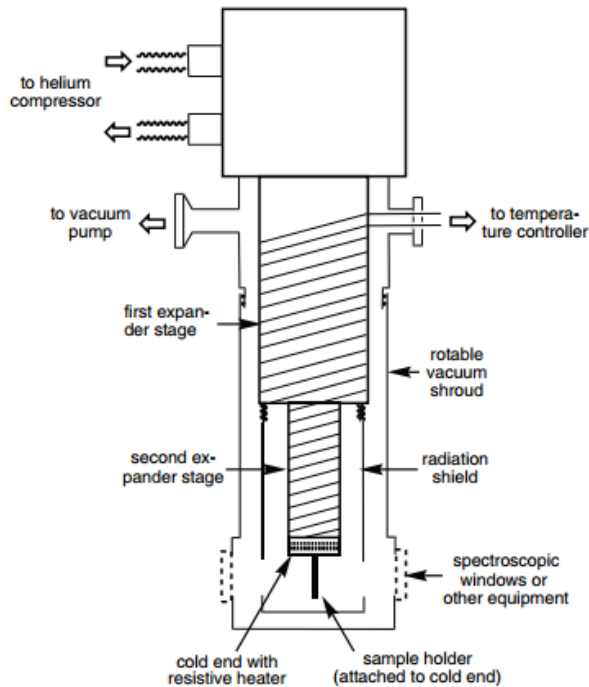
Figure 9. Closed-cycle cryostat [68].

Vacuum shield is designed to isolate low temperature equipment from the room temperature environment. This is a measure against thermal energy transfer through molecular collisions. In addition to this, the second expander

region is surrounded by a radiation shield which stops thermal energy transfer by radiation. Vacuum is also a useful measure against sample pollution.

Experiment can be divided into two parts – deposition of the sample and the registration of the spectra. First of all, the nozzle is turned towards spectral window with a very small distance between them so that gas mixture could be deposited evenly. During spectra registration, the shield is rotated so that the radiation could pass through the window and to the detector. At the very end of the experiment, the sample is evaporated.

The spectral window on which the sample is deposited has to be transparent for the electromagnetic irradiation used during the experiment. In the case of infrared, the most suitable materials are diamond and its cheaper alternative cesium iodide. Unlike sodium chloride or potassium bromide, cesium iodide is not brittle and is less likely to be damaged due to constant temperature change. In case of Raman scattering spectroscopy, the sample window is replaced with a mirror.

2.2. Quantum chemistry calculations

Quantum chemistry calculations use mathematical methods to determine physical and chemical properties of molecules and their systems. The most important properties of any system are its energy and the structural geometry on which the aforementioned energy depends. In the context of experimental works and spectroscopy specifically, the calculated vibrational spectra help interpret the experimentally obtained data. Structure and energy of any molecule depend on interactions between positively charged nuclei and negatively charged electrons. For static parameters, the information about lowest energy electron states is sufficient. For dynamic properties such as excited molecule spectra or allowed transitions between electronic levels it is important to know electron distribution in excited states and even its time-dependent dynamics. For transitions between rovibrational levels only, this information about excited states is not necessary. In addition to the calculation of vibrational frequencies, other spectroscopic parameters, charge distribution, dipole and higher multipolar moments, rotational constants, cross-sectional areas of collision with other particles can be found by quantum chemistry methods [166-168].

Different approaches can be used to model the structure of molecules – molecular mechanics, *ab initio*, density functional methods. Molecular

mechanics is usually used to describe large molecular systems. The latter two methods (*ab initio* and DFT) are described in more detail further on. In order to describe static and dynamic properties of a molecule, Schrödinger equation has to be solved. The larger the molecule, the more resources the calculations demand. To solve Schrödinger equation for a system of more than two particles, approximations eliminating the movement of nuclei and simplifying electronic interactions are employed.

2.2.1. *Ab initio* methods

Ab initio (Latin for "from the beginning") is based on the basic equations and constants of quantum mechanics [168]. The behavior of the nuclei and electrons in the molecule is described by Schrödinger's equation, the solution of which for larger particle systems can be simplified by applying various approximations. One of them is Born-Oppenheimer principle, in which the mass of a nucleus is considered to be much bigger than that of an electron. Because of this assumption, the motion of nuclei can be eliminated from the system and the electrons can be described as moving in the electrostatic field generated by stationary nuclei. In this case, it is possible to separate nuclear and electronic wave functions and show that the electronic energy depends on the coordinates of the nuclei in a parametric manner.

$$\Psi = \Psi_{el}(q, Q)\Psi_n(Q),\tag{4}$$

here q represents electronic and Q – nuclear coordinates. In this case, electronic operator solutions (real values and functions) will be calculated separately for each set of nuclear coordinates. For this reason, it becomes possible to find the most stable geometric arrangement of molecules – finding the most stable system becomes equivalent to calculating the energy minimum. For molecules in these minima, the vibrations can be described by harmonic approximation where electronic wavefunction depends on internal nuclear coordinates:

$$\left(H_{el} + U(Q)\right)\Psi_{el}(Q) = E_{vib}\Psi_{el}(Q),\tag{5}$$

here $U(q)$ – potential energy function. If, upon solving this equation, there are imaginary values in the list of vibrational frequencies, it means that instead of a true minimum, there is a saddle point.

The application of Born-Openheimer approximation is not enough to solve Schrödinger's further for larger, more complex molecules so further simplifications are needed to describe them. If approximate separation is not possible, the multi-body system can be modeled as a single pseudo-particle by averaging the interactions. This is the Hartree-Fock approximation. Hartree proposed a method for solving Schrödinger's equation, assuming that one electron senses the averaged potential field of all other electrons [166]. This reduces the accuracy of molecular energy calculations due to the elimination of specific interelectronic interactions but this step is still the basis for many more accurate calculations.

Dirac and Heisenberg proposed an asymmetry condition for electronic wavefunctions that fulfills Pauli exclusion principle. Due to these conditions, the lowest energy state of a particle is described as a determinant of single-particle states (Slater determinant) – when two rows or columns are swapped, the sign of the determinant changes, and when two rows or columns become identical, the value of determinant becomes zero. When there are three or more electrons in the system, the Slater determinant for the asymmetric wavefunction can be written as follows:

$$\Psi(1,2,\dots,N) = \frac{1}{\sqrt{N!}} \begin{vmatrix} \varphi_1(1) & \varphi_2(1) & \dots & \varphi_N(1) \\ \varphi_1(2) & \varphi_2(2) & \dots & \varphi_N(2) \\ \vdots & \vdots & \ddots & \vdots \\ \varphi_1(N) & \varphi_2(N) & \dots & \varphi_N(N) \end{vmatrix}, \tag{6}$$

where $\varphi_i(j)$ is a single-electron wave function. Hartree-Fock approximation was derived after applying the Slater determinant to the Hartree method [169, 170]. Here, the Coulomb and exchange operators are used to describe the electron wavefunction. The Coulomb integral can be interpreted according to the classical mechanics - it describes the electrostatic interaction between two electrons characterized by their probability density. The exchange integral is of quantum nature and arises from the condition of the asymmetry of the wavefunction with respect to the operator of exchange. This term describes the overlap between orbitals and their mutual attraction.

Hartree-Fock equations are solved using the SCF (self-consistent field) method. In this case, information about the analyzed system such as the

coordinates and charges of the nuclei, the number of electrons and the initial molecular orbitals, is collected first. Then, using the initial orbitals, the one- and two-electron integrals are computed in order to find the Fock matrix, and so the electronic eigen functions and energy values are obtained. The problem is solved using the variational method which is based on comparing the obtained molecular orbitals to the initial orbitals. If the difference is less than a certain set threshold, the results are accepted as true functions. If the difference is larger, the same process is repeated again, only the calculated orbitals are now taken as the initial ones. Hartree-Fock approximation can be refined in various ways such as coupled cluster methods.

Another method that improves on the accuracy of Hartree-Fock is Møller–Plesset perturbation theory [166, 171]. The main principle of perturbation theory is that after obtaining a precise solution to a specific problem, the Hamiltonian is supplemented by an extra term which represents perturbation. If the perturbation is small, the new solution is equal to the known precise solution and a correction value. In terms of Schrodinger equation, the Hamiltonian is written as a sum of two parts representing a reference and a perturbation operator.

$$(H_0 + \lambda H')\Psi = W(H_0 + \lambda H'). \tag{7}$$

Here λ is a parameter which indicates the strength of the perturbation. The reference Hamiltonian in Møller–Plesset is the sum of Fock operators which represents the average interaction of the electrons. If the perturbation is equal to zero, the eigenfunction is the zeroth-order or unperturbed wavefunction Φ_0 and W is the zeroth-order energy E_0. The first-order energy is the energy obtained by Hartree-Fock method. Higher order energy corrections are given names of MPn methods, with n denoting the order of perturbation. MP2 is used most widely because higher-order methods are much more resource-consuming.

2.2.2. Density functional theory

Density functional theory (DFT) is based on the proof that the lowest energy electronic state can be fully described by the electronic density $\rho(r)$ [166-168]. A functional (indicated by square brackets) is a mathematical entity that depends not only on the value of a function at a single point, but

also on its behavior over a given range. The wavefunction and the electronic density are functions, and the energy that depends on them is a functional. At the beginning of the development of the density functional method, attempts were made to express all energy components as an electronic density functional. Unfortunately, these methods were inaccurate and there was a constant need to return to methods based on the search for the wavefunction [167, 172]. An appropriate correction was suggested by Kohn and Sham, who argued that the kinetic energy of electrons should be calculated from a set of auxiliary orbitals representing the electron density [173]. In this case, only the exchange-correlation energy, the value of which is relatively small, remains unknown. The simplest DFT model is LDA (local density approximation), which assumes that the electronic density is a slowly varying quantity [168]. In this case, the exchange-correlation energy is calculated using formulas derived for homogeneous electronic density. There are also more sophisticated methods that calculate this part of the energy more accurately. DFT-based calculations are similar to the Hartree-Fock method, but give more accurate results.

The main idea of Kohn-Sham theory is to split the kinetic energy into two parts - the precisely calculated and the correction part, included in the exchange-correlation functional. For the first part, it is assumed that the electrons do not interact with each other. This is similar to Hartree-Fock theory, in which the wavefunctions of orbitals describe non-interacting electrons. In DFT theory, the electron density, like the molecular orbitals in Hartree-Fock theory, can be calculated using the variational principle. The full DFT energy is expressed as follows:

$$E_{DFT}[\rho(\boldsymbol{r})] = T_S[\rho(\boldsymbol{r})] + E_{NE}[\rho(\boldsymbol{r})] + J[\rho(\boldsymbol{r})] + E_{XC}[\rho(\boldsymbol{r})], \qquad (8)$$

here $T[\rho]$ is kinetic energy, E_{NE} – term used to describe the attraction between the nuclei and electrons, J – Coulomb term and E_{XC} – exchange-correlation term [163]. It describes not only the quantum mechanical phenomena of exchange and correlation, but also the correction for the difference between the kinetic energies of classical interactions and the kinetic energies of non-interacting electrons and real systems.

There are various theoretically derived and empirical methods of DFT, the accuracy of which depends largely on the expression of the exchange-correlation potential. The local density method is based solely on the electron density function. More sophisticated and accurate calculations use electron

density and its gradient or hybrid methods that combine functionals with other methods using Hartree-Fock theory. One of the most widely used hybrid functionals is B3LYP (which stands for Becke 3-parameter, Lee–Yang–Parr). This method uses Becke exchange functional and the correlation functional of Lee, Yang and Parr to express the exchange-correlation potential [174-176]. B3LYP is widely recognized as one of the best methods in organic molecule vibrational spectra calculation.

2.2.3. Basis sets

Basis sets are groups of mathematical functions that can be used to express an unknown wavefunction, such as a molecular orbital. The main disadvantage of this solution is that the basis set can only be considered complete when the number of functions is infinite. With a finite number of basis functions, some information is inevitably lost. The results of the calculations are also influenced by the type of the basis functions - choosing suitable functions means obtaining sufficiently accurate results with a reduced size of the basis set. Obviously, smaller sets are more suitable for computer modeling due to lower time consumption [166-168, 177].

The most commonly used basic functions are Gaussian (GTO) and Slater orbitals (STO) [163, 175, 176]. The latter are similar to hydrogen atomic orbitals, their shape in the polar coordinate system is described by equation (9).

$$\chi_{\zeta,n,l,m}(r,\theta,\varphi) = NY_{l,m}(\theta,\varphi)r^{n-1}\exp(-\zeta r), \qquad (9)$$

here N – normalization coefficient, $Y_{l,m}$ – spherical harmonic functions. The exponential dependence on the distance between the nucleus and the electron corresponds to the description of hydrogen orbitals. The biggest problem is that the integrals of a two- or four-center two-electronic systems cannot be solved analytically. Therefore, STOs are commonly used to accurately describe the distribution of electrons in monoatomic and diatomic systems, but are no longer suitable for even only slightly larger molecular systems. Instead, approximate Gaussian orbitals are often used, and their expressions in the polar and Cartesian coordinate systems can be written as follows:

$$\chi_{\zeta,n,l,m}(r,\theta,\varphi) = NY_{l,m}(\theta,\varphi)r^{2n-2-l}\exp(-\zeta r^2), \qquad (10)$$

$$\chi_{\zeta,l_x,l_y,l_z}(x,y,z) = N x^{l_x} y^{l_y} z^{l_z} \exp(-\zeta r^2). \qquad (11)$$

The main advantage is that the overall result of Gaussian distributions with different maximum positions is also expressed as a Gaussian distribution. Here the sum of l_x, l_y, l_z indicates the type of orbital. The d-type GTO described by spherical functions has five members ($Y_{2,2}$, $Y_{2,1}$, $Y_{2,0}$, $Y_{2,-1}$, $Y_{2,-2}$) while in the Cartesian coordinate system there are six (x_2, y_2, z_2, x_y, x_z, y_z). These six functions can be converted to five spherical d-functions and one additional s-function ($x^2 + y^2 + z^2$). When there are many d-functions in the analyzed system, such spherical functions significantly simplify the calculations. In addition, using only spherical functions reduces the problems that arise due to linear dependence of large basis sets.

There are several notations used in the context of basis sets. The STO-nG sets refer to Slater orbitals approximated by the number n of Gaussian orbitals [166, 168]. It was found that the sufficient results are obtained when n = 3. The STO-3G is a minimal set of basis functions, with only one function assigned to each orbital, and three Gaussian orbitals corresponding to each Slater orbital.

The k-nlmG basis sets, designed by Pople and coworkers, are of the split-valence type [166]. Here k denotes how many Gaussian orbitals are used to describe the internal coordinates, and nlm indicates the number of functions into which the valence orbitals are split, as well as the number of Gaussian orbitals that describes them. Values written before G indicate the s- and p-functions in the basis set, and values after G describe the polarity. This type of basis sets uses the same exponential to describe the s- and p-functions. This speeds up calculations but reduces accuracy.

For example, in 3-21G set, three Gaussian functions describe the internal orbitals, and the split-valence functions use two separate groups to describe the electron distribution of the valence layers. This set allows the expansion or contraction of valence orbitals depending on the changing molecular environment. The internal valence orbitals are described by two Gaussian functions and the external ones by one. Methods 6-31G, 6-311G are described accordingly.

Each set of basis functions can be supplemented by diffusion and/or polarization functions. Diffusion functions are usually of the s- and p-function type and are denoted by + or ++, written before G. The first plus indicates one set of diffuse s- and p-functions in the heavy atoms and the second plus

denotes the diffuse s-function for the hydrogen atom. The polarization functions are indicated after G. For example, the notation 6-311 ++ G (2df, 2dp) refers to valence orbitals divided into three parts with additional functions: diffuse sp-, two d- and one f-function for heavy atoms, and diffuse s-, two p- and one d-function for hydrogen. With only one set of polarization functions, the base can be marked with an asterisk. 6-31G * base is identical to 6-31G (d) and 6-31G ** to 6-31G (d, p).

These are not the only basis functions that can be used. Another type of basis functions is Dunning functions which do not follow the format of Pople style basis sets [163]. Dunning, or Dunning-Huzinaga functions were developed as contracted forms of primitive GTO bases [180, 181]. The notation is usually as follows (for the first-row atoms): (9s5p/4s2p). This means that 9 s-type primitive GTOs are contracted to generate 5 s-type contracted GTOs (CGTOs) and that 5 p-type primitive GTOs are contracted to make 2 separate p-type CGTOs. This is known as DZ type of basis set. Another commonly distinguished type is TZ where (10s6p) is contracted to [5s3p]. The two types of basis sets described in this chapter are often used but there are more, both Dunning type and others [182].

CHAPTER III. EXPERIMENTAL PART

3.1. Experimental and theoretical details
3.1.2. Experimental methods

Acetylacetone (99 %), trifluoroacetylacetone (98 %) and hexafluoroacetylacetone (99 %) from Sigma-Aldrich and chloromalondialdehyde (95 %) from Acros were degassed in the vacuum system by using freeze-pump-thaw cycle and used without further purification. Malondialdehyde is an unstable substance and was synthesized before measurements, according to the procedure described in [183]. Malondialdehyde sodium salt was prepared from 1,1,3,3-tetramethoxypropane (> 99 %, Sigma Aldrich) and hydrochloric acid solution (1 M). Precipitation of impure malondialdehyde sodium salt was obtained by adding acetone and leaving the mixture to stand. The mixture was later filtered and the collected solid was dried under a primary vacuum for 48 hours at room temperature. Water was filtered and distilled using EASYpure RoDi (Thermo Fisher Scientific) water purification system and degassed in the system by using the same freeze-pump-thaw cycle. Nitrogen (99.999 %), argon (99.999 %), xenon, neon and carbon monoxide gases from Elme Messer Gaas were used without additional treatment. Doubly deuterated acetylacetone was prepared using technique described in [83]. Salicylic acid (Sigma–Aldrich, 99 %) and acetylsalicylic acid (Alfa Aesar, 99 %) were used in powder form and heated in order to obtain sufficient evaporation to make a matrix sample mixture.

Several different setups were used in the experiments. In the first one (in Vilnius, Lithuania), sample and matrix gases were mixed in glass vacuum system with their ratios estimated by measuring partial gas pressures. In a typical experiment, 1 mbar of the sample molecule and 500 mbar of the matrix gas were mixed. In the experiments with acetylacetone-water complex formation, the ratios of these molecules were varied in a wide range (1 mbar of acetylacetone and 0.5 to 5 mbar of water). This was done in order to obtain spectra with different amounts (in comparison to monomers) and sizes (e.g. one water and one acetylacetone molecule, or two water and one acetylacetone molecule) of complexes. In a typical experiment approximately 20 mmol of gas mixture were deposited in 90 minutes onto a spectral window (cesium iodide) held at 10 K in a closed cycle He cryostat (Leybold-Heraeus RW2).

In more recent experiments, with salicylic acid and acetylsalicylic acid specifically, the low temperature system was upgraded. The old cryostat was replaced with the new three stage cooling system capable to cool down to 3K (JANIS SHI-4-1). The optical head and deposition system were adapted to fit existing spectrometer optics. The cryogenic system can be easily adjusted from IR spectroscopy to Raman experiments by replacing the spectral window with a mirror and moving the cryostat in a position where the Raman spectrometer source laser beam would focus on the sample. During the measurements of SA and ASA, the optimal heating system was developed to obtain spectra of these low vapor pressure molecules.

Infrared absorption spectra were recorded in the 500-4000 cm^{-1} range using Bruker IFS 113 spectrometer at 1 cm^{-1} resolution. The background spectra and the sample spectra were measured under the same conditions, measuring and averaging 256 spectra. In order to follow complex formation in the matrix sample annealing experiments were performed. The spectra were recorded at higher temperatures (up to 30 K) before the sample was cooled down back to 10 K and additional spectrum was recorded. During Raman experiments, similar procedure was performed. The mixture ratio for a typical experiment was 1:100 of analyte (in this case, trifluoroacetylacetone) molecule to matrix gas in order to obtain a better signal intensity for Raman scattering. The spectra were registered in 50-5000 cm^{-1} range with Bruker FT-Raman spectrometer at 4 cm^{-1} and 1 cm^{-1} resolution. Duration of the deposition, in this case on a mirror inside of the cryostat instead of a spectral window, was set to about 2-3 hours. The procedure was a little different for salicylic acid and acetylsalicylic acid samples and will be described below.

Two different matrix isolation experimental setups were used for IR studies in Orsay, France. The first one had sample mixed with argon or neon gases and contained in the system (sometimes for days) before deposition. The other set-up was used mainly for parahydrogen experiments since it required lower temperatures and ortho-para conversion to be performed before each experiment. In this case, mixing of the sample and matrix gas occurred simultaneously with the deposition. It included two closed cycle helium cryostats, connected by a stainless steel tube. First cryostat was used for the ortho/parahydrogen conversion process (Air Products, Displex DE202) with Fe_2O_3 powder (Sigma-Aldrich 99 %) as catalyst, and the other for the sample deposition (ICE: Innovative Cryogenic Engineering, RDK 415D, He Compressor: Sumitomo F-50). In the ortho/para- conversion

cryostat, the temperature was raised to 18 K after conversion around 15 K, and pH_2 was sent in the tube. A small reservoir containing the sample was attached to this tube. Two Swagelok micro valves allowed controlling the host gas flux (pH2) and the amount of vapor from the sample. The mixture of gases arrived directly in front of the internal diamond window (2.8 K) fixed to the cold head of the second cryostat. This cryostat was pumped by a turbomolecular pump (Oerlikon, Leybold vacuum, Turbovac 600C, pumping speed for H2: 570 l.s-1), which meant pressures below 10^{-6} mbar at 293 K were reached. The pH2 converter was pumped by a diffusion pump (CIT Alcatel). For molecules with high vapor pressure, cooling ice and salt baths could be used in order to control the evaporation.

The spectra were measured using Fourier transform infrared spectrometer (Nicolet Nixus 670/680) with a globar (heated SiC) source and a MCTA (HgCdTe – Mercury Cadmium Telluride) detector cooled by liquid nitrogen. The number of accumulated scans was usually 1024 (although sometimes shorter scans of 256 or 512 were performed), the spectral range was 500-4000 cm^{-1}, the typical resolution 0.5 cm^{-1}. Background spectra were registered before every experiment under the same conditions. The spectrometer was controlled using *Omnic 7.3* software but the analysis was mostly carried out using *OPUS*.

The molecules of salicylic and acetylsalicylic acid have low vapor pressure, so the samples have to be heated in order to obtain a matrix sample. In a set-up such as this, it is impossible to know the exact ratio of guest to host. The samples in powder form were placed in a container situated on the tube through which matrix gases enter the cryostat. During the first experiments, the container with salicylic or acetylsalicylic acid powder was heated with a resistive heating element and the temperature was controlled by the amount of voltage. Later, higher signal to noise ratio and fewer thermal dissociation products were observed in the spectra of the samples obtained when the container was heated with a stream of hot air. This set-up was constructed so that the thermocouple connected to the sample container showed temperature of 40 ºC. Matrix gas flowed through the tube at the same time, and "picked up" the sample molecules so that the mixture was deposited on the spectral window in the cryostat (or a mirror, in case of Raman spectroscopy). In infrared absorption experiments in Vilnius, argon was usually used as the matrix host and the deposition took up to an hour with the hot air stream heating method. The deposition during Raman scattering experiments took about four hours, nitrogen gas was usually used

here. A constant temperature of 17 K was maintained during the deposition in both set-ups. In addition to this, experiments with salicylic and acetylsalicylic acids were carried out in Orsay, France, mostly in parahydrogen matrices. The heating temperature was set to be about the same (40-50 ºC) in order to obtain best matrix sample and minimize the concentration of thermal dissociation products.

Photochemistry experiments were performed exclusively in Orsay, France. The ultraviolet irradiation of the samples was performed by Optical Parametric Oscillator nanosecond laser from Continuum which was pumped by the 355 nm line of a tripled Nd:Yag (neodymium-doped yttrium aluminum garnet) laser, with 10 Hz repetition rate. Irradiation times varied from 10 minutes to about 40 minutes. Usually, long irradiations at the same wavelength were carried out in steps and infrared spectra were measured in between.

3.1.2. Theoretical calculations

Density functional theory (DFT) at the B3LYP/6-311++G(3df,3dp) level was used to optimize the geometries and calculate harmonic frequencies of the analyzed molecules, their higher energy isomers and complexes with water consisting of one analyte and one water molecule. All the molecules were modeled in Gaussview 5.08 and the calculations were performed using Gaussian 09 program package [184] at the High Performance Computing Center "HPC Sauletekis" in Vilnius University Faculty of Physics. In a typical calculation *nosymm* keyword was used in order to ensure that calculation program did not enforce incorrect symmetry of the molecules. This was found to be very important in the calculations of acetylacetone, as potential minimum for the torsional rotation of CH_3 groups is very shallow. The calculated wavenumbers in tables and figures thereafter are presented without scaling factor unless otherwise indicated. Some calculations at MP2 level were performed in collaboration with Alejandro Gutiérrez-Quintanilla in ISMO, France.

3.2. Chloromalondialdehyde
3.2.1. Introduction

2-chloromalondialdehyde (chloromalondialdehyde, ClMA) is a chlorinated derivative of a malondialdehyde (MA). Like its parent molecule, it exhibits resonance assisted intramolecular hydrogen bond which stabilizes its enol form as opposed to the keto one. The chlorine atom, being both bigger and more electronegative than hydrogen, disturbs the geometry of the molecule in comparison to malondialdehyde. The intramolecular hydrogen bond strength is highly dependent on these effects and so is the proton transfer process. Most of the studies involving malondialdehyde and chloromalondialdehyde molecules, focus on exploring this process by both theoretical and, in the case of MA, experimental methods [48, 118-120].

(a)   (b)
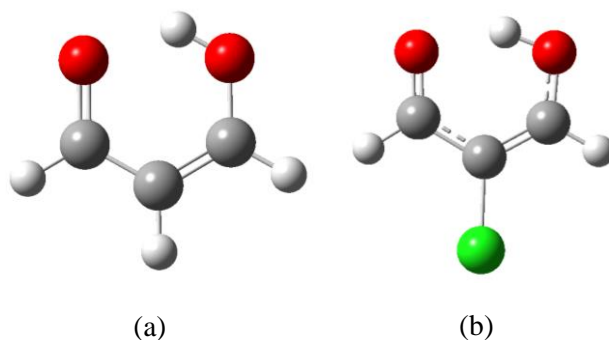
Figure 10. The most stable enol tautomers of (a) malondialdehyde and (b) 2-chloromalondialdehyde molecules.

In this work, several experiments were performed with chloromalondialdehyde molecule isolated in argon, neon and parahydrogen matrices. The obtained results offer insight into the proton tunneling process in these molecules.

Because of the changes in molecular structure, the conformational variety is also expected to change from malondialdehyde to chloromalondialdehyde and this change should be observed in the infrared absorption spectra. In order to obtain four out of eight possible open enol isomers which will be discussed later, photoisomerization experiments were performed at different wavelengths for chloromalondialdehyde molecules isolated in argon matrix.

3.2.2. Theoretical calculations

The hydrogen bond strength for both chloromalondialdehyde and its parent molecule was evaluated by theoretical and experimental parameters such as the interatomic distances in O-H…O groups, γOH vibrational mode frequency and the energy difference between CCC and CCT isomers (Table 1). The level of π electron delocalization is expressed here by the delocalization factor λ, equal to $\lambda = \frac{1-\frac{Q}{0.32}}{2}$, where $Q = d_{C-O} - d_{C=O} + d_{C-C} - d_{C=C}$.

Table 1. Theoretical and experimental parameters of ClMA and MA molecules (CCC isomers).

	dO…O, Å	dO-H, Å	λ, Å	v_{th} (C=O), cm^{-1}	v_{th} (γOH), cm^{-1}	v_{exp} (γOH), cm^{-1}	ΔE^*, kJ/mol
MA	2.570	0.999	0.26	1697.2	942.9	884.0	51.0
ClMA	2.578	0.995	0.24	1700.7	909.5	823.5	47.2

The calculations for geometrical optimization of both molecules prove that the hydrogen bond is weakened upon chlorination of the molecule. The distance between oxygen atoms is larger, and the O-H bond length is smaller for chloromalondialdehyde, meaning that the hydrogen is forming a stronger bond with one of the oxygen atoms and is farther away from the other one thus weakening the intramolecular hydrogen bond. In addition, the delocalization parameter shows lower level of π-electron delocalization which is reinforced by the fact that the C=O stretching band is shifted towards higher vibrational frequencies. The difference between isomer energies, which is not always a reliable parameter since it is influenced by other parameters apart from IHB, also confirms the weaker hydrogen bond in chloromalondialdehyde.

The reason for this weakening of hydrogen bond could be the electrostatic attraction between electronegative chlorine atom and hydrogen atoms of C-H groups. Chlorine pulls the hydrogens towards itself, thus "opening" the molecule and increasing O-H…O distance. However, it is worth mentioning that the differences between parameters of these two molecules are not very large. One other possible effect that can influence such intramolecular hydrogen bond is the steric effect. In molecules such as

chloroacetylacetone, the steric effect dominates since the bulky chlorine atom pushes the methyl groups away from itself thus increasing the internal hydrogen strength in comparison to the parent molecule, acetylacetone. In the case of malondialdehyde derivatives, however, chlorine has plenty of space and molecule does not need to be rearranged in order to fit it in.

In addition, the electronegative chlorine can have an effect on the charge distribution of the entire molecule by pulling the electron cloud towards itself. This could weaken the O-H bond and strengthen the involved oxygen atom as a donor. However, it can also weaken the other oxygen atom as an acceptor of hydrogen bond at the same time which means the overall strength of hydrogen bond would remain fairly unaffected.

3.2.3. Experimental results
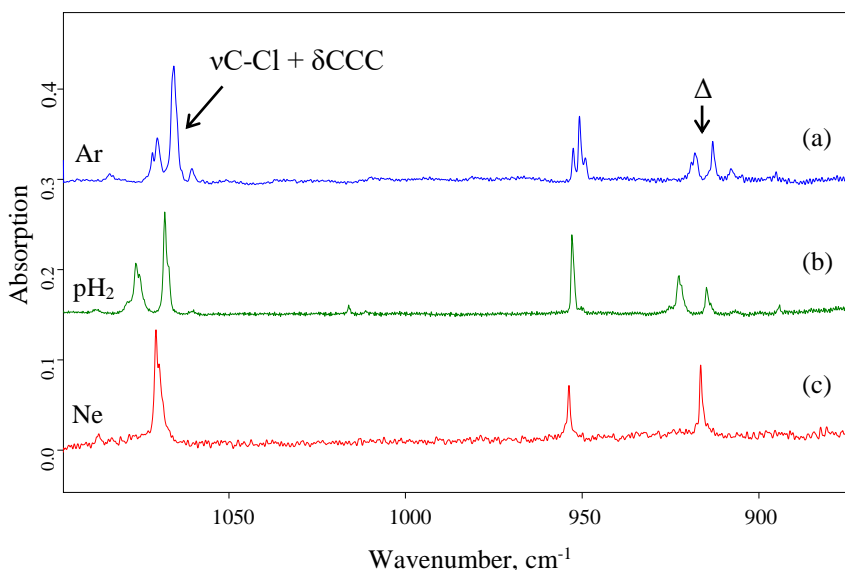
Figure 11. Infrared absorption spectra for chloromalondialdehyde molecule isolated in (a) argon, (b) parahydrogen and (c) neon matrices.

As previously stated, the chloromalondialdehyde molecule was isolated in argon, parahydrogen and neon matrices in order to explore the effect of different environments. In this section, the infrared spectra are analyzed in the context of the proton tunneling manifesting as the splitting of vibrational

levels. To that end, figure 11 shows a close up of the spectra at the 1100 – 900 cm^{-1} region where the largest splitting of the bands can be observed.

Band splitting is observed in the experimental spectra, specifically in argon and parahydrogen matrices. Before discussing the evidence for proton tunneling in more detail, other reasons for the doublet appearance should be considered. First of them could be the isotopic effect. It manifests as a doublet with small vibrational frequency difference and relative intensities that correspond to natural abundances of specific isotopes. For chlorine, it is ^{35}Cl and ^{37}Cl with respective natural abundances of 75.78 % and 24.22 %. Naturally, the mode that directly involves chlorine should be the most affected. In this case, the isolated C-Cl stretching motion is observed in a low energy part of the spectrum (predicted to be at 470.7 cm^{-1}) and thus of no importance in the infrared absorption experiments. The other isolated C-Cl modes are of even lower frequencies, all due to the relatively large mass of chlorine atom.

Apart from this one, the bands of two other modes shown in figure 11 (at 1070.6 cm^{-1}, which corresponds to combination of vibrations including stretching of C-Cl bond, and at 916.5 cm^{-1}) were more carefully analyzed. The band at 1070.6 cm^{-1} in neon matrix spectrum has a shoulder at 1069.5 cm^{-1} and the experimental difference of 1.1 cm^{-1} corresponds well with the value calculated for the two isotopes (1.2 cm^{-1}). For the 916.5 cm^{-1} band, this theoretical difference is 0.3 cm^{-1} while experimentally, the value is slightly larger – 0.6 cm^{-1}, but it can still be explained by the isotope effect. The relative intensities of these components also match the isotope abundance distribution quite well (1:0.33 experimentally, and 1:0.32 theoretically). The doublet bands in argon and parahydrogen matrix spectra have shoulders towards the lower wavenumber region that can be assigned to the ^{37}Cl isotopologue as well.

Secondly, there are always matrix effects to consider, since different gases can form a more or less perturbing environment for the sample molecule to be isolated in. One of these matrix effects means that spectral bands are often slightly shifted and the value of this wavenumber shift varies from matrix to matrix and also depends on the mode in question. For example, a "soft" matrix like parahydrogen allows large amplitude motions that can become hindered in other environments such as neon. In the spectra of chloromalondialdehyde, isolated in three different matrices, there is another obvious difference (figure 11). The spectral bands of the molecule isolated in both argon and parahydrogen matrices exhibit splitting while in neon matrix spectrum, single

bands are observed at the same wavenumbers. Some of this splitting is present only in argon and since the wavenumber difference between the peaks is very small (< 3 cm^{-1}), it could be attributed to site effects. However, site effects should not be observed for parahydrogen matrix, unless there is presence of impurities such as ortho hydrogen which was not the case there. The possible explanation of spectral structure because of Fermi resonance or combination bands for the 1070.6 cm^{-1} and 916.5 cm^{-1} modes was also discarded after anharmonic calculations were performed.

In conclusion, the best explanation for band structure in the experimental spectra is the splitting of vibrational levels (figure 11) that occurs because of proton tunneling between two stable states near oxygen atoms. Intuitively, it is easy to tell that stronger bond, and the π electron delocalization as well, means a lower potential barrier height for the proton transfer. If the partial negative charge on the C=O group oxygen increases in value, the proton tunneling becomes more likely. Specific vibrational modes also enhance the transfer possibility. Besides the isolated O-H stretching mode, the modes involving ring deformation (coupled to O-H stretching) can strengthen the probability of proton transfer.
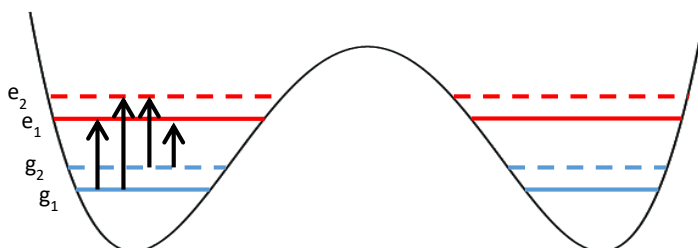

Figure 12. Simplified structure of chloromalondialdehyde energy levels.

The tunneling splitting depends on the vibrational level and vibrational mode since other modes coupled to OH vibrations can enhance or hinder the proton transfer. In acetylacetone, for example, the transfer is coupled to methyl group rotations. In the case of chloromalondialdehyde, the in plane deformations of the molecule are the most important. The tunneling splitting can be further increased or reduced by the matrix environment. In this case, argon exhibits lower values since it is a more perturbing matrix than parahydrogen. Neon does not exhibit tunneling splitting at all, likely because of the geometry of the molecule trapping sites. The proton transfer is very

sensitive to even the slightest interactions between the host and the guest molecules so it is important how much space the molecule has around it in the matrix and what intermolecular forces could change its structure and break the symmetry. In addition, experiments in argon are performed in different conditions than those in parahydrogen which require temperatures no higher than 3 K. Argon samples were deposited in a large range of temperatures, from 7 K to 17 K, in order to bring out the tunneling splitting effects in the infrared absorption spectra.

In figure 11, the band at 1070.6 cm^{-1} in neon corresponds to a combination of νC-Cl, ring in-plane and CH deformation modes. The 916 cm^{-1} band is assigned to ring and OH in-plane deformation vibrations. These in plane ring deformations are symmetric with respect to the transition state (the C_{2V} state of the molecule where hydrogen is directly in the middle between two oxygen atoms, or, in the energy level diagram – the maximum between two symmetric wells). According to [94], symmetric modes coupled to proton transfer tend to increase the tunneling splitting.

In argon and parahydrogen spectra, both of the mentioned bands are observed as doublets split by approximately $\Delta\nu_{Ar} = 5 \text{ cm}^{-1}$ and $\Delta\nu_{pH2} = 8 \text{ cm}^{-1}$. In the case of proton tunneling, both ground and excited vibrational states should be split into two thus making four different transitions available (figure 12). However, unless the difference between split ground levels is low enough for both of them to be populated, transitions from only lowest energy ground level will be observed. As mentioned previously, the calculated tunneling splitting for chloromalondialdehyde is 12 cm^{-1} [120]. This difference would correspond to approximately 8 % of population of the higher energy level at 7 K (argon sample deposition temperature) and only 0.3 % at 3 K (parahydrogen sample deposition temperature). In any case, the g_1-e_1 and g_1-e_2 transitions should definitely be present in both matrices in case of the tunneling splitting, and the difference between bands of these two transitions should be the same as for the g_2-e_1 and g_2-e_2. In case of the argon matrix and the higher energy mode out of the two that are discussed here, the band at 1066 cm^{-1} corresponds to g_1-e_1 and the one at 1070 cm^{-1} to g_1-e_2 transition. Similarly, the bands at 913 cm^{-1} and 918 cm^{-1} correspond to these respective transitions for the lower energy mode. If the 5 cm^{-1} value is taken as excited level splitting value, the Boltzmann distribution gives 27 % population of higher energy level e_2. There are other bands around these regions in argon matrix spectra but they cannot be assigned to transitions from g_2. Even if these can be observed which is likely given the higher temperature, the intensity of

the bands should still be lower and they likely overlap with more intense bands. This overlap would present as band structure which can also be isotopic in nature or, in the case of argon, due to site effects.

Annealing experiments were performed on the sample isolated in argon matrix. Ideally, such change in conditions would result in the relative intensity changes for the bands assigned to different transitions between split ground and tunneling levels. However, the spectra registered after temperature increase yielded bands that were too broad for their intensities to be properly evaluated.
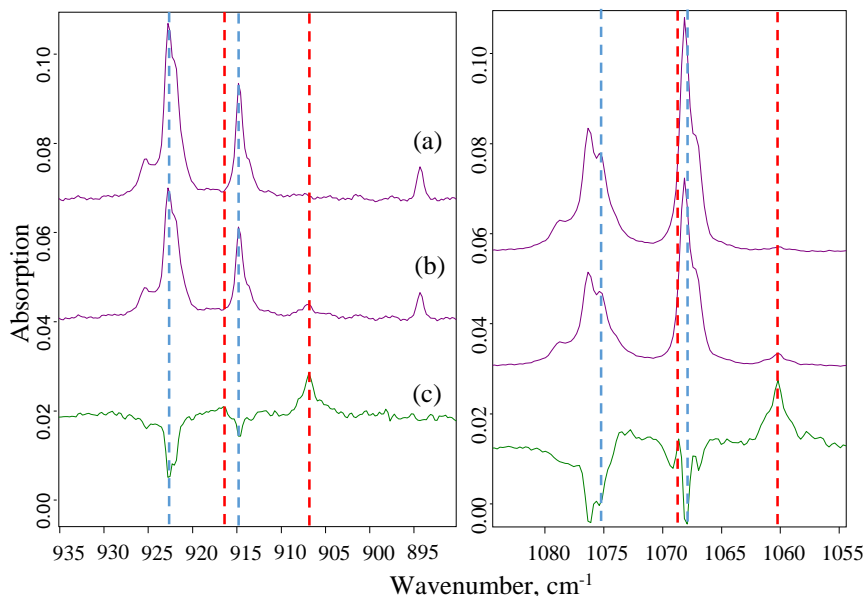
Figure 13. Infrared absorption spectra of chloromalondialdehyde isolated in parahydrogen at (a) 3 K, (b) 5 K, (c) the difference spectra between (a) and (b).

In contrast, the annealing experiments in parahydrogen matrix allowed a better assignment of vibrational transitions. In figure 13, the spectra of chloromalondialdehyde isolated in parahydrogen at different temperatures of 3 K and 5 K, and the difference spectra between these two are shown. As temperature is increased, the population of higher ground level grows as well. With the average level difference of 8 cm^{-1} in parahydrogen spectra, the population of g_2 would be 2 % at 3 K, and 9 % at 5 K. The difference spectra show the changes best and confirm that the band at 1068 cm^{-1} corresponds to g_1-e_1 and the one at 1076 cm^{-1} to g_1-e_2 transition (with a slight shift in

comparison to argon). The bands at 915 cm^{-1} and 923 cm^{-1} correspond to these respective transitions for the lower energy mode.
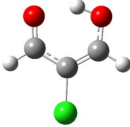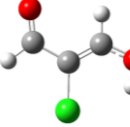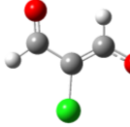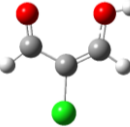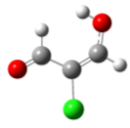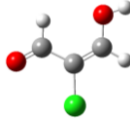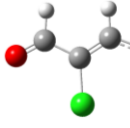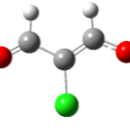
The bands at 907 cm^{-1} and 1060 cm^{-1} show greater increase for two respective modes and can be assigned to g_2-e_1 transition. Since the 8 cm^{-1} difference is calculated from first set of bands, it can be used here to confirm the position of the g_2-e_2 bands. In fact, there is slight intensity increase at 916 cm^{-1} and 1068 cm^{-1} wavenumbers and the respective differences correspond to 8 cm^{-1} value quite well. So it can be concluded that the vibrational splitting of ground and excited levels of chloromalondialdehyde molecule due to proton tunneling and the transitions between these levels can be observed in parahydrogen matrix.

3.2.4. Photoisomerisation experiments

The enolic chloromalondialdehyde molecule has eight isomers, the most stable of which is CCC. The other isomers are obtained by the rotation of around C-C, C=C and C-O bonds, their calculated parameters are summarized in table 2. Most of the isomers are of much higher energy (around 30 kJ/mol and higher) and so will not be observable in experimental spectra. The isomers CTC and TTC are of slightly lower energy because their geometry allows for electrostatic attraction between electronegative chlorine and hydrogen of OH group. That also results in the slight increase of the O-H distance for these two isomers (0.97 Å in comparison to 0.96 Å for other open enol isomers).

The energy difference between lowest energy isomer CCC and CTC is calculated to be 14.4 kJ/mol which corresponds to 0.3 % of CTC in room temperature. The respective difference between CCC and TTC is 10.1 kJ/mol and which corresponds to 1.6 % of TTC in room temperature. That means there is possibility to observe TTC isomer in the deposited samples without performing photoisomerization experiments.

Table 2. Open enol isomers of chloromalondialdehyde and their parameters.

	CCC	CTC	CTT	CCT
ΔE, kJ/mol	0	14.4	27.2	47.1
population, %	98	0.3	≪ 0.01	≪ 0.01
dO-H, Å	1.00	0.97	0.96	0.96
	TCC	TCT	TTC	TTT
ΔE	41.0	39.5	10.1	27.3
population, %	≪ 0.01	≪ 0.01	1.6	≪ 0.01
dO-H, Å	0.96	0.96	0.97	0.96

As was mentioned before, the intramolecular hydrogen bond in the lowest energy isomer CCC means the O-H stretching bands are extremely broad and virtually unobservable in experimental spectra. The 4000-3000 cm^{-1} region becomes more relevant in the photoisomerization experiments since the appearance of OH stretching bands indicates the breaking of the intramolecular hydrogen bond and the presence of open enol isomers. This region is also useful for gauging the amount of water in the sample. Water can form intermolecular hydrogen bonds with the analyte molecules and thus influence molecular structure, intramolecular hydrogen bond strength and other properties. In the experimental spectra, band shifts and new bands might be observed because of this water-sample molecule complex formation. However, in the case of the chloromalondialdehyde samples, the water content

was rather low as can be seen in subsequent figures both in the OH stretching region and from the 1650 cm^{-1} band which belongs to the deformational vibration of the H_2O molecule.

In order to find the specific irradation wavelength to induce the desired isomer transformation, UV absorption spectra of chloromalondialdehyde sample were measured first. They were recorded using a deuterium lamp as the light source and a 0.6 m Jobin Yvon grating monochromator coupled to a CCD camera (Andor DH720) as a detector. The deposition window of the setup was changed from CsI (for IR) to sapphire for the measurement of UV absorption. UV irradiations of the samples were performed with a tunable pulsed laser (Continuum Surelite II + OPO (Optical Parametric Oscillator) Horizon system, repetition rate: 10 Hz, pulsewidth: 4 ns), operating in the 200–300 nm range. The energy per pulse did not exceed 1 mJ on the sample.
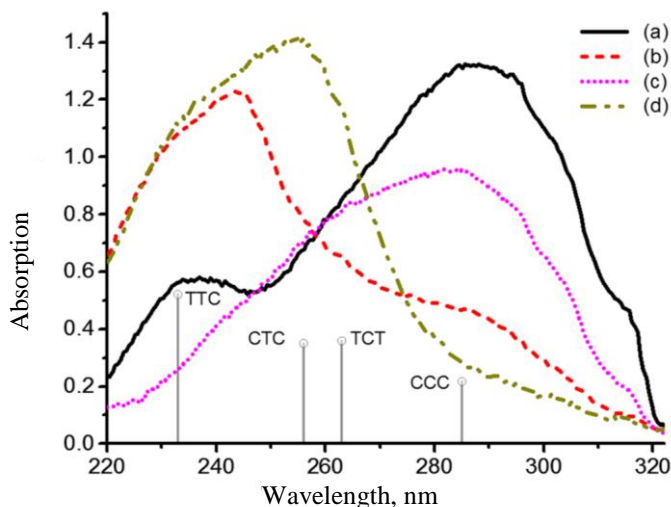

Figure 14. UV spectra of ClMA in Ne: (a) as-deposited sample, (b) after 15 min of irradiation at 290 nm + 15 min of irradiation at 260 nm, (c) after additional 15 min of irradiation at 235 nm, and (d) after additional 15 min of irradiation at 300 nm. The vertical lines are placed at the calculated S2 ← S0 vertical transition wavelengths of the specified conformers.

The UV absorption spectra were measured with chloromalondialdehyde molecule isolated in neon matrix. The shift between different matrices should be small, with an expected slight blue shift from the argon matrix to the neon matrix. In figure 14, the spectrum recorded after deposition (a) is compared to the spectra obtained after irradiating the sample with various wavelengths (in

UV region). Two main bands can be seen in the UV absorption spectrum of the as-deposited sample. The one at around 285 nm, with higher intensity, is assigned to the π–π ∗ transition in the CCC form. The second band at around 235 nm corresponds to another isomer which exists in smaller quantity in the as-deposited along with CCC. This isomer, as will be discussed later in the part of IR absorption spectra analysis, is very likely to be TTC. The effect of UV irradiation on the conformer formation was explored with the OPO laser tuned at various wavelengths in the 230–300 nm spectral range. The irradation wavelength was changed in order to optimize the production of specific isomers. The UV absorption spectra were measured between several of these irradiations, and examples of such spectra are shown in figure 14. It is clear that after some sequences of laser irradiation, the absorption profile exhibits a strong absorption between the two bands assigned to CCC and TTC (see figure 14(d)) which proves that other open enol conformers are being produced in the matrix.

Infrared absorption spectra, measured in between UV irradiation and UV absorption spectra measurement, indicated that the UV broadband source slightly advances the interconversion between isomers during the acquisition of the UV spectrum. Consequently, there are some, albeit slight, errors while determining the composition of the samples. Figure 14 shows a specific sequence of irradiation with the production of samples with mainly TTC (14b) and CCC (14c). An additional irradiation in the 290–300 nm range depletes the CCC form, but the IR spectrum shows a combination of CTC and TTC with a small amount of TCT (figure 14(d)). So the maxima of absorption in Ne for a mixture of CTC and TCT is around 255 nm.

In infrared absorption experiments, the as-deposited spectra of chloromalondialdehyde was analyzed first of all (figure 15). UV absorption experiment results and theoretical results predict the presence of at least two isomers in the deposited sample.
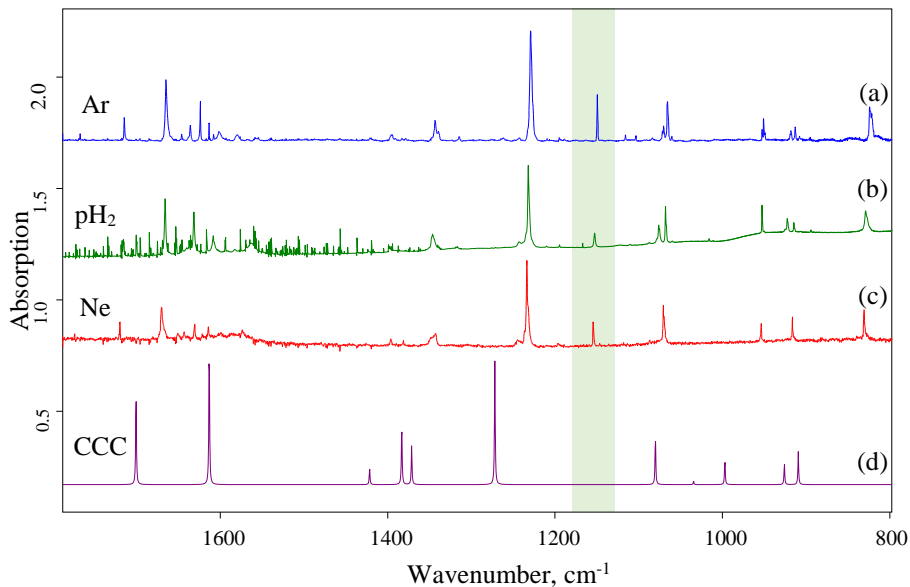
Figure 15. Infrared absorption spectra for chloromalondialdehyde molecule isolated in (a) argon, (b) parahydrogen, (c) neon matrices, (d) calculated spectrum of ClMA isomer CCC. The most intense TTC band is highlighted by a green strip.

The CCC isomer, being most stable one due to IHB, should correspond to around 98 percent of the sample in the room temperature according to Boltzmann distribution. When performing matrix isolation experiments in low temperatures, it is possible to "freeze" the room-temperature isomer distribution if the potential barrier heights for isomer interconversion are high enough. If the opposite is true, the higher energy isomers quickly convert into the most stable one. In the experimental spectra of ClMA isolated in each matrix, the bands can be mostly assigned to the vibrational modes of CCC isomer and thus it can be concluded that this isomer is definitely the most abundant one in the as-deposited matrix samples. There are, however, several additional lower intensity bands, observable in all the experimental spectra.

The most intense one is around 1150 cm^{-1} (exact position depends on the matrix). It fits well with the calculated band of TTC isomer (1160 cm^{-1}), assigned to stretching vibrations of C-C and deformational vibrations of OH and CH groups. The intensity looks fairly high in the comparison with all the CCC bands but calculations predict this band to be one of the most intense bands for TTC. The experimental band is also quite narrow, and when integration was performed for bands in neon matrix spectrum (1050 cm^{-1} for

65

TTC and 1070 cm^{-1} for CCC) the obtained TTC to CCC ratio was 0.03 to 1. This value was calculated according to the band intensities predicted by theoretical methods, and is only slightly higher than the predicted TTC concentration of 1.6 %.

The other open enol isomers were obtained by irradiating the sample. The irradiation was started off at $\lambda_1 = 290$ nm wavelength, followed by $\lambda_2 = 270$ nm, $\lambda_3 = 235$ nm and $\lambda_4 = 300$ nm irradiations. The irradiation at longer wavelengths (λ_1) decreased intensity of CCC bands and produced new bands of first group of isomers. The comparison with theoretical spectra confirms the presence of CTC and a smaller amount of another isomer (figure 16). The irradiation at 270 nm wavelength began diminishing the amount of CTC and growing the second group of isomers.
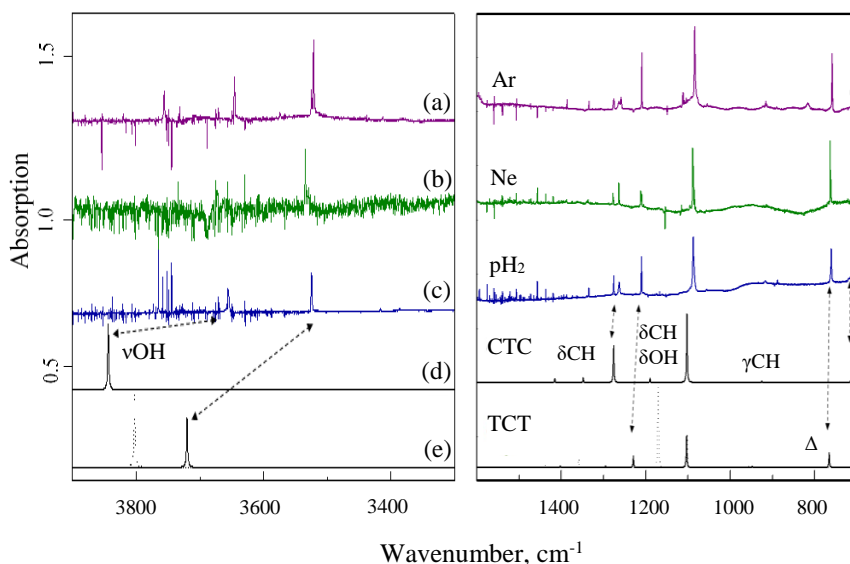

Figure 16. Infrared absorption spectra of first isomer group of 2-chloromalondialdehyde in (a) argon, (b) neon and (c) parahydrogen matrices; obtained by subtracting CCC and the second isomer group spectra. Theoretical calculation of (d) CTC, (e) TCC (full line) and TCT (dotted line) isomers with 0.98 scaling factor, Δ – in plane deformation of the molecule.

Theoretical calculations proved that TTC was the sole isomer of the second group. Finally, the irradiation at the shortest wavelength started converting TTC isomer back to CCC. Lower wavelength (higher energy) irradiation evaporated some of the sample and at the same time initiated CO

fragmentation, seen as new bands appearing at 2140 cm^{-1} – 2040 cm^{-1}. The sample was also irradiated at the wavelength of 300 nm which again began converting CCC to the first group of isomers.

Figure 16 shows OH stretching region of the first group of isomers. The spectrum in neon matrix only shows one band of low intensity. In contrast, argon and especially parahydrogen have several structured bands. The shift between bands in theoretically calculated spectra seems to favor TCC as the second isomer but in any case, the match between theoretical and experimental spectra is not perfect here. Thus it is not yet possible to conclude which isomer is observed together with CTC, although calculations show that for chloromalondialdehyde, the TCC and TCT isomers have inverted energy positions in comparison to malondialdehyde.

The second part of the spectra shown in figure 16 (1600 cm^{-1} – 700 cm^{-1} region) clearly indicates the presence of two isomers and is more convenient for comparison with theoretical spectra. The band with maximum intensity, corresponding to the in plane ring deformation (at 1100 cm^{-1}) has identical positions for both CTC and TCT isomers. However, the bands at 1210 cm^{-1} and 1270 cm^{-1} (corresponding to in plane bending of CH mode) can be each assigned to a different isomer after comparison to the theoretical spectra. Similar comparison can be made in the region of 800 cm^{-1} – 700 cm^{-1} where the bands are assigned to in plane deformation of the whole molecule (table AI-2).
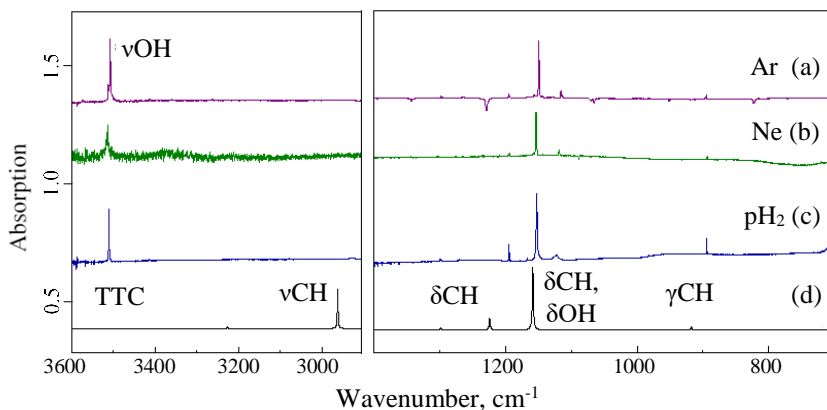

Figure 17. Infrared absorption spectra of second isomer group of 2-chloromalondialdehyde in (a) argon, (b) neon and (c) parahydrogen matrices; obtained by subtracting CCC and the first isomer group spectra. (d) Theoretical calculation of TTC isomer with 0.98 scaling factor.

3.2.5. Summary and comparison to malondialdehyde

Matrix isolation studies offer insight into proton tunneling process and the conformational variety of chloromalondialdehyde molecule. In comparison to its parent molecule, malondialdehyde, chloromalondialdehyde has a weaker intramolecular hydrogen bond. The reason for that is the replacement of alpha position hydrogen by electronegative chlorine atom which pulls hydrogen atoms of CH groups towards itself, effectively opening the molecule. Despite this effect, the hydrogen bond is strong enough for proton tunneling to be observed in the molecule via the splitting of vibrational levels. Band structure was observed in the infrared absorption spectra of the molecule isolated in argon and parahydrogen matrices, unexplainable by site and isotopic effects. The doublets are separated by 5 cm^{-1} in argon and 8 cm^{-1} in parahydrogen, which corresponds quite well to the theoretically calculated value of 12 cm^{-1}. The smaller value of splitting in argon is due to the fact that it is a more perturbing matrix while parahydrogen is soft and allows large amplitude motions of the guest molecule. Both of the split ground-state levels are populated in both argon and parahydrogen matrices. Annealing experiments performed in the latter matrix allowed identification of the bands that belong to the transitions between both of the split ground-state levels to both of the excited-state levels. In argon, however, there are a couple more bands whose presence is attributed to site effects, as well as band broadening due to increased temperatures during the annealing experiments. For these reason, all the transition bands in argon could not be clearly identified.

It is useful to compare the proton tunneling splitting in chloromalondialdehyde to its parent molecule, malondialdehyde. There are many theoretical studies performed to evaluate the proton tunneling parameters in MA, and it has been experimentally observed in studies employing supersonic jet. According to these studies, the value of the ground state splitting for MA is around 22 cm^{-1}. No vibrational splitting was observed in malondialdehyde isolated in xenon, neon, argon and nitrogen matrices. The matrix environment, as previously mentioned, can influence and even stop the proton transfer. The sites in which the molecules are isolated may stabilize the molecular structure where hydrogen is in the position near one of the oxygen atoms. So essentially, the molecule-host interaction changes the energy surface so that the symmetric double well potential becomes asymmetric. There is also a possibility that the matrix environment interferes with the proton transfer due to dynamic friction along the proton tunneling coordinate.

The latter reason is usually given to explain the absence of proton tunneling effects in the spectra of malondialdehyde isolated in low temperature matrices.

The conformational variety of chloromalondialdehyde molecule was explored by theoretical and experimental methods. The most stable isomer CCC is confirmed to be the most abundant at the room temperature. However, calculations predict that one of the open enol isomers, TTC, should exist in observable quantities because of its relatively low energy (11 kJ/mol higher than CCC). The reason why this isomer is so stable compared to the rest is the attraction between electronegative chlorine and OH group hydrogen.

The spectra registered immediately after sample deposition contain more bands than could be attributed to one isomer. Based mostly on the OH stretching region where CCC does not have any spectral bands, the other deposition isomer is identified as TTC. The presence of the other relatively stable isomer CTC can also be confirmed in this region. According to the intensities of experimental bands, there is a little more than 3 % of TTC in neon matrix. Chloromalondialdehyde is the first member of the β-aldehyde and β-diketone families which has stable open enol isomers at the room temperature.

Other open enol isomers were obtained by the irradiation process. The summary of the isomer bands evolution is depicted in figure 18. First of all, the infrared spectrum was registered immediately after deposition and CCC isomer was observed along with traces of second isomer group (TTC isomer). The first step of irradiation was at $\lambda_1 = 290$ nm wavelength (point 2 in figure 18). This produced the first group of isomers, containing CTC and TCT. In addition to this, rapid decline of CCC and slower growth of TTC was also observed. For the $\lambda_2 = 270$ nm (point 3 in figure 18) irradiation started diminishing the amount of the first group of isomers, resulting in rapid production of TTC and some conversion back to CCC. The $\lambda_4 = 235$ nm irradiation prompted the conversion of the second isomer group back to CCC. An increase in first group of isomers was also observed.
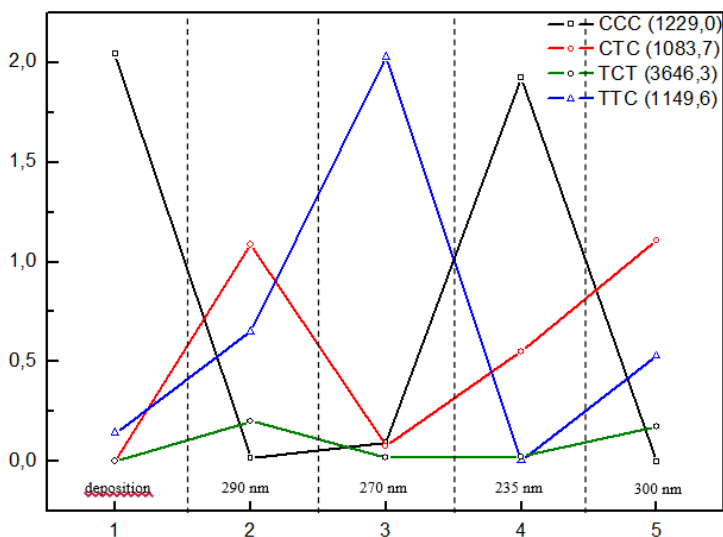
Figure 18. The spectral band intensity evolution during irradiation process:
(1) deposition, after (2) 290 nm irradiation, (3) after 270 nm irradiation, (4)
after 235 nm irradiation and (5) after 300 nm irradiation.

So it can be concluded that even if eight enol isomers are predicted by theoretical, only four of them can be observed in the experimental spectra, includidng CCC. These isomers correspond to the most stable form in each XYT-XYC pair. Within these pairs, isomers differ only by the position of the OH group so it is likely that the less stable forms disappear because of a tunneling process through the OH rotational barrier. In comparison to malondialdehyde, the irradiation with ultraviolet laser produced two groups of isomers for both molecules. The first group contained CTC isomer in both cases but the additional isomer was different. Theory predicted an inversion of energy positions for TCC and TCT isomers from malondialdehyde to chloromalondialdehyde. The calculated energy gap was very small and could be easily disregarded taking into account error margins. However, experimental spectra seem to confirm that TCC isomer is observed for malondialdehyde and TCT is observed for chloromalondialdehyde along with CTC in the first group of isomers.

3.3. Acetylacetone derivatives
3.3.1. Introduction

Acetylacetone is a β-diketone class molecule with a chemical formula $CH_3COCH_2COCH_3$. It is dimethyl derivative of malondialdehyde (figure 19, R1=R2=CH_3) and just like its parent molecule, it has an intramolecular hydrogen bond that stabilizes its enol form and exhibits π electron delocalization. Some of the molecules analyzed here were fairly symmetric (with identical -R groups) – acetylacetone, deuterated acetylacetone, hexafluoroacetylacetone. However, the intramolecular hydrogen bond strength and therefore the structure differed depending on specific molecule. In comparison to malondialdehyde, the intramolecular hydrogen bond strength is also different, and the proton tunneling has a lower potential barrier since the tunneling process is coupled to methyl group rotations.
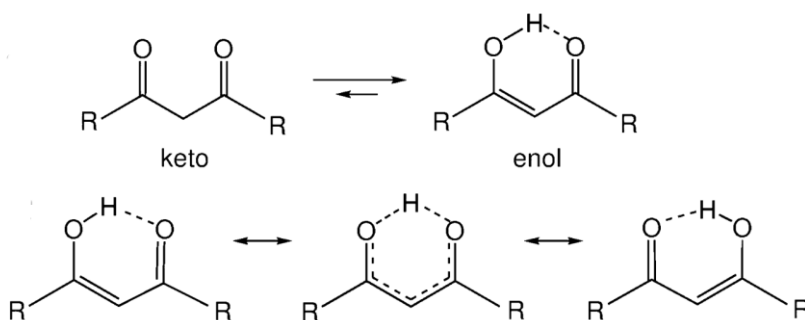

Figure 19. β-diketone structure (a) keto-enol conversion, (b) enol to enol interconversion with the middle state of C_{2v} symmetry [187].

Acetylacetone molecule has been well analyzed before by both theoretical and experimental methods. The symmetry of the molecule is one of the interesting questions [185-187], along with the hydrogen bond strength [52] and proton transfer [60, 120, 188, 189], π electron delocalization [190, 191] conformational variety [56, 79, 121, 192, 193] and keto-enol equilibrium in different environments [56, 103, 194]. In this work, more attention was paid to acetylacetone derivatives, especially those with clearly asymmetric structure, as well as the conformational variety and associates with water.

The results of the experiments and calculations of acetylacetone molecule were mainly used as a benchmark for the analysis of its derivatives.

In total, five acetylacetone derivatives were explored, formed by deuteration and halogenation of acetylacetone molecule (figure 20). The molecules presented in figure 20 are the most stable structures – some of their open enol isomers can be produced by photoisomerization using laser irradiation. In addition to this, there are a few molecules with an asymmetric structure and an asymmetric double well potential. They have two different closed enol conformations which both exhibit same intramolecular hydrogen bond but are still different in energy. They will be denoted as (CO) or (OH) depending on which side of the molecule the replacement group is (both are depicted in figure 20).

In general, the structural modifications of acetylacetone can be sorted into two different categories: changes made to OH and olefinic hydrogen atoms and modifications of the methyl group or groups. While other molecules are used as model systems to observe how structural changes of other atomic groups in the molecule can influence intramolecular hydrogen bond strength, in the deuterated acetylacetone molecule the O…H-O bond is directly replaced by O…D-O bond. The most significant change this substitution brings is to the vibrational frequencies of OD (compared to OH of acetylacetone) bond and, subsequently, to the zero-point energy of the molecule.
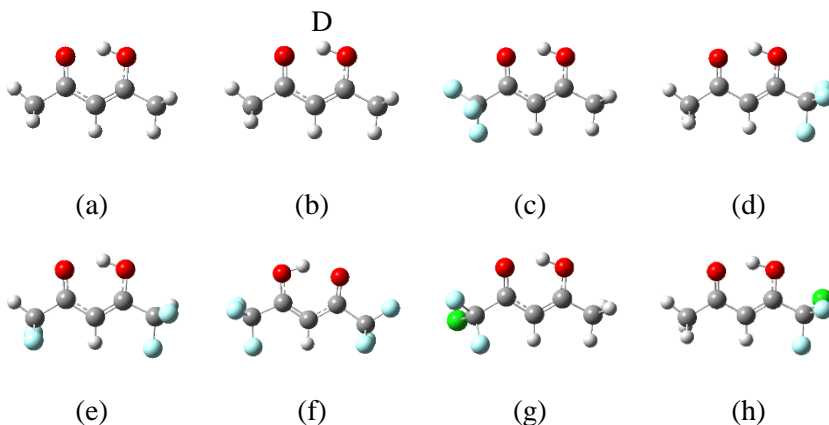

Figure 20. Acetylacetone derivatives analyzed in this work: (a) acetylacetone AcAc, (b) deuterated acetylacetone dAcAc, (c) trifluoroacetylacetone AcAcF3(CO), (d) trifluoroacetylacetone AcAcF3(OH), (e) tetrafluoroacetylacetone AcAcF4, (f) hexafluoroacetylacetone AcAcF6, (g) chlorodifluoroacetylacetone AcAcF2Cl(CO), (h) chlorodifluoroacetylacetone AcAcF2Cl(OH).

The second group consists of fluorinated acetylacetone derivatives. The molecules studied were hexafluoroacetylacetone (AcAcF6) where all the hydrogen atoms from methyl groups were replaced by fluorine atoms, trifluoroacetylacetone (AcAcF3) and chlorodifluoroacetylacetone (AcAcF2Cl) molecules with asymmetric structure and two coexisting isomers, and tetrafluoroacetylacetone (AcAcF4) where two hydrogens from each methyl group were exchanged by fluorine atoms. Trifluoroacetylacetone was most thoroughly analyzed out of all of these molecules, determining the effect of the matrix environment and the presence of water on the distribution of two lowest energy isomers. The results for trifluoroacetylacetone molecule here are mostly compared with the parent acetylacetone and the symmetric hexafluoroacetylacetone molecule.

The influence of hydrogen-replacing halogen atoms can be described through steric and electrostatic effects. The former arises from the atomic bulk and is important in determining the structure and reactivity of molecules. Since the chlorine atom is bigger than fluorine, and they both are much larger than a hydrogen atom, the molecule structure has to be rearranged to fit them in. In addition, the electrostatic forces come into play as the halogens have higher electronegativity than hydrogen atom (4.0 for fluorine, 3.0 for chlorine, 2.2 for hydrogen).

In this work, the intramolecular hydrogen bond strength for different molecules was evaluated by methods mentioned previously: theoretically calculated geometrical and vibrational frequency values, as well as experimentally observed OH bond related vibrational bands. Other geometric parameters of the optimized structures were important in determining the level of π electron delocalization. The positions of C=C stretching vibration band in experimental spectra can also confirm these findings. After evaluating intramolecular hydrogen bond strength, the intermolecular hydrogen bond formed between acetylacetone derivatives and water molecules was explored for all the molecules. In this case, the stretching OH region was of most interest since the position of bound OH group in water molecule exhibits clear increasing shift with increasing bond strength.

The influence of this intermolecular bond on molecular structure was analyzed – mostly by comparing the changes of IHB evaluation parameters that were mentioned above. The case of trifluoroacetylacetone was explored in more depth, both in regards to the interplay between hydrogen bond strength and π electron delocalization, and to the influence of water and matrix

environment on the molecular structure. Finally, the stabilization of certain open enol isomers was investigated by photoisomerization using laser irradiation and calculations of isomer structures, energies and spectra in order to better understand the experimental results.

The above mentioned acetylacetone derivative molecules were analyzed experimentally by using low temperature infrared absorption spectroscopy. Additionally, Raman scattering spectra were also measured for some molecules. All the molecules were isolated in argon matrix, most of them in nitrogen as well. In most cases, experiments were repeated for different concentrations of the sample, or different ratios of acetylacetone molecule to water. For some of the molecules, like tetrafluoroacetylacetone, the higher limit for number of experiments was unfortunately determined by amount of the sample available. The optimized geometries and vibrational spectra were calculated for all the molecules using DFT B3LYP with 6-311++G(3df,3pd) basis sets.

3.3.2. Theoretical calculations

The parameters for intramolecular hydrogen bond strength evaluation are presented in table 3. Deuteration of the molecule does not change the molecular geometry, since the charge and size remain the same. However, the mass increase from hydrogen to deuterium significantly affects all the vibrational modes involving H/D atom. Mode frequencies add up to modify the zero-point vibrational energy which, in turn, determines the strength of the hydrogen bond. This specific change means that the comparison between deuterated-parent molecules is of interest for the analysis of intramolecular hydrogen bond. However, both theoretical and experimental investigations have been conducted on deuterated acetylacetone derivatives before. In this work, the main focus is on acetylacetone-water associate formation in cryogenic matrices, the strength of intermolecular hydrogen bond and its influence on the internal structure of the molecules.

Table 3. Properties of acetylacetone and its derivatives. γOH – out-of-plane vibrational OH mode, Q – coordinate of π bond delocalization ($Q = d_{C-O} - d_{C=O} + d_{C-C} - d_{C=C}$). Experimental data taken from IR absorption spectra of molecules isolated in argon matrix. All γOH bands are broadened.

	AcAc	dAcAc	AcAcF3 (CO)	AcAcF3 (OH)
γOH, cm^{-1} (calc)	1010.0	750.9	961.7	972.3
γOH, cm^{-1} (exp)	996.3 (broad)	718.6	998-934	898
νC=C, cm^{-1} (calc)	1676.9	1663.2	1689.7	1700.7
νC=C, cm^{-1} (exp)	1637.5	1632.4	1646.5	1658.1
dO…H(D), Å	1.614	1.614	1.663	1.628
Q, Å	0.151	0.151	0.135	0.175
λ, Å	0.26	0.26	0.29	0.23
ΔE$_{(CCT-CCC)}$, kJ/mol	63.2	63.1	51.7	53. 3
	AcAcF4	AcAcF6	AcAcF2Cl (CO)	AcAcF2Cl (OH)
γOH, cm^{-1} (calc)	912.0	884.2	941.5	954.6
γOH, cm^{-1} (exp)	932.0	819.5	900-875	882.2
νC=C, cm^{-1} (calc)	1704.0	1723.3	1688.2	1695.2
νC=C, cm^{-1} (exp)	-	1696.0	1648.3	1658.2
dO…H, Å	1.684	1.703	1.667	1.620
Q	0.161	0.168	0.139	0.171
λ	0.25	0.24	0.28	0.23
ΔE$_{(CCT-CCC)}$, kJ/mol	44.6	41.4	52.5	55.9

Considering only hydrogenated molecules, the hydrogen bond is strongest for derivatives with a bulkier atoms or groups in alpha position and weaker for the ones with electronegative atoms replacing hydrogens in methyl groups. The overall trend (according to geometrical parameters) is as follows: AcAcCH3 > AcAcCl > AcAc > AcAcF3(OH) > AcAcF3(CO) >

AcAcF2Cl(OH) > AcAcF2Cl(CO) > AcAcF4 > AcAcF6. The only discrepancy with the open-closed isomer energy difference is the order of AcAcF3 and AcAcF2Cl isomers which asks for further theoretical and experimental investigation. The AcAcCH3 and AcAcCl are molecules that have not been analyzed in depth here but they are shown in overall hydrogen bond strength tendency in order to explore what molecular modifications can actually increase it.

This overall tendency can be explained by steric effects dominating in AcAcCl where the chlorine atom in alpha position "pushes" the methyl groups away due to its size therefore reducing O…O and O…H distances and strengthening the bond. The same effect was visible in deuterated molecule (in comparison to simple deuterated acetylacetone), but not in chloromalondialdehyde when comparing it to the parent malondialdehyde molecule. The same effect is significant for AcAcCH3 molecule since CH_3 group is substantially bulkier than any single atom.

On the other side of acetylacetone, fluorinated molecules exhibit the tendency to weaken hydrogen bond with the number of added fluorine atoms. They, and chlorine atom in AcAcF2Cl as well, are always in methyl group position so the steric effect is not a major influence in these molecules. The electronegative fluorine and chlorine atoms do, however, significantly change the charge distribution. Because of electrostatic forces, their pull on the electron cloud decreases partial negative charge on one or both oxygen atoms. Depending on the positions of fluorine atoms, this decrease can change in magnitude. The electrostatic effect explains why the intramolecular hydrogen bond strength decreases with each added fluorine atom and why the bond is stronger in (OH) rather than (CO) isomers of the asymmetric molecules AcAcF3 and AcAcF2Cl. As long as the CF_3 (or CF_2Cl) group is on the same side as the proton, the electrostatic effect is stronger for OH group. The partial negative charge decreases for both oxygen atoms upon fluorination but the relatively greater influence for the OH group oxygen weakens its hold on the proton and therefore the covalent OH bond, strengthening the intramolecular hydrogen O…H bond at the same time.

The calculated geometries predict symmetric positions of CH_3 groups while in all the fluorinated derivatives, these groups are in relatively rotated positions. The internal rotations of these groups (CH_3, as well as CF_3 and CF_2Cl) are also important since they couple with the OH vibration and can influence proton transfer.
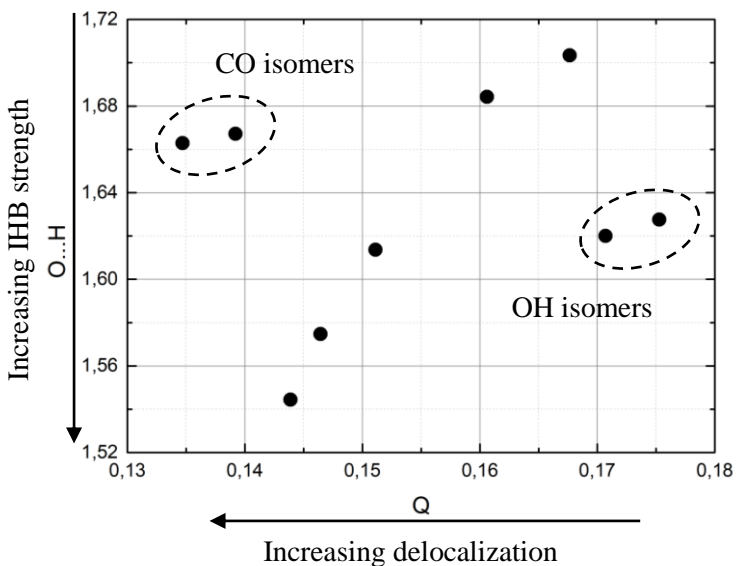
Figure 21. Comparison between intramolecular hydrogen bond strength and
π electron delocalization using O…H distance and Q as the parameters.
O…H and Q values are in Angstroms.

Another part worthy of deeper investigation is the interplay between hydrogen bond strength and π electron delocalization in these asymmetric molecules. According to the definition of resonance assisted hydrogen bond, π electron delocalization should strengthen the hydrogen bond by making the partial charge on the proton donor more positive and the one on the acceptor – more negative. The relationship between hydrogen bond strength, expressed as O…H interatomic distances, and π electron delocalization, expressed as coordinate of π bond delocalization Q, is depicted in figure 21. For most molecules, this relationship is directly proportional – the stronger the π electron delocalization, the stronger the intramolecular hydrogen bond. That can be seen in the figure in the central part of the graph with the dots representing (in order from lowest) AcAcCH3, AcAcCl, AcAc, AcAcF4 and AcAcF6. The isomers of the two assymetric molecules, AcAcF3 and AcAcF2Cl, do not follow the same trend as the other acetylacetone derivatives.

As discussed above, the intramolecular hydrogen bond is stronger in AcAcF3(OH) isomer, but the AcAcF3(CO) is more stable and abundant. In fact, calculated energy of AcAcF3(CO) is lower by 4.3 kJ/mol than that of AcAcF3(OH) which, according to Boltzmann distribution, would correspond

to a room temperature mixture of 85 % AcAcF3(CO) and 15 % AcAcF3(OH). For the AcAcF2Cl molecule, the energy difference was calculated to be 6.3 kJ/mol, and so the percentages in room temperature mixture are 93 % and 7 % for (CO) and (OH) isomers, respectively.

Usually the intramolecular hydrogen bond stabilizes the molecule. However, (CO) isomer shows all the signs of higher level of π electron delocalization. This discrepancy in the otherwise expected dependency of hydrogen bond strength on the level on π electron delocalization is an interesting property of asymmetric acetylacetone derivatives that could help understand more about intramolecular hydrogen bonding in π conjugated systems.
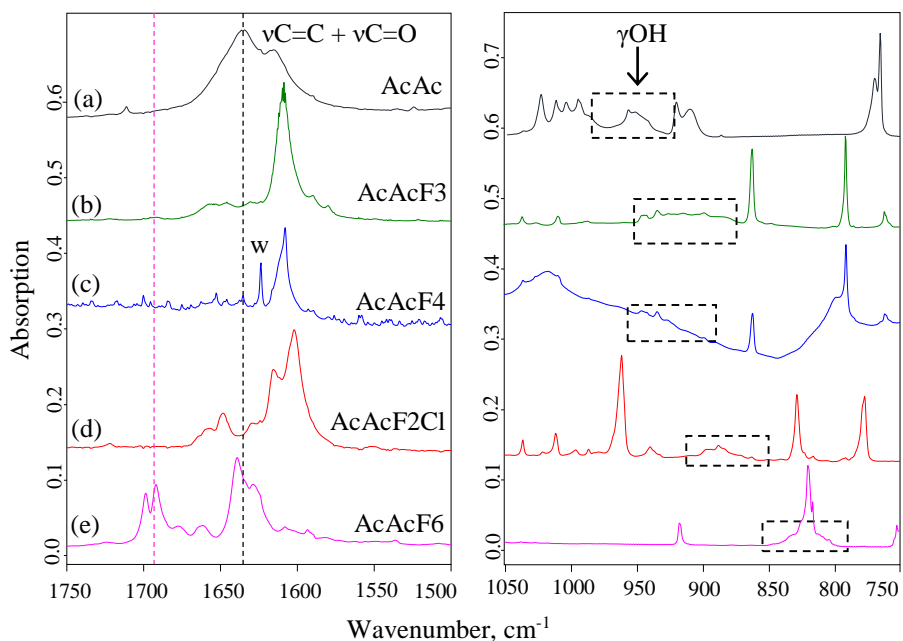
3.3.3. Experimental results

Figure 22. Infrared absorption spectra of (a) AcAc, (b) AcAcF3, (c) AcAcF4, (d) AcAcF2Cl and (e) AcAcF6 isolated in argon matrix, the 1750 cm^{-1} – 1500 cm^{-1} region (left) and 1050 cm^{-1} – 750 cm^{-1} region (right).

Since all of the fluorinated acetylacetone derivatives have been investigated in the environment of argon matrix, these spectra were chosen for

78

comparison (figure 22). In the region from 1750 to 1500 cm^{-1}, DFT calculations predict two bands, first belonging to coupled stretching C=C and C=O vibrations, and second to coupled C=C stretching and in plane OH deformations. Since two bands are predicted for each isomer of the asymmetric molecules (AcAcF2Cl and AcAF3), and their relative intensities and frequencies are quite different, this region serves as a good gauge for presence of (OH) isomers.

As previously stated, bands of any vibrational mode involving OH will be broadened, as seen in both of the spectral regions shown in figure 22. The coupled stretching C=C, C=O and in plane OH deformational vibrations produced very broad bands in the spectra of acetylacetone. The bands for the fluorinated derivatives are a little narrower although the overlap of different isomer bands (for AcAcF3 and AcAcF2Cl) and possibly some water impurities could change the spectral band shape. The water band is most clearly observed in the spectra of AcAcF4 at 1624 cm^{-1} and its high intensity is mostly due to low concentration of the molecule itself. The bands in this region are of very low intensity for AcAcF6 molecule and they exhibit some splitting as well. The same doublet structure is observed in nitrogen and even parahydrogen matrices which points to the intrinsic dynamics in the AcAcF6 molecule. The weak bands in between these two doublets are most likely combination bands.

The vibrational frequency of C=C and C=O bonds is one way to determine the level of π electron delocalization from experimental results. The more pronounced the delocalization, the more similar C-C and C=C bonds become (the same applies to C=O bond). In this case, the C=C bond in a localized system should have a higher vibrational frequency since it is closer to a real double bond, so to say – stronger. And vice versa, when the system exhibits higher π electron delocalization, the C=C vibrational band should shift towards lower frequencies in response to the weakening of this bond. The theoretical results predict a delocalization trend more or less in line with the intramolecular hydrogen bond strength, the only exception being the asymmetric molecules. In the experimental spectra, the assignment of the bands is a little more complicated due to the reasons discussed previously – broadening due to OH tunneling, isomer band overlap, low band intensities and/or presence of water. However, it is quite obvious that for AcAcF6, the νC=C/νC=O band is observed at much higher frequency (the doublet is at 1692 and 1699 cm^{-1}) than for AcAc (band at 1637 cm^{-1}). The vibrational frequencies for this mode fall somewhere in the middle for both isomers of

AcAcF3 and AcAcF2Cl molecules (1645 and 1648 cm^{-1}, respectively), and the band is virtually unobservable for AcAcF4 due to low intensity. However, the νC=C/δOH band for this molecule is at a similar position as in the spectrum of AcAcF3 so it could be concluded that the level of π electron delocalization is similar as well.

The next region shown in figure 22 includes the bands assigned to γOH vibrations whose position can be used to evaluate intramolecular hydrogen bond strength. This vibration, although easier to observe than other OH modes, is delocalized as well, even in AcAcF6 where the IHB is supposed to be weakest. However, even if γOH vibrations cannot be assigned to a band at a specific wavenumber, it is possible to confirm that the hydrogen bond strength more or less follows the predicted theoretical trend. It is strongest for the molecules with only one replaced methyl group, weaker for tetrafluoroacetylacetone and weakest for hexafluoroacetylacetone. Both regions will be explored more in the section dedicated to AcAcF3, especially in regards to the coexistence of (CO) and (OH) isomers in the environment of different matrices.

3.3.4. Associates with water
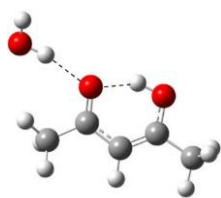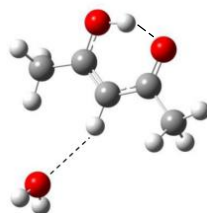
AcAc + H$_2$O (I)   AcAc + H$_2$O (II)   AcAc + H$_2$O (III)
E$_B$ = 15.8 kJ/mol   E$_B$ = 9.5 kJ/mol   E$_B$ = 3.5 kJ/mol
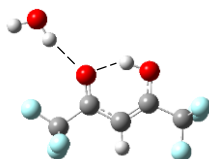
AcAcF6 + H$_2$O
E$_B$ = 6.2 kJ/mol

Figure 23. Possible configurations of acetylacetone and water molecular complex and the most stable geometry of hexafluoroacetylacetone and water complex, with their binding energies noted below.

In solutions, water molecules create a solvation shell with complex interactions between water and solute molecules. In the case of matrix isolation, it is possible to control the amount of these interactions by having low water concentration and controlling water molecule movement through the solid by slowly increasing the temperature of matrix samples. In those cases, associates of two molecules (that is to say, one analyte – one water molecule) form in the matrix environment and provide a small model system which helps analyze the intermolecular hydrogen bond, its strength and the consequences of its formation to the molecular structure and properties.

Table 4. Properties of acetylacetone and water molecular complexes. γOH – out-of-plane vibrational OH mode, Q – coordinate of π bond delocalization ($Q = d_{C-O} - d_{C=O} + d_{C-C} - d_{C=C}$), d_1O…H(D) – intramolecular hydrogen bond distance, d_2O…H(D) – hydrogen bond distance between acetylacetone and water. Experimental data taken from IR absorption spectra of molecules isolated in argon matrix.

	AcAc+H$_2$O (I)	AcAc+H$_2$O (II)	dAcAc+ D$_2$O	AcAcF6+ H$_2$O
E_B, kJ/mol	15.8	9.5	17.5	6.2
νOH(OD), cm^{-1} (H$_2$O/D$_2$O free OH(OD), calc)	3885.2	3889.9	2835.2	3895.2
νOH(OD), cm^{-1} (H$_2$O/D$_2$O bound OH(OD), calc)	3640.8	3737.4	2638.2	3779.4
γOH(OD), cm^{-1} (calc)	987.4	1009.4	738.7	884.2
νC=C, cm^{-1} (calc)	1668.1	1678.9	1647.4	1722.7
d_1O…H(D), Å	1.63	1.57	1.65	1.73
d_2O…H(D), Å	1.91	1.99	1.91	2.07
Q, Å [AcAc]	0.13	0.16	0.13	0.16

For a water-acetylacetone associate, there are multiple bonding sites, a few of which were explored in this work and depicted in figure 23 and described in table 4. The intermolecular hydrogen bond strength of these complexes can be determined from the frequency of OH stretch in water molecule. The

stronger the bond, the lower the frequency of the bonded OH stretching mode in comparison to the free OH stretch.

According to theoretical calculations, the energy of acetylacetone-water complex where OH group in water is bonded to C=O group in acetylacetone, is energetically favored out of all possible complex types. If the complex energy is calculated as the difference of absolute complex energy and the sum of absolute energies of two molecules (equation 12), the value for the mentioned structure is almost 16 kJ/mol.

$$E_B = E_{complex} - (E_{water} + E_{AcAc}). \tag{12}$$

The next most stable associate (with H_2O bonded to C-O-H group) has energy difference of only 9.5 kJ/mol. According to these energy differences and Boltzmann distribution at room temperature, the amount of the most stable structure is around 93 %, the amount of the second (C–O–H side) structure – 6 %, and the missing 1 % corresponds to the least stable complex in which oxygen atom of the water molecule is bonded to the olefinic hydrogen of acetylacetone. Therefore, it is expected that most stable structure would dominate in the experimental sample, with only a small possibility of observing second structure bands.

The deuteration of the molecule does not change its electronic structure. So the dAcAc-D_2O complex energy calculations yield exactly same results as for the simple acetylacetone and water molecules. However, adding the vibrational zero-point energy changes complex energy so that the deuterated associate is lower in energy by 1.7 kJ/mol than that of the hydrogenated one. Hexafluoroacetylacetone molecule was chosen for further studies in order to investigate the influence of mass and electronic changes in acetylacetone on the formation of the hydrogen bonded complex with water. According to the calculations, hydrogen–fluorine exchange has a major influence on the structure and binding energy of the complex. The most stable structure of the hexafluoroacetylacetone-water complex is different from acetylacetone-water since the repulsion between electronegative oxygen in water and fluorine atoms in AcAcF6 increases the intermolecular distance. The only possible counter force for this repulsion is the attraction between the hydrogen atom of the free OH group in the water molecule and the CF_3 group in hexafluoroacetylacetone. The hydrogen of the OH group is turned towards the fluorine atoms in CF_3 group but the intermolecular distance in this case is too large and cannot compensate for the repulsion between oxygen and fluorine.

In comparison to the AcAc–water complex, the binding energy of the most stable AcAcF6-water complex structure is much smaller, around 6.2 kJ/ mol (table 4).
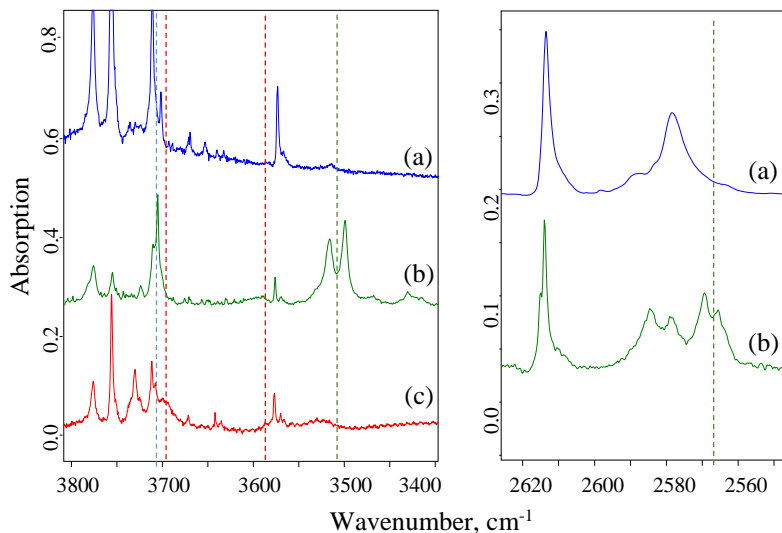

Figure 24. Infrared absorption spectra of water (a), acetylacetone and water (b), hexafluoroacetylacetone and water (c) isolated in argon matrix (left); infrared absorption spectra of deuterated water (a) and deuterated acetylacetone and deuterated water (b), isolated in argon matrix (right).

The matrix isolation experimental technique makes it possible to stabilize weak complexes and prevent formation of larger structures which would hinder detection of such complexes. In figure 24, the νOH region for acetylacetone-water mixture samples isolated in argon matrix are presented. This region is where the most obvious spectral changes should occur since the vibrational band belonging to water's bound OH vibration should exhibit a significant shift in frequency upon formation of the intermolecular bond. The acetylacetone-water mixture spectrum exhibits several bands that are not present in either pure acetylacetone or pure water spectra which indicates that at least one type of the complex is formed. The region depicted in figure 25 (with γOH vibrational bands) is helpful in identifying the influence of intermolecular hydrogen bond on the intramolecular one. In the most stable complex, the C=O group in acetylacetone is the same that participates in the intramolecular hydrogen bond O…H-O and so it functions as a double

acceptor. This should mean that IHB weakens upon acetylacetone-water complex formation – this effect could be observed as a red shift of γOH band in the experimental spectra.

The spectra of acetylacetone–water mixtures isolated in argon matrices are presented in figure 24. Most of the bands seen in the 3800 – 3700 cm^{-1} region can easily be assigned to water monomers. The water dimer OH stretch band is observed at 3573 cm^{-1}, and the low intensity trimer band appears at around 3514 cm^{-1}. According to the calculations, in the AcAc-water and AcAcF6-water complexes, the νOH frequency of the group not participating in the hydrogen bond is only slightly shifted from the νOH of water monomer. The value of this shift is about 30 cm^{-1} for both complexes. The shift of bound OH stretch is more pronounced – the band is calculated to be at 3641 cm^{-1} for AcAc (shift from monomer band around 270 cm^{-1}) and 3779 cm^{-1} (shift around 140 cm^{-1}) for AcAcF6. In the spectra of both AcAc and AcAcF6, the band at 3705.9 cm^{-1} can be attributed to the free OH stretch of water bound to acetylacetone, based on the calculations and annealing experiments, although in both of these spectra they are slightly overlapping with water band at 3710 cm^{-1}.

In spectra of acetylacetone and water, the band of bound OH stretch which would allow estimation of intermolecular HB strength, is present as a doublet at 3512 cm^{-1} and 3495 cm^{-1}. The first band could technically be water trimer band but its shape and exact position differs slightly. Comparisons with theoretical calculations, annealing and increasing water concentration experiments all allow the conclusion that both of these bands belong to the same molecular species. This means that intermolecular hydrogen bond strength in acetylacetone-water complexes is similar to that in the water trimer. In the case of the hexafluoroacetylacetone, the shift from water monomer OH stretch to bound OH stretch of water in a complex is much smaller. According to calculations, the shift should be approximately 140 cm^{-1}, placing the experimental band of bound OH stretch at around 3600 cm^{-1}. Spectrum subtraction manipulations show that there is indeed an indication of a new band (with peak value at 3580 cm^{-1}) although the water dimer band is much more intense here. If this band can be assigned to AcAcF6-H$_2$O complex, that means the HB strength here is comparable to that in the water dimer. One additional band in the spectra of hexafluoroacetylacetone and water is observed at 3695 cm^{-1} which clearly grows together with increasing temperature and water concentration. Calculations do not predict this band but they do predict geometry change

from AcAc-H$_2$O complex to AcAcF6-H$_2$O. Perhaps in some cases the distance between CF$_3$ groups and hydrogen in H$_2$O is smaller, and the interaction strength slightly bigger than predicted, and this band represents stretching mode of these particular OH groups.

The O–D stretch region of D$_2$O and deuterated acetylacetone isolated in the argon matrix is presented in figure 24 as well. From the experiments using different concentrations of D$_2$O and dAcAc, it was possible to identify two spectral bands associated with the bound O–D stretch of D$_2$O bonded to dAcAc (2569 and 2564 cm^{-1}). The separation between this doublet is smaller than in the case of normal water – only 5 cm^{-1} in comparison to 12 cm^{-1} for AcAc. The doublet separation change from hydrogen to deuterium can be associated with the matrix cage effect, as heavier deuterium atom vibration is probably less perturbed by surrounding argon atoms. The complex band is close to the D$_2$O trimer band just like it was in the case of normal water. The experimental spectral shift of the water O–H stretch from the monomer to the acetylacetone–complex is 250 cm^{-1} in the hydrogenated complex and 220 cm^{-1} in the deuterated complex. A smaller shift in the deuterated system exhibits a weaker hydrogen bond. This effect is called the negative Ubbelohde effect and is in agreement with theoretical predictions for weakly bounded hydrogen bond complexes involving water [195]. A similar effect upon deuteration is also observed for the water trimer [72, 196]. It is interesting to note that this experimental observation contradicts theoretical predictions at the DFT B3LYP (6-311++G(3df, 3pd)) level where a deuterated form is predicted to be slightly stronger, but confirms Car–Parrinello molecular dynamics studies where water involving hydrogen bond complexes is expected to have a slightly weaker hydrogen bond upon deuteration.
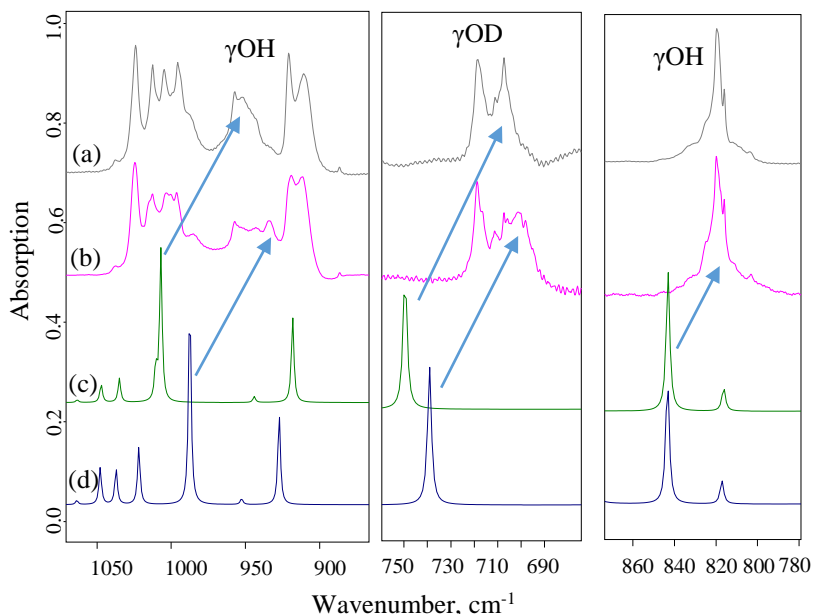
Figure 25. The infrared absorption spectra of (a) acetylacetone and (b) acetylacetone and water isolated in argon matrix, (c) calculated spectrum of AcAc, (d) calculated spectrum of AcAc+H$_2$O (leftmost panel). The spectra in the same order for deuterated acetylacetone and deuterated water are shown in center panel, and for hexafluoroacetylacetone and water – in rightmost panel.

In order to see the effect of intermolecular hydrogen bond on the IHB, the regions of γOH (or γOH for deuterated derivatives) are shown in figure 25. Calculations predict a 23 cm^{-1} red shift upon hydrogen bond formation (see Table AI-4) and a 24 cm^{-1} red shift is observed in argon matrix experimentally (γOH band is at 960 cm^{-1} for pure AcAc and 937 cm^{-1} for AcAc–water complex). Similar values can be extracted from dAcAc-D2O spectra – the theoretical shift is calculated to be 10 cm^{-1} and the experimental one is around 8 cm^{-1}. The calculations predict practically no shift for hexafluoroacetylacetone and water complex formation. The small band shifts of the AcAc molecule upon complex formation and remaining broad bands in the argon matrix confirm that water, hydrogen bonded to the AcAc molecule, has only a weak influence on the intramolecular hydrogen bond strength.

3.3.5. Trifluoroacetylacetone

In this section, the asymmetric acetylacetone derivatives, especially trifluoroacetylacetone, are explored further. The broken symmetry of AcAcF3 molecule means that hydrogen is more likely to be localized near one of the oxygen atoms. All the theoretical and experimental studies performed on trifluoroacetylacetone agree that the AcAcF3(CO) isomer, in which hydrogen is localized on the same side as CH_3 and not CF_3 group, is more stable. The AcAcF3(OH) isomer is a local minimum and the calculated energy difference between these two isomers is to be very dependent on the chosen calculation method [119]. According to the calculations performed at B3LYP 6-311++G(3df, 3pd) level, this difference is 4.3 kJ/mol which corresponds to 85 % AcAcF3(CO) and 15 % AcAcF3(OH) mixture at room temperature according to Boltzmann distribution.

In order to confirm the presence of higher energy isomer, both infrared absorption and Raman scattering spectroscopical methods were employed together with matrix isolation. AcAcF3 was isolated in carbon monoxide, nitrogen, argon, neon and parahydrogen matrices in order to estimate the influence of different environments. The CO matrix is most similar to nitrogen, which is known to be more interacting than argon. Parahydrogen matrix is a very interesting environment for exploration since it allows large amplitude motions of the trapped molecule. In addition, studies with AcAcF3–water mixtures were performed in order to determine the influence of intermolecular hydrogen bond on the stability of the two isomers. The obtained results are compared with the similar studies of acetylacetone and hexafluoroacetylacetone, explored previously.

Another molecule similar to AcAcF3 in its asymmetry is AcAcF2Cl, which was explored only in argon and nitrogen matrices using infrared absorption spectroscopy. These results will be compared to AcAcF3 at the end of this section.
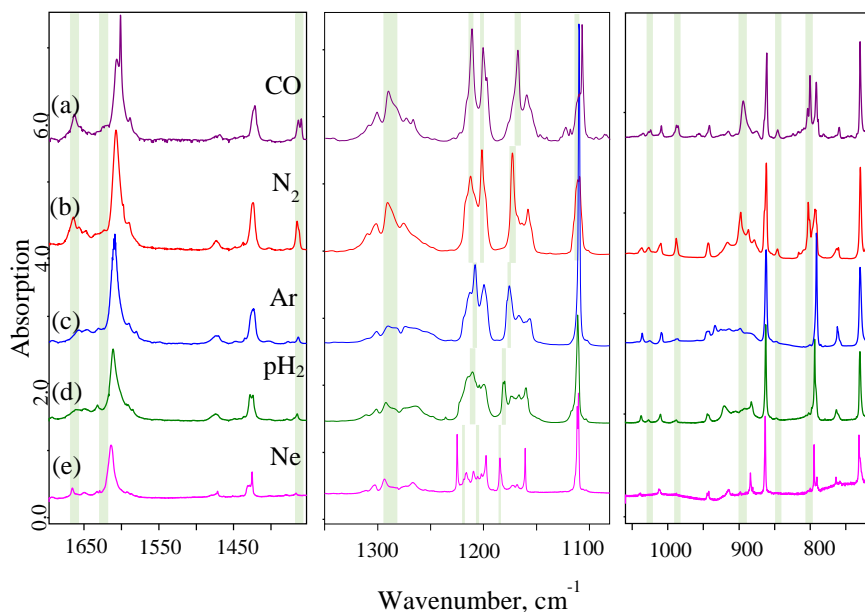
Experimental results

Figure 26. IR absorption spectra of AcAcF3 isolated in (a) CO, (b) N_2 (c) Ar, (d) pH_2 and (e) Ne matrices (T=3-12 K) in three spectral ranges: 1300 cm^{-1} – 1750 cm^{-1}, 1050 cm^{-1} – 1350 cm^{-1} and 700 cm^{-1} – 1100 cm^{-1}. Green vertical strips highlight positions of CCC(OH) bands.

Infrared spectra of the AcAcF3 molecule isolated in different matrices are depicted in figure 26. Since it is possible for pH_2 matrix to carry some ortho-hydrogen impurities after conversion from normal hydrogen, the molecule was isolated in normal hydrogen as well. No significant changes were observed and so, only spectra of AcAcF3 isolated in pH_2 are shown here. The number and relative intensities of bands observed in the spectra of different matrices definitely suggest that there is more than one isomer. The AcAcF3(OH) band positions were determined after comparison between different experimental spectra and theoretical calculations and are highlighted here by light green vertical strips. The concentration of AcAcF3(OH) is much higher in more interacting matrices of N_2 and CO than in Ar and seems to be very low in Ne. These differences in concentration can be quantitatively evaluated by integrated well-separated bands of two isomers which will be discussed in more detail later. The amount of AcAcF3(OH) seems to be higher in pH_2 than in either of rare gases. However, the samples in pH_2 contained

some water impurities and water seems to have a stabilizing effect on AcAcF3(OH) as will be discussed later.

The bands in the C=C and C=O stretching region shown in the leftmost panel in figure 26 are fairly easy to assign. They are broadened due to coupling with δOH mode, however, it is still possible to identify AcAcF3(CO) and AcAcF3(OH) bands with the help of calculated spectra and the host-dependent band intensities. According to DFT calculations, AcAcF3(CO) isomer has an intense band at 1658 cm^{-1} and a less intense one at 1770 cm^{-1} – they can be assigned to the 1610 and 1650 cm^{-1} bands in the experimental spectra. The AcAcF3(OH) isomer is predicted to have bands at 1695 cm^{-1} and 1769 cm^{-1}, second of which should be twice more intense. They can be identified in experimental spectra at 1630 and 1660 cm^{-1}. The positions of these bands in the experimental spectra also confirm the theoretical prediction that AcAcF3(CO) isomer exhibits higher level of π electron delocalization. Another important observation in this spectral region is the band at 1365 cm^{-1} which is quite well separated from others and can serve as a gauge for the presence of the higher energy isomer.

The range of 1350 to 1100 cm^{-1} (figure 26, middle panel) is fairly complicated. Firstly, it exhibits a broad structure around 1280 cm^{-1} which can be assigned to in-plane deformational OH vibration. The slightly better localized peak at 1290 cm^{-1} is assigned to AcAcF3(OH) mainly because of the already observed host dependency. The many overlapping bands in the region from 1230 cm^{-1} to 1150 cm^{-1} are attributed to CF stretching modes in CF$_3$ group. The assignment to specific ones is quite complicated but tentatively performed by comparing experimental AcAcF3 spectra to both calculated values and the spectra of AcAcF6 which exhibits similar structure in this region. Finally, there is an intense band at 1110 cm^{-1}, seen in all the matrices. Theoretical calculations predict an intense band at 1138 cm^{-1} for AcAcF3(CO) and 1148 cm^{-1} for AcAcF3(OH). Therefore, it can be concluded that these two bands overlap here in experimental spectra and are responsible for broader peaks in the spectra of N$_2$ and CO matrices.

The best region for determining the amount of the AcAcF3(OH) in different environments is from 900 to 700 cm^{-1}. The γCH band (calculated to be at 813 cm^{-1} for AcAcF3(CO) and 834 cm^{-1} for AcAcF3(OH)) can be clearly observed in N$_2$ and CO matrices at around 792 and 802 cm^{-1}, respectively. The relative intensities of this band can help assign other bands to AcAcF3(OH) isomer, including the band of γOH vibration. Theoretical calculations predict γOH vibrational band to be at 904 cm^{-1} for AcAcF3(CO) and 921 cm^{-1} for

AcAcF3(OH). However, as previously discussed, this band in experimental is very broad and, in this case, with a structure that depends on matrix environment. The only band that seems more localized and could be assigned to AcAcF3(OH) due to its intensity is at 898 cm^{-1} in N_2 and 894 cm^{-1} in CO. The AcAcF3(CO) band is then the broad structure in the region from 930 to 875 cm^{-1}. In neon matrix, there are two more bands that can be identified – at 884 and 915 cm^{-1} (at 883 and 921 cm^{-1} in pH$_2$) that could belong to out-of-plane bending motion of OH group in AcAcF3 molecule.
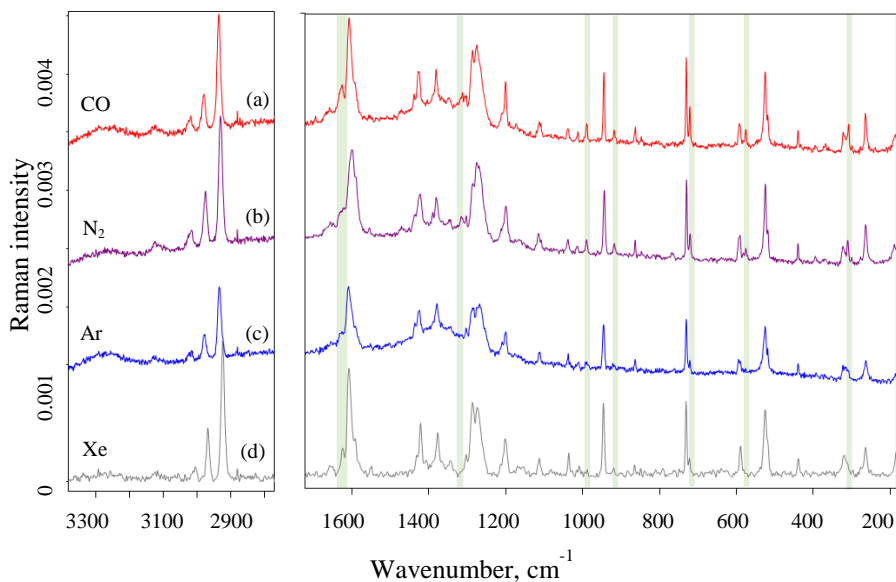

Figure 27. Raman scattering spectra of AcAcF3 isolated in (a) CO, (b) N_2, (c) Ar, (d) Xe matrices (T=12-20 K) in two spectral ranges: 3200 cm^{-1} – 2850 cm^{-1} and 1800 cm^{-1} – 200 cm^{-1}. Green vertical strips highlight positions of CCC(OH) bands.

Experiments using Raman spectroscopic methods were also performed for trifluoroacetylacetone. In this case, AcAcF3 molecule was isolated in CO, N_2, Ar and Xe matrices. The most relevant regions of the spectra are depicted in figure 27. As in IR spectra, more bands are present in CO and N_2 than in Ar, and some weak bands show higher intensity in the first two matrices. Besides the fact that some modes that were not active in IR spectra can be observed in Raman, the latter method also allows the observation of low-frequency
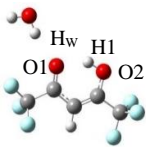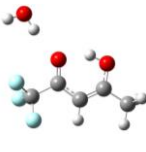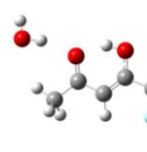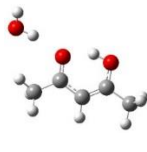
vibrations. In this region (800 cm^{-1} to 200 cm^{-1}), the bands are quite narrow and easy to assign. There are two bands that work as especially good gauges of AcAcF3(OH) isomer. They are observed at 310 and 575 cm^{-1} in both N$_2$ and CO, and correspond to calculated values of 308 (Δ vibrational mode) and 585 cm^{-1} (δCH$_3$-C-O vibrational mode).

Bands in other regions are quite broad and tend to overlap. For example, in the CH stretching region (3200 cm^{-1} to 2800 cm^{-1}), only AcAcF3(CO) modes are observed but due to their bandwidth, the AcAcF3(OH) band could be hidden underneath. It is hard to observe any AcAcF3(OH) bands in the 1200 cm^{-1} – 1400 cm^{-1} region as well. A broad band with structure is observed around 1280 cm^{-1}, corresponding to OH in-plane bending and the chelated ring motions in AcAcF3(CO). The same mode in AcAcF3(OH) is predicted to have low Raman activity and is not clearly visible even if it is present. However, the bands observed in the low frequency region are enough to confirm the presence of AcAcF3(OH) in the four matrices.

Effect of water, temperature and irradiation

Theoretical calculations predict that the most stable complex formed from one acetylacetone molecule and one water molecule has the structure where hydrogen of water molecule is bonded to oxygen of C=O group in acetylacetone molecule (see table 5). This type of bonding geometry remains similar for all the acetylacetone derivatives, the only change being H$_2$O rotation away from CF$_3$ groups in AcAcF3(CO) and AcAc6F (the molecules where CF$_3$ group is at the same side of the molecule as the C=O group) because of repulsion between oxygen of water molecule and fluorine of AcAc molecule. The calculated values are summarized in table 5.

Table 5. Calculated parameters of acetylacetone-water complexes (B3LYP/6–311++G(3df,3dp)). E_B is complex binding energy, ΔE is the energy difference between AcAcF3(CO)–water and AcAcF3(OH)–water isomers.

	AcAcF6 +H_2O	AcAcF3(CO) +H_2O	AcAcF3(OH)+ H_2O	AcAc+H_2O
E_B, kJ/mol	6.2	8.9	9.5	15.8
ΔE, kJ/mol	-	0	0.7	-
$d_{O1...H1}$, Å	1.73	1.68	1.65	1.63
d_{O2-H1}, Å	1.00	0.99	1.00	1.00
$d_{O1...Hw}$, Å	2.07	2.03	1.96	1.91
H_2O νOH_{bound}, cm^{-1}	3779.4	3754.5	3691.6	3640.8
AcAc γOH, cm^{-1}	884.2	943.6	941.3	987.4

The trifluoroacetylacetone-water spectra are shown in figure 28, along with the spectrum of pure water. As discussed previously, the bound OH band is observed at 3495 cm^{-1} for AcAc and 3580 cm^{-1} for AcAcF6. The medium strength band around 3705 cm^{-1} is attributed to the free OH stretch (water OH group not involved in hydrogen bonding) for all the acetylacetone derivatives. The situation is more complicated in case of water bound to AcAcF3 molecule. In the OH stretch region besides water bands three additional bands can be observed at 3545, 3590 and 3711 cm^{-1}. The latter one is easily attributed to the free OH stretch of water bound to AcAcF3.
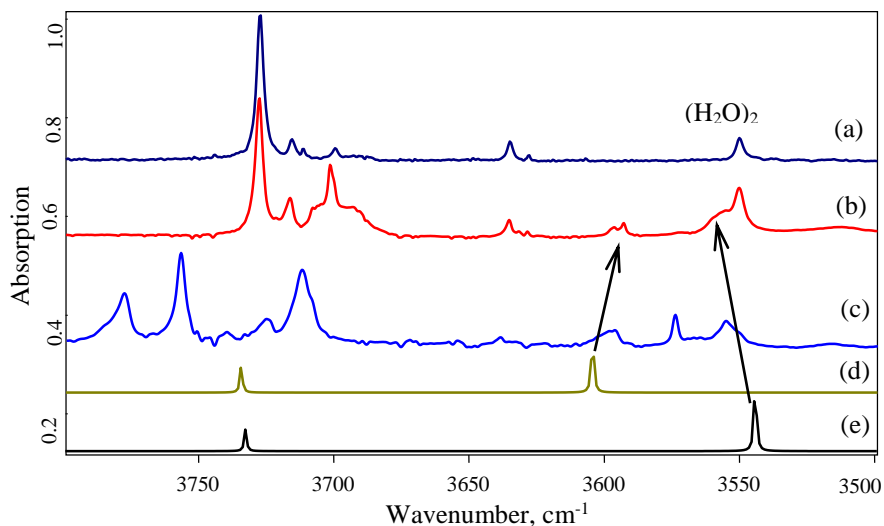
Figure 28. IR absorption spectrum in the OH stretch region of (a) water in argon matrix, (b) trifluoroacetylacetone and water in argon matrix, (c) trifluoroacetylacetone and water in argon matrix, (d) calculated AcAcF3(CO)+H$_2$O and (e) calculated AcAcF3(OH) spectra. Scaling factor of 0.96 was used for all calculated spectra.

However, remaining two bands at 3590 and 3545 cm^{-1} seem to point to the existence of two distinct structures of AcAc-water complexes. The theoretical calculations predict that the strongest hydrogen bond is in the structure of AcAcF3(OH)-water complex. Calculated hydrogen bond energy is 9.5 kJ/mol (see table 5). The second strongest hydrogen bond is in the structure of AcAcF3(CO)-water complex and the calculated bond energy is 8.9 kJ/mol. However, the overall electronic energy is lower for the AcAcF3(CO)-water complex by 0.6 kJ/mol. Thus observation of complexes of both isomers at similar concentrations can be expected. Comparison of calculated and experimental spectra (figure 28) suggest assignment of the band at 3545 cm^{-1} to the AcAcF3(OH)-water complex, and the band at 3590 cm^{-1} to the AcAcF3(CO)-water complex. This assignment correlates well with calculated hydrogen bond strength of the complexes. AcAcF3(OH)-water complex with the stronger hydrogen bond exhibits a larger bound OH stretch red shift from the free OH stretch, and weaker complex of AcAcF3(CO)-water has a smaller bound OH stretch wavenumber red shift.
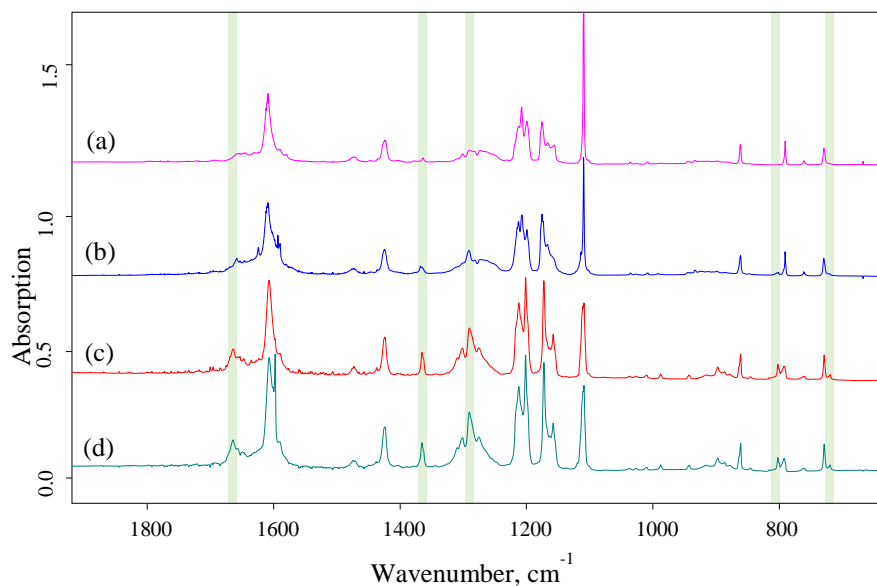
Figure 29. IR absorption spectra of (a) AcAcF3 isolated in Ar, (b) AcAcF3 and water (1:2) isolated in Ar, (a) AcAcF3 isolated in N_2, (b) AcAcF3 and water (1:1) isolated in N_2. Green vertical strips highlight positions of CCC(OH) bands.

The spectra depicted in figure 29 show the effect of water on the distribution of two AcAcF3 isomers. The bands that were assigned to AcAcF3(OH) are absent or very weak in the spectrum of pure AcAcF3 isolated in argon. However, upon addition of water, these bands grow in intensity. Since the AcAcF3(OH)-water complexes have higher binding energy, it makes sense that water molecules help stabilize higher energy isomer and increase the AcAcF3(OH)/AcAcF3(CO) ratio. According to spectral band integration, and keeping in mind the calculated intensities of the bands, this ratio increases from 0.42 (pure AcAcF3 deposited in N_2) to 0.5 (AcAcF3+H_2O mixture in N_2), and from around 0.01 (pure AcAcF3 deposited in N_2) to 0.05 (AcAcF3+H_2O mixture in N_2).

Another external effect that can change this ratio is temperature of the sample. These effects are detected during the annealing process but specific results depend on matrix environment as well. In general, annealing should irreversibly increase the amount of lower energy isomers. However, in the experimental spectra of N_2 and CO, the AcAcF3(OH) band intensity increases after this process (figure 30, table 6). In Ne and pH_2, a weak increase is also

94

observed, but these samples had some water impurities and its diffusion through matrix during annealing could have affected the result. The only matrix in which no change is observed is argon.
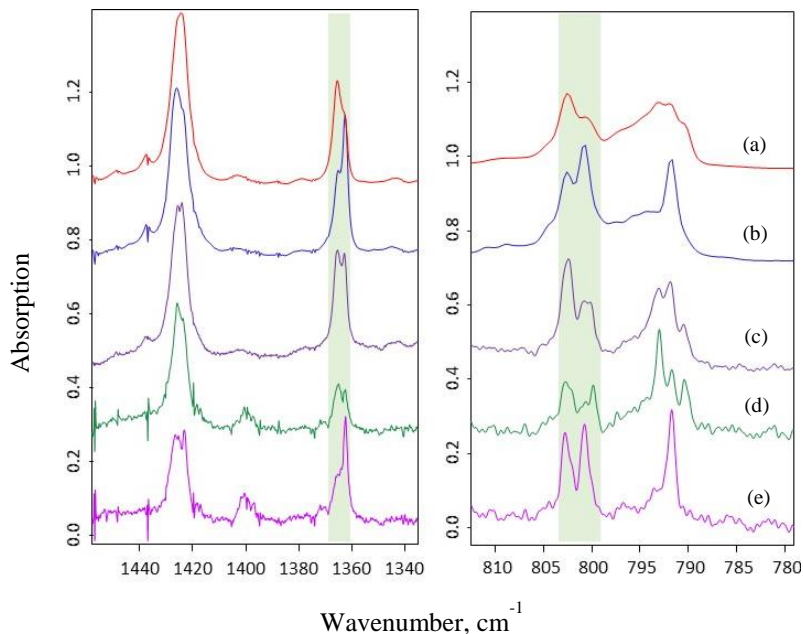

Figure 30. Spectra of trifluoroacetylacetone in nitrogen matrix, two different samples: first sample (a) before (red) and (b) after annealing (blue); second sample (c) as deposited (violet), (d) after successive UV irradiation (green), (e) after successive UV irradiation and annealing (purple). Green vertical strips highlight CCC(OH) bands.

The effects of UV irradiation are also depicted in figure 30. The irradiation was performed in other matrices besides N_2 (pH_2, Ne, Ar) in order to produce open enol isomers. However, here only the effect on the AcAcF3(OH)/AcAcF3(CO) ratio is shown. While annealing increases this ratio, irradiation decreases it. The latter effect (figure 30, (c)−(d)) is easier to observe and so can be very useful in identifying the bands of two isomers in the more complex parts of the spectra. The information about AcAcF3(OH)/AcAcF3(CO) ratio changes upon irradiation is also necessary in future photoisomerization experiments.

In some matrices, the annealing effect could also be tied into AcAcF3-water complex formation which also affects isomer ratio. In any case, the role

of the environment is extremely important to the stabilization of higher energy isomer. For example, in the case of CO and N_2, after annealing the AcAcF3 molecules become positioned in the matrix site in such a way that the CO (or N_2) and OH group interaction is strengthened, thus further stabilizing AcAcF3(OH) isomer. This is a similar effect to what was observed upon the addition of water. The summary of annealing and irradiation effects on AcAcF3(OH)/AcAcF3(CO) ratio is presented in table 6. Here, infrared absorption bands were used for the calculations, several pairs were picked in order to confirm the findings but information from only one pair (793 cm^{-1} and 803 cm^{-1}) is shown in the table, since the values were similar for all the calculations. These calculations were not performed for all the spectra since high water content or easy evaporation of some matrices could give innacurate results.

The band at 793 cm^{-1} belongs to AcAcF3(CO) and the one at 802.5 cm^{-1} – AcAcF3(OH), both correspond to the same vibrational mode (γCH). The intensity ratio was predicted to be 1.19 (MP2), 1.68 (M06-2X) or 1.12 (B3LYP-D3). The ratios here are calculated from integrated band areas taking into account the intensities of M06-2X calculations.

Table 6. AcAcF3(OH)/AcAcF3(CO) ratio values extracted from the spectroscopic results in the various probed hosts.

Matrix gas	Isomer ratio in as-deposited sample	Isomer ratio after annealing	Isomer ratio after irradiation
Ne	> 0.007	-	-
Ar	> 0.01	> 0.01	-
pH$_2$	> 0.08	-	-
N$_2$	0.42±0.08	1.2±0.3	0.35±0.01
CO	0.8±0.2	1.5±0.3	-

3.3.6. Conclusions and AcAcF3 comparison to AcAcF2Cl

Theoretical calculations performed at the B3LYP 6-311++G(3df, 3pd) level and matrix isolation infrared absorption experiment results confirm that acetylacetone and water form hydrogen bonded complexes in argon and nitrogen matrices. Only one complex with the most stable structure was observed experimentally for acetylacetone, deuterated acetylacetone and hexafluoroacetylacetone. Both of the trifluoroacetylacetone isomers formed complexes with water in the matrix environment.

The spectral bands of the complex were identified and assigned to the normal vibrations of water and acetylacetone participating in the formation of the complex. The bond strength in the complex is similar to the bond strength in the water trimer – this is confirmed by the calculations and similar spectral shifts of the bound O–H stretch observed in the water trimer and the acetylacetone–water complex. In spite of a moderate hydrogen bond strength only very small changes of the AcAc bands are observable. The observation that O–H out-of-plane deformation band does not shift much upon the formation of an intermolecular hydrogen bond with water suggests that water has a very minor influence on the strength and dynamics of an intramolecular hydrogen bond in an AcAc molecule. The deuteration of water and acetylacetone O–H and C–H bonds results in a slight decrease of the complex hydrogen bond energy upon the deuteration. This is manifested in a smaller water molecule O–D stretch shift from the monomer to the complex compared with the corresponding O–H stretch shift. The fluorination of CH_3 groups in acetylacetone results in a different complex geometry and a significant binding energy decrease manifested both in the DFT calculated energy and the observed smaller OH stretching shifts from the monomer to the complex bands.

The experimental and calculated data revealed that both isomers of AcAcF3 coexist in matrix environment with their ratio highly dependent on the host. The higher energy isomer AcAcF3(OH) was observed in all the matrices but the AcAcF3(OH)/AcAcF3(CO) ratio was much higher for more interacting CO and N_2 solids. Because of this, the assignment of AcAcF3(OH) vibrational bands (more than 20) was made easier. The temperature and irradiation effects on the isomer ratio were also explored in nitrogen matrix. It seems that while the amount of AcAcF3(OH) surprisingly increases after annealing, it decreases after UV irradiation.

The addition of water leads to the trifluoroacetylacetone-water complex formation. This is well manifested in the appearance of new bands in the OH stretch region attributed to the free and bound OH stretches of water molecule bonded to trifluoroacetylacetone. The analysis of the calculated and experimental spectra leads to the conclusion that complexes of water with both isomers of trifluoroacetylacetone coexist in argon and nitrogen matrices. Association with water stabilizes the less stable isomer with CF_3 group on OH group side of trifluoroacetylacetone molecule. The strongest intermolecular hydrogen bond is formed in acetylacetone-water, weaker one in trifluoroacetylacetone-water and the weakest one in hexafluoroacetylacetone-water complexes. These experimental observations are in good agreement with calculated complex binding energies. The formation of hydrogen bond with water slightly weakens the intramolecular hydrogen bond of the trifluoroacetylacetone based on theoretical calculations. However, the experimental data does not show the perturbation of trifluoroacetylacetone vibrations from formation of hydrogen bond with water due to the highly broadened bands involving OH vibrations.

The results of AcAcF3 can be briefly compared with another asymmetric molecule that was studied by the same methods. According to the calculations, AcAcF2Cl has two isomers with (CO) being 7.8 kJ/mol lower in energy than (OH). Just like in AcAcF3, the (OH) isomer has stronger IHB but lower π electron delocalization level. In the experimental spectra, shown in figure 31, additional bands can be seen in nitrogen matrix in comparison to argon.

As in the spectra of AcAcF3, the band assigned to δOH mode has additional peaks in nitrogen matrix spectrum (1255 cm^{-1}). The calculations also predict this band to be a little shifted and of higher intensity for AcAcF2Cl(OH) isomer. Another well separated band can be seen at 980 cm^{-1} – it can be assigned to the calculated band at 1004 cm^{-1}, belonging to rocking vibrations of CH_3 group and deformations of the ring. In addition to that, there is a tiny doublet at 1365 cm^{-1}. It is a single band in argon and a doublet in nitrogen which would be unusual for a single isomer since argon is more likely to exhibit splitting due to site effects. This band is also very interesting because the same band with same characteristics appeared in the spectra of AcAcF3.
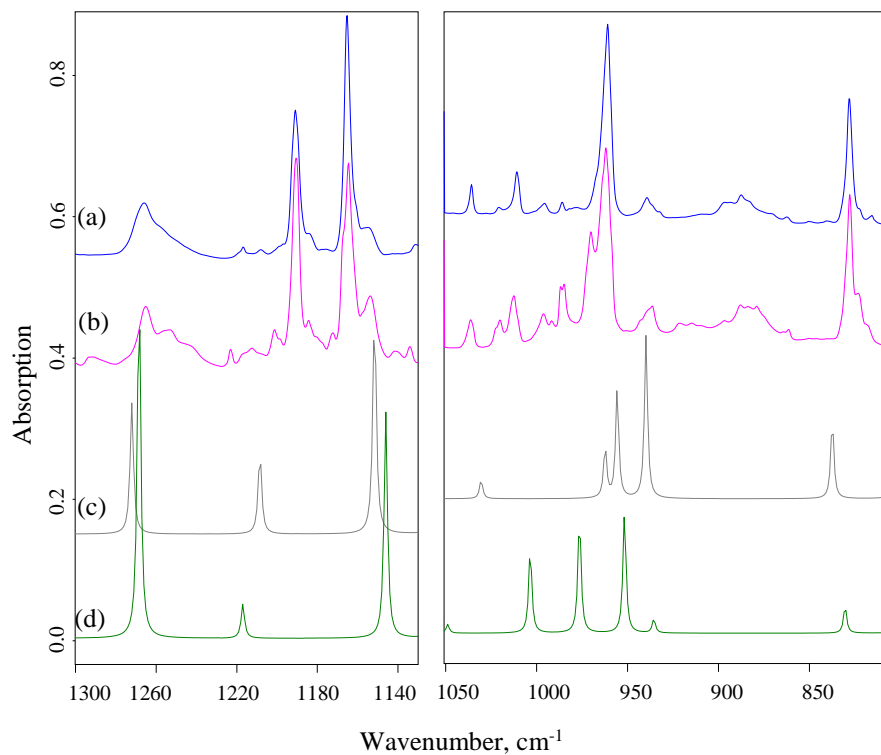
Figure 31. The infrared absorption spectra of AcAcF2Cl isolated in (a) argon and (b) nitrogen matrices, calculated spectrum of (c) AcAcF2Cl(CO) and (d) of AcAcF2Cl(OH).

Overall, the differences are perhaps not as well pronounced for AcAcF2Cl as they were in the spectra of AcAcF3 but the calculated energy difference is also bigger – with 6.3 kJ/mol difference, the amount of higher energy isomer of AcAcF2Cl molecule should equal to 7 % according to the Boltzmann distribution.

99

3.4. Salicylic acid and acetylsalicylic acid

Acetylsalicylic acid (ASA, more commonly known as aspirin) is a non-steroidal anti-inflammatory drug which has been widely used for over 100 years for prevention of clotting and reduction of fever, inflammation and pain. The molecule itself is an aromatic compound with carboxy and ester groups at the *ortho* positions. ASA is synthesized from salicylic acid ($C_7H_6O_3$) and excess of acetic anhydride ($C_4H_6O_3$) in the presence of acidic catalyst. During the reaction, the hydroxyl group of salicylic acid is replaced by an ester group to give the by-product acetic acid.
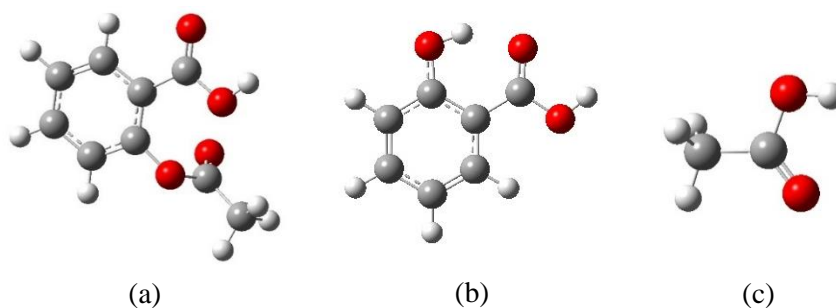

(a) (b) (c)

Figure 32. Acetylsalicylic acid (a), salicylic acid (b) and acetic acid (c) molecules.

The molecular structure of both salicylic acid and acetylsalicylic acid has been explored by theoretical methods and the experimental studies mostly dealt with their crystalline forms. Only one study was performed with salicylic acid isolated in low-temperature matrices. It was carried out by gently heating SA and mixing it with matrix gas simultaneously [141]. One stable isomer of SA was observed in argon matrix and other two were produced by UV photoisomerization. However, there have not been any low temperature matrix isolation experiments performed with ASA. The reason for the small amount of matrix isolation studies is low vapor pressure and rapid thermal dissociation, especially in the case of ASA. When heated to over 100 degrees, the mass loss occurs by elimination of acetic acid and evaporation of both salicylic acid and acetic acid (AA). The vapor pressure of ASA is also lower than that of SA (3.3 mPa and 10.9 mPa respectively).
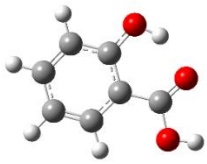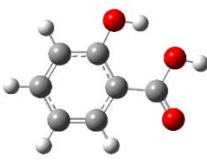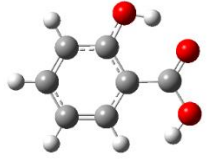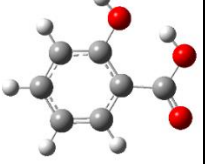
Because of this, finding optimal experimental conditions becomes quite a complex task. The temperature at which sample is heated is of utmost importance but the sample placement in the system and the speed of deposition matter as well. The heating temperature has a minimum value – that at which the evaporation is just intense enough to obtain an observable concentration in the final sample. This threshold concentration is especially important in Raman spectroscopy where the signal is weak and the concentration has to be much larger for it to be distinguished from the noise. When temperature is too high, the thermal dissociation products complicate the spectra. It is impossible to avoid them completely, especially in the case of ASA, but there are certain heating temperature values at which their concentration can be minimized.

In addition to thermal dissociation, there is a number of other reason why the spectra might be complicated to analyze. First of all, the samples of ASA and SA come in a form of powder which can absorb water. When the sample is heated, water evaporates easily and its concentration gradually diminishes if the experiments are performed with the same sample. The water has its own spectra and can also form molecular complexes with both the analyte molecule and the thermal dissociation products. These molecules (ASA, SA, AA) themselves can form intermolecular hydrogen bonds and additional bands belonging to molecular associates can then be observed in the experimental spectra. Finally, both salicylic acid and acetylsalicylic acid molecules can exist in different conformational forms. Most of them are much higher in energy than the most stable form but a couple might be observed in the spectra as weak additional bands.

3.4.1. Theoretical calculations

In the case of salicylic acid, the second lowest energy isomer is 15.7 kJ/mol higher in energy than the most stable one. This would correspond to around 0.1 % population at room temperature according to the Boltzmann distribution. Needless to say, it is very unlikely to be observed under the experimental conditions in question. Other isomers are of even higher energy, and could only be possibly obtained by photoisomerization of the sample.

Table 7. Energetic parameters of four lowest energy isomers of salicylic acid.
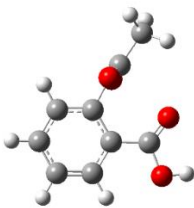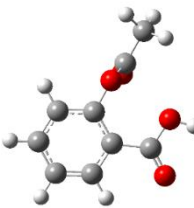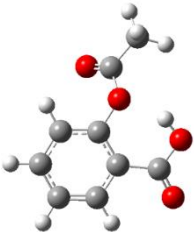
E	R	O	H
$\Delta E = 0$ kJ/mol	15.7 kJ/mol	22.0 kJ/mol	38.2 kJ/mol

In the most stable isomer of salicylic acid, the hydrogen of COOH group is oriented inwards and the hydrogen of OH group is facing towards the C=O oxygen of COOH group. The distance between these hydrogen and oxygen atoms is lower for E (and O) isomers (1.7 Å) when compared to R and H (1.8 Å). The increase in energy in the case of R isomer is due to the fact that OH group hydrogen is oriented towards OH oxygen in COOH group, and not C=O as it is in isomer E.

The isomer distribution is different for acetylsalicylic acid (table 8) where the two lowest energy isomers are separated by less than 4 kJ/mol. ASA molecule, unlike SA, is not planar and the $COOCH_3$ group orientation differs for all the isomers even if only slightly. The lowest energy isomer, denoted 1a, has the COOH group in the same plane as the carbon ring and the hydrogen of this group facing inwards and bound to the oxygen farther away from $COOCH_3$ group. The next most stable isomer (2a) is 3.8 kJ/mol higher in energy than the 1a isomer. This amount of energy difference means around 17 % concentration of the higher energy isomer should be observed in room-

temperature samples. For isomer 4a which is the next most stable, this concentration is around 0.8 %, and so it is again very unlikely to be observed in experimental spectra.

Table 8. Energetic parameters of four lowest energy isomers of acetylsalicylic acid.
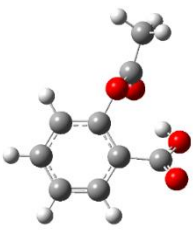
1a	2a	4a	5a
$\Delta E = 0$ kJ/mol	3.8 kJ/mol	11.8 kJ/mol	13.8 kJ/mol

The structural and energetic parameters were calculated for molecular associates of SA-water and ASA-water as well. Only the lowest energy isomer for SA and two lowest energy isomers for ASA were taken into account during these calculations.

3.4.2. Experimental results

The experiments were performed with acetylsalicylic and salicylic acid molecules isolated in argon, nitrogen, neon and parahydrogen matrices. The sample heating temperatures varied from 30 ºC to 120 ºC. For all the temperatures above 100 ºC, acetic acid dominated the sample.

The experiments were usually started by letting matrix gas pass by the sample without heating it. However, the spectra obtained this way contained either no bands at all or at least none that could be distinguished from the noise. The samples were then heated by placing a resistive heating element at the bottom of the sample container and controlling the temperature by increasing or decreasing the voltage. Later on, the method of heating was changed to a hot air stream which could heat the sample container up to 50 ºC.

This method was better than the resistive heating element method because its influence was less localized, meaning that the sample container was heated from all the sides and so were the tubes through which the sample and matrix gas travelled towards the spectral window in the cryostat.

Some of the early spectra of molecules isolated in argon matrices are shown in figure 33. Observing these spectra, it is clear that – for all the reasons listed above – SA and ASA spectra are similar. The minimal changes that appear are most clearly seen in the region between 1800 cm^{-1} and 1650 cm^{-1} where C=O stretching vibrations can be observed. Another possible source of impurities is the molecules that get "stuck" in the system so that in the spectra of salicylic acid, acetylsalicylic acid might sometimes be observed because there were traces of it in the system from previous experiments.
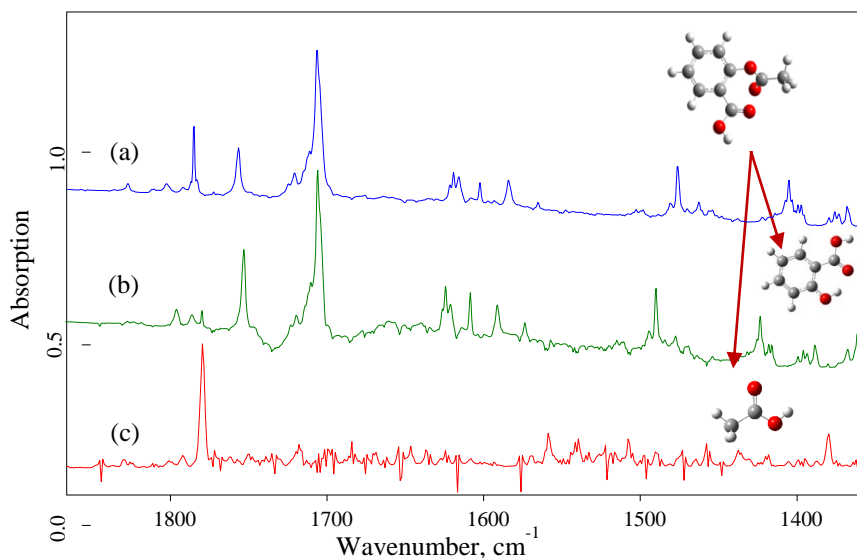
Figure 33. Infrared absorption spectra of acetylsalicylic acid isolated in the argon matrix (a) and thermal dissociation products salicylic acid (b) and acetic acid (c).

The most intense of characteristic bands for acetic acid is observed around 1778 cm^{-1} for its one and only C=O group while SA has an intense band at 1705 cm^{-1}. ASA has two bands at 1752 and 1719 cm^{-1}. The difference between these two bands corresponds well to the theoretically calculated values of C=O

stretching vibrations (1828 cm^{-1} in ester group and 1780 cm^{-1} in carboxy group).
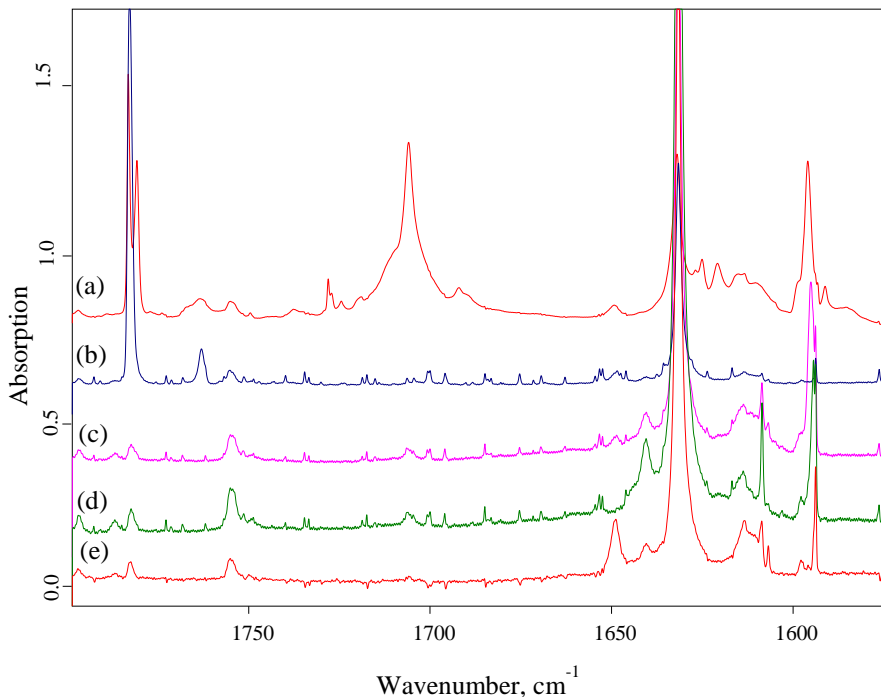
Figure 34. Infrared absorption spectra of acetylsalicylic acid, isolated in parahydrogen matrix. The sample was heated to (a) 100 ºC, (b) 70 ºC, (c) 60 ºC, (d) 55 ºC and (e) 50 ºC.

In order to better explore this region, spectra of ASA heated to different temperatures and isolated in parahydrogen matrices are presented in figure 34. There is a relatively large amount of water in all of these samples, as can be seen from the intense bands in the region from 1650 cm^{-1} to 1580 cm^{-1}. The most dramatic difference is observed between the spectra of ASA heated to 100 ºC (a) and the spectrum of ASA heated to 70 ºC (b). The intense band at 1752 cm^{-1} which has already been assigned to SA decreases to almost nothing. The amount of acetic acid (manifesting as 1778 cm^{-1} band) drops when the sample heating temperature is further lowered from 70 ºC to 60 ºC. The best spectra were obtained by heating ASA sample at 50 ºC – here only acetylsalicylic acid and water bands are observed.
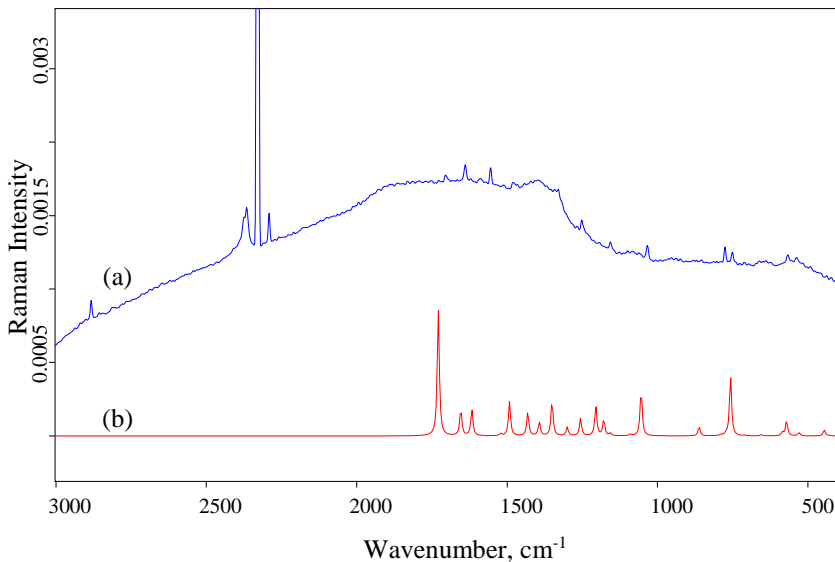
Figure 35. Raman scattering spectrum of SA, isolated in nitrogen matrix (a), and calculated spectrum of SA molecule.

Sometimes, the information obtained from infrared absorption experiments can be supplemented by data of Raman spectroscopy. However, the sample deposition procedure is even more complicated for Raman spectroscopy than infrared because it demands higher concentration of the sample. The excitation source – laser beam – has to be focused on a small area where the amount of molecules has to be high enough for Raman signal to be observable. The experiments were carried out only with salicylic acid and were repeated several times, depositing the samples for at least four hours and at very low speeds. One of the spectra with the best signal to noise ratio is shown in figure 35.

In this spectrum, the most intense band can be observed at 2328 cm^{-1} and is assigned to stretching vibrations of N_2 molecule of the matrix. One of the smaller bands at the foot of it (at 2290 cm^{-1}) can be assigned to the stretching vibrations of nitrogen isotope ($^{15}N_2$). The other one belongs to nitrogen lattice phonon vibrations. The presence of nitrogen bands confirms that the laser beam is focused on the matrix sample. This is one of the reasons why the nitrogen matrix was the first choice for Raman experiments, the possibility to observe N_2 Raman bands allows easier optical allignement of the cryostat with the spectrometer. In addition to nitrogen, experiments were carried out using argon gas. However, it seems that only this slight change in the experimental conditions prevented a formation of sufficiently concentrated matrix sample.

According to the comparison between experimental and calculated spectra in figure 35, salicylic acid is present in this sample. The spectral band at 1732 cm^{-1} in the calculated Raman spectrum corresponds to the experimental band at 1641 cm^{-1}. The theoretical 1053 cm^{-1} band is observed at 1036 cm^{-1} in the experimental spectrum, and the 757 cm^{-1} band is observed at 780 cm^{-1}. Some bands in the range of 1130 cm^{-1} to 1700 cm^{-1} in the theoretical spectrum are also visible in the experimental spectra, but most of their intensities are too low to be observed. There is also a band at 1555 cm^{-1}, which can be assigned to oxygen molecule and its presence can be explained by oxygen impurities in the nitrogen gas.

3.4.3. Photoisomerisation experiments

Both salicylic acid and acetylsalicylic acid can exist in different isomeric forms. As with open enol isomers of chloromalondialdehyde, they will only be observed in experimental spectra if certain conditions are fulfilled. First of all, the energy difference between these isomers has to be low enough so that the concentration of less stable isomer is sufficiently large and, more importantly, the potential barrier between these two states has to be high enough so that the molecule cannot easily be converted to the lower energy isomer.

Interconversion between these isomers could happen if there is enough external energy provided for the molecule to overcome the potential barrier between the two minima representing two different structures. First of all, if the surrounding temperature is high enough, the thermal energy alone is sufficient to trigger these transitions. In this case, the less stable isomers would convert into the most stable form which would be observed during annealing experiments. The only other way for the conformational interconversion to happen is through the photoexcitation of the molecule.
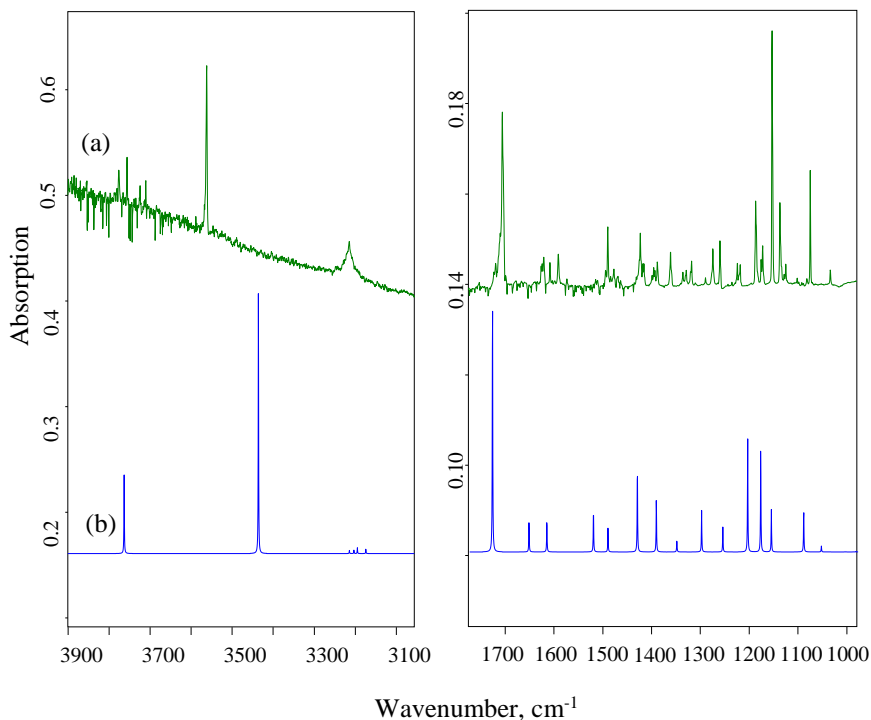
Figure 36. Infrared absorption spectra of SA isolated in argon matrix (a) and calculated spectrum of most stable isomer of SA molecule (b).

Theoretical calculations predict that the most stable isomer of salicylic acid makes up 99.8 % of the sample at room temperatures. The remaning 0.2 % is divided between higher energy isomers, none of which should be observed in the experimental spectra. The spectrum of salicylic acid isolated in argon matrix, and the calculated spectrum of the most stable SA isomer, E, are shown in figure 36. The OH stretching region is quite simple to interpret. There are two calculated bands of SA, corresponding to stretching OH vibrations in COOH and COH groups (at 3764 and 3436 cm^{-1}, respectively). The shift between them can be explained by the local environment in the groups, more specifically, by intramolecular hydrogen bond formed between hydrogen atom in COH and oxygen atom in COOH. In the experimental spectrum, there are bands at 3777, 3756, 3725, 3710, 3563 and 3214 cm^{-1}. The first four bands correspond to the vibrational modes of water molecule. The band intensities are quite low so the water impurities must be present, but not abundant, in the matrix sample. The other two bands, at 3563 cm^{-1} and

3214 cm^{-1} should correspond to OH stretching vibrations in the SA molecule. The difference between band positions in the experimental spectrum (349 cm^{-1}) is quite similar to the value predicted by the theoretical calculations (329 cm^{-1}). In the theoretical spectrum shown in figure 36, there are several bands due to CH vibrations in the ring of SA molecule. They are, however, of much lower intensity and are barely observable further on in the experimental spectrum. Overall, this region does not show any additional bands that could be assigned to higher energy isomers.

The situation is a little different in the region from 1800 to 600 cm^{-1} where many narrow bands can be observed. The calculations predict fewer bands than are observed in the spectrum but there is a good match between those that are predicted. The rest of the bands can be assigned to possible impurities in the sample. For example, the most intense calculated band is at 1729 cm^{-1} and corresponds well to the band at 1705 cm^{-1} in the experimental spectrum. There is an observable ASA band at 1752 cm^{-1} and several water bands in the 1640 cm^{-1} – 1650 cm^{-1} region. Here, the bands predicted by the calculations (1654 and 1617 cm^{-1}) can be seen as the structure of the water bands with which they overlap. Throughout the rest of the spectrum, there are no additional bands that suggest a second isomer could be seen experimentally which matches well with the theoretically calculated energy gap between these isomers.
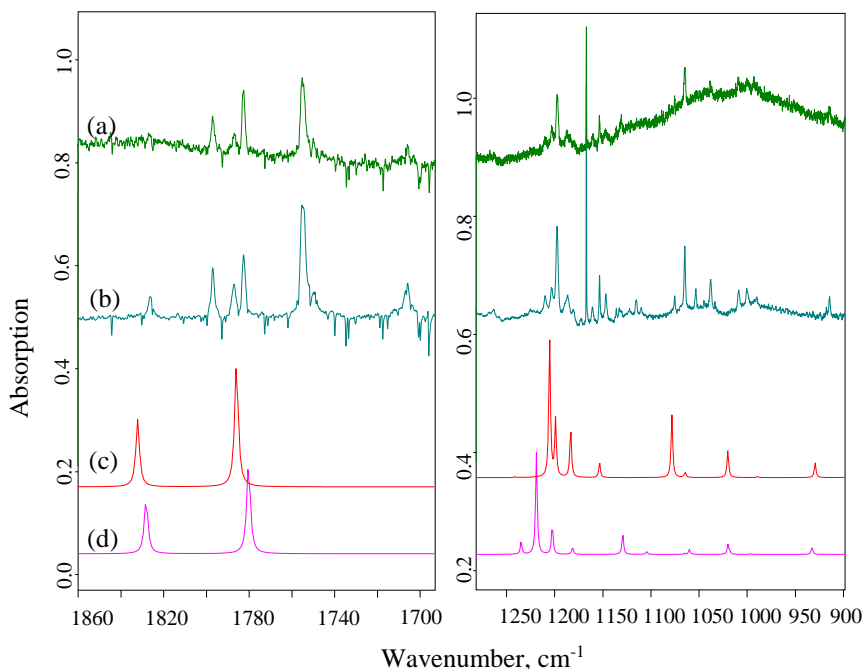
Figure 37. Infrared absorption spectra of ASA isolated in parahydrogen matrix with sample heating temperature of 50 ⁰C and 55 ⁰C (a, b) and calculated spectra of ASA isomers: 1a (c), 2a (d).

In contrast, the calculations predict a couple of ASA confomers to be closer in energy. The difference between the most stable isomer, 1a, and the isomer 2a is only 3.8 kJ/mol. That should correspond to 17 % concentration of higher energy conformer 2a in the room temperature sample according to Boltzmann distribution. Looking at the experimental spectrum of ASA in parahydrogen, and comparing it to the calculated spectra of 1a and 2a isomers (figure 37), it can be concluded that the second isomer is observed at small quantities. The OH stretching region is not depicted here because ASA OH vibrational bands have relatively low intensity and are difficult to observe in the presence of more intense bands of water impurities.

In figure 37, in the region from 1860 to 1700 cm^{-1} where C=O and C=C stretching vibrations can be observed, the bands between these two isomers should have a slight shift. Indeed, in both of the experimental spectra (of ASA sample heated to 50 ⁰C and 55 ⁰C), there are several bands which could be assigned to different isomers. First of all, the impurities should be identified. The band at 1705 cm^{-1} which has higher intensity in figure 37(b) (corresponding to the sample heated to slightly higher temperature) belongs

110

to SA. Comparison to calculated spectra and to experimental spectra of pure materials (pure AA samples) and relative intensity values allow the assignement of 1780 cm^{-1} band to acetic acid. The calculations for the 1a and 2a forms predict two bands with only slight shifts when comparing the two isomers. Since the 2a isomer should be less abundant, the intensities of the spectral bands assigned to it should be much lower. In this case, if the 1752 cm^{-1} band is assigned to ASA 1a isomer, the low intensity band at the foot of it (at 1749 cm^{-1}) could be the band of ASA 2a. The frequency shift would be similar to the calculated one. Then, the bands 1797 cm^{-1} and 1787 cm^{-1} could be assigned to the ones at 1832 cm^{-1} and 1829 cm^{-1} in the calculated spectrum. The frequency shift here is larger, and the relative intensities don't quite match. It is possible that the bands of two isomers overlap in the 1797 cm^{-1} band.
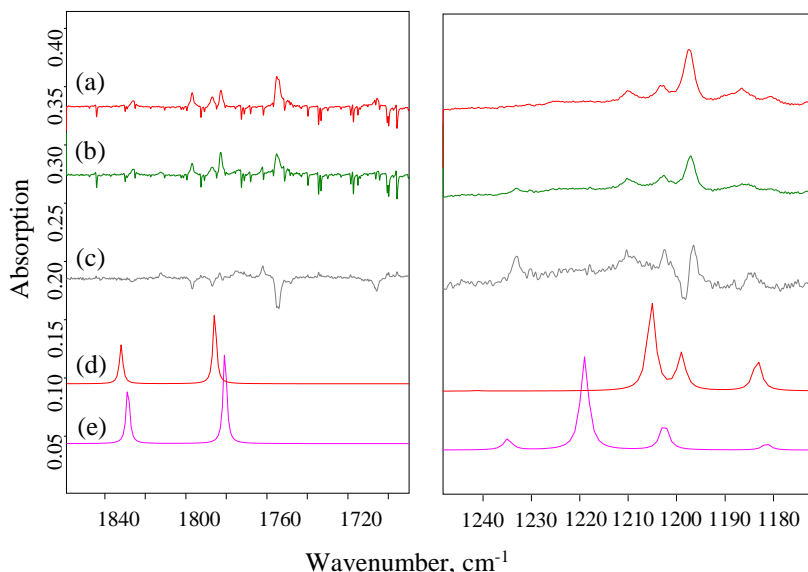
Figure 38. Infrared absorption spectra of acetylsalicylic acid isolated in parahydrogen matrix (a) after deposition; (b) after irradiation of the sample at 270 nm for 40 minutes; (c) difference spectrum of (b)-(a); calculated spctra of ASA (d) 1a and (e) 2a isomers.

In order to better evaluate the conformational variety, irradiation experiments were also performed on the samples with best ASA to dissociation products ratio. The irradiation was performed with a tunable

pulsed laser, at wavelengths of 300 nm, 290 nm and 270 nm. The biggest differences are observed after irradiation at 270 nm (figure 38). The same regions are shown in this figure as in figure 37.

The decrease of 1752 cm^{-1} band indicates disappearance of ASA, or at least the most stable isomer. As seen from the calculated spectra (figure 38, right) and discussed before, the shift between the most intense bands of the two isomers is only of several wavenumbers. Thus the changing shape of 1752 cm^{-1} could prove that isomer interconversion is observed in the matrix. One of the more obvious differences between 1a and 2a isomers is in the range of 1250 cm^{-1} – 1180 cm^{-1}. The band that decreases the most with irradiation of the sample is at 1199 cm^{-1} and could be assigned to the calculated 1a isomer band at 1205 cm^{-1}, belonging to ring deformation and νCO vibrations. The slight increase of intensity at 1210 cm^{-1} could be explained by growing intensity of 1219 cm^{-1} calculated band of 2a. There is also a band appearing at 1232 cm^{-1} that could fit well with the 2a isomer band, calculated to be at a similar position, even if the relative intensity change seems a little too big in comparison to others.

3.4.4. Associates with water

The annealing experiments were also performed for salicylic acid and acetylsalicylic acid molecules. First and foremost, they help detect the molecular complexes forming in matrix samples and identify new or growing spectral bands belonging to them. Since water molecules are small and move around more easily with given amounts of heat energy, most common complexes are water-water dimers and molecular associates of one SA (ASA) and one water molecule. For acetylsalicylic acid, the purest spectra were measured in parahydrogen matrix but the amount of the molecule is quite small and the annealing experiments don't show any changes in the OH stretching region. One of the more obvious differences there becomes clear when comparing the spectra of the samples heated to different temperatures. In the region 3580 cm^{-1} – 3560 cm^{-1}, there are at least three overlapping bands whose relative intensities depend on the sample heating temperatures. It is possible that these are molecular complexes but, as already mentioned, their intensities are not altered during annealing experiments.

SA + H₂O (I)   SA + H₂O (II)   SA + H₂O (III)
$E_B = 39.6$ kJ/mol $E_B = 16.7$ kJ/mol $E_B = 9.0$ kJ/mol
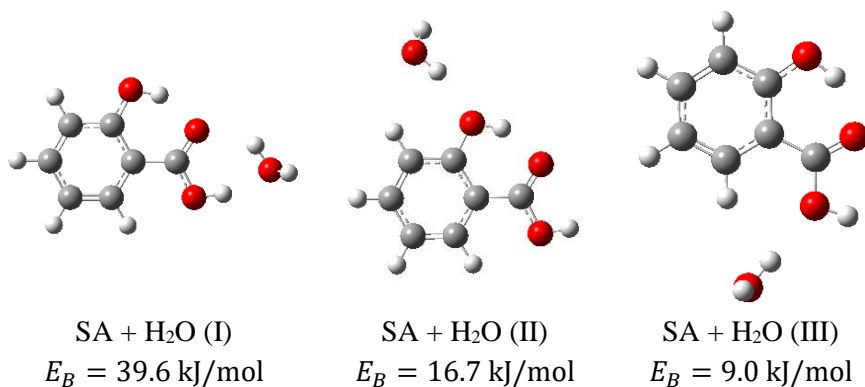
Figure 39. Possible configurations of salicylic acid and water molecular
complex and their binding energies.

As for salicylic acid, several different associates with water could be
formed in the matrix. Some of them with their calculated binding energies are
presented in figure 39. The most stable structure is the one where H_2O
molecule is bound to COOH group in salicylic acid molecule. The oxygen of
water molecule forms an intermolecular hydrogen bond with the hydrogen of
the OH group in SA, and one of the H_2O OH groups is turned towards oxygen
in C=O group of SA. The binding energy of this complex is 39.6 kJ/mol which
is significantly higher than the values calculated for acetylacetone and water
associates. Therefore, larger shifts in experimental spectra can be expected.

A few other associates were modeled, with some resulting in the most
stable complex. Two other shown here have significantly lower binding
energies and should not be experimentally observed.
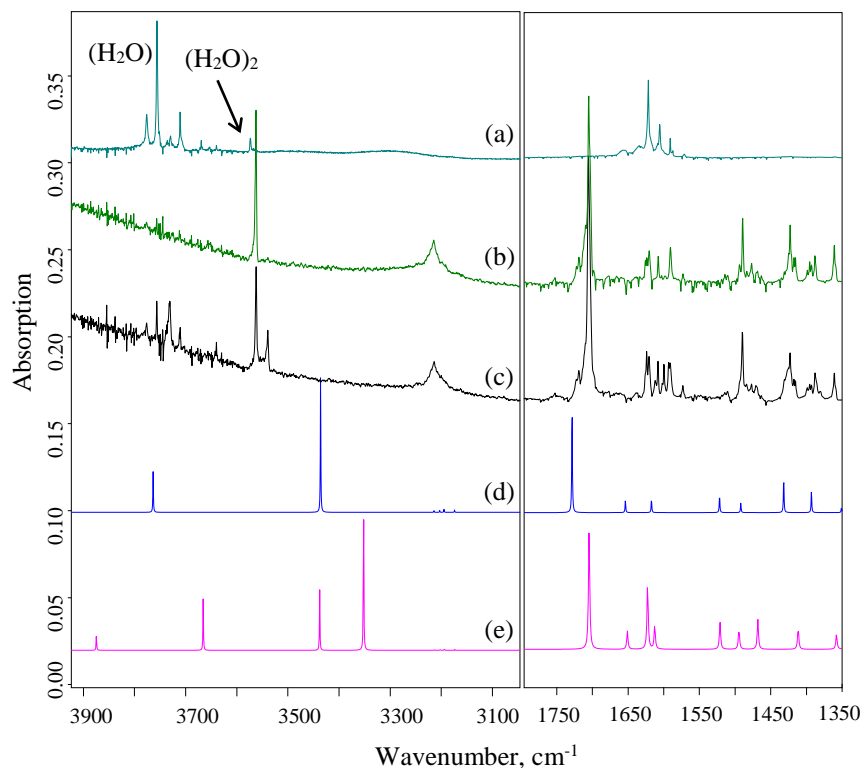
Figure 40. Infrared absorption spectra of (a) water, (b) SA, (c) SA and water, isolated in the argon matrix at 17, and calculated spectra of (d) SA, (e) SA+H$_2$O (I).

Figure 40 shows the OH stretching region of SA isolated in argon matrix. As mentioned previously, calculations predict two bands for SA in OH stretching region – at 3764 cm^{-1} for COOH and 3426 cm^{-1} for COH group. These can be observed in the experimental spectrum at 3563 cm^{-1} as a high intensity narrow band, and at 3215 cm^{-1} as a low intensity broad band. The shift and the broadness are due to intramolecular hydrogen bond in SA molecule.

A new band growing along with the water concentration (at 3540 cm^{-1}) can be clearly observed in figure 40(c). After comparing the experimental spectra with the calculated ones and in accordance to calculated binding energies, it can be determined that the water molecule is bound to the COOH group in the salicylic acid molecule. Therefore, the νOH of COH group does not exhibit a spectral shift upon addition of water, and the OH stretching band of COOH

group is shifted by about 300 cm^{-1}. Since there are two well-defined bands in the spectrum of salicylic acid, they can be attributed to these vibrational modes. Thus, in the salicylic acid and water spectrum, the band at 3540 cm^{-1} is assigned to the bound νOH mode in water, and the band formed on the slope of the 3200 cm^{-1} band belongs to the νOH of the COOH group participating in the intermolecular hydrogen bonding in the SA-water associate. The shift is quite large, and is in accordance with calculated energies, confirming a strong intermolecular hydrogen bond in salicylic acid and water associates.

Another region that is quite important for HB formation is the 1750 cm^{-1} – 1600 cm^{-1} region where water molecule δOH bands and SA molecule νC=O band can be observed. The water bands are at 1624 cm^{-1}, 1608 cm^{-1} and 1593 cm^{-1}. SA also has bands in this region at 1620 cm^{-1} and 1591 cm^{-1}, assigned to νC-C and νC=C vibrations in the ring combined with δOH deformations. There are several bands in the SA and water (figure 40(c)) that are not observed in either pure water or pure SA spectrum. These new bands are at 1612 cm^{-1} and 1599 cm^{-1}, and fit quite well with calculated bands of SA+H$_2$O complex (at 1623 cm^{-1} and 1651 cm^{-1}). Calculated and observed shift values between single molecule and complex bands are of several wavenumbers in both the experimental and calculated spectra. Exact values are difficult to calculate because the calculations predict three vibrational bands for SA+H$_2$O, each one assigned to combination of δOH in SA and δOH in the water molecule.

The νC=O values were calculated to be 1729 cm^{-1} for SA and at 1705 cm^{-1} for SA+H$_2$O. In the experimental spectra, this band can be observed at 1705 cm^{-1} and seems to not change at all upon the addition of water. However, closer observation does prove that the band shape is slightly altered with the intensity growing slightly in the lower wavenumber side. This could confirm νC=O band shift upon complex formation, even if the value is much lower than calculations predict. This shift is quite similar to the ones observed in acetylacetone and water samples where the calculations predicted small shift of νC=O band upon water complex formation and the experimental values were even lower.

3.4.5. Conclusions

Acetylsalicylic acid or aspirin, a non-steroidal anti-inflammatory drug, is both produced from salicylic acid and dissociates into it in the presence of water and upon being heated. Both ASA and SA are used in medicine to relieve pain and stop inflammation. The structural properties of molecules themselves had been mostly explored by theoretical methods. In this work, they were studied by the methods of low temperature matrix isolation and vibrational spectroscopy. The sample preparation was a complex procedure due to the low vapor pressure of these molecules and their tendency to dissociate while heated, especially in the case of ASA.

The optimal temperature for heating these samples was found to be around 50 ⁰C. In the case of SA, most of the infrared absorption spectra of the molecule isolated in argon matrix showed few impurity bands. SA was also isolated in nitrogen matrix for Raman scattering spectroscopy which is a new combination of methods that could provide more structural information. However, this method requires even longer and more difficult sample preparation. The infrared absorption spectra of ASA isolated in parahydrogen exhibited a fairly good signal to noise ration with least amount of thermal dissociation products. The analysis of these spectra and photoisomerization experiments revealed the presence of two isomers (1a and 2a), confirming theoretical calculations.

For SA, only one isomer was observed in as-deposited samples but more could be induced in further experiments with UV laser irradiation. As some of the SA samples had water impurities coming from the crystalline powder form of the sample, the complex bands were identified. The experimental data and the theoretical calculations confirmed that in the SA-water associate, water molecule forms an intermolecular hydrogen bond with COOH group in SA molecule.

CONCLUSIONS

1. It has been shown that proton tunneling can be observed for 2-chloromalondialdehyde molecule at very low temperatures in argon (7 K) and parahydrogen (3 K) but not neon matrices. Experimentaly observed band splittings of 5 cm^{-1} in Ar matrix and 8 cm^{-1} in pH$_2$ matrix are in good agreement with theoretically calculated value of 12 cm^{-1}.

2. Two out of eight predicted enol isomers of chloromalondialdehyde are observed in low temperature matrices – CCC and TTC. Out of XYC and XYT pairs, one isomer can be selectively produced by irradiation at specific wavelengths in 230-300 nm range.

3. Experimental and theoretical results show that for fluorinated acetylacetone derivatives, the strongest intramolecular hydrogen bond is in acetylacetone, weakest – in hexafluoroacetylacetone, with trifluoroacetylacetone in between. Intermolecular hydrogen bond in associates with water follows the same pattern, and has little effect on the strength of the IHB.

4. The more abundant isomer of trifluoroacetylacetone (AcAcF3(CO)) is stabilized by π electron delocalization in the chelated ring. However, both isomers were observed at low temperatures in different matrix environments (neon, argon, parahydrogen, xenon, nitrogen, carbon monoxide), with higher concentrations of AcAc(OH) in nitrogen and carbon monoxide matrices, as well as in samples with more water impurities.

5. Salicylic and acetilsalycic acid can be observed in low temperatures if the samples are heated in the range of 50 ⁰C. Thermal dissociation products were observed upon heating samples at higher temperatures.

6. One isomer of SA and two of ASA are present in the samples. The most stable structure of the associate formed from one SA and one H$_2$O molecule is where water molecule is bound to COOH group in SA.

SANTRAUKA LIETUVIŲ KALBA
ĮVADAS

Vandenilinis ryšys yra be galo svarbus visuose biologiniuose ir biocheminiuose procesuose, kasdien vykstančiuose mūsų pasaulyje. Vandenilinio ryšio stipris gali varijuoti nuo labai silpno (1 kJ/mol) iki stipraus, prilygstančio kovalentiniams ryšiams (150 kJ/mol) [5, 7]. Tai labai svarbu biologinėse sistemose, kurios turi būti dinamiškos ir nuolat prisitaikyti prie besikeičiančių aplinkybių. Pavyzdžiui, DNR gijos, surištos vandeniliniais ryšiais, turi atsiskirti prieš vykstant replikacijos procesui. Dviguboje spiralėje vandeniliniai ryšiai stiprina vienas kitą ir stabilizuoja sistemą, o kai reikia DNR kopijuoti – kiekvieną sekantį ryšį vis lengviau nutraukti [28]. Toks ryšio stiprinimas (silpninimas) daug vandenilinių ryšių turinčioje sistemoje vadinamas kooperatyviniu (antikooperatyviniu) efektu, geriausiai jis ištirtas vandens molekulių sistemose.

Molekulinė struktūra ir tiek vidiniai, tiek tarpmolekuliniai vandeniliniai ryšiai yra vienas nuo kito priklausomi. Pavyzdžiui, molekulėse su aromatiniais žiedais π elektronai delokalizuojasi ir toks krūvio persiskirstymas gali reikšti, kad padidėja vandenilinio ryšio akceptoriaus dalinis neigiamas, o donoro – dalinis teigiamas krūvis, todėl vandenilinio ryšio stipris didėja [36-43]. Pasikeitus molekulinei struktūrai, pavyzdžiui, pakeičiant vieną atomą kitu, didesniu arba labiau elektroneigiamu, paveikiamas ir vandenilinis ryšys [44-46]. Apibendrinant galima teigti, kad minėta π elektronų delokalizacija molekulėse su vidiniais vandeniliniais ryšiais, šiuo ryšius stiprina. Tai vadinama rezonanso stiprinamu vandeniliniu ryšiu (RAHB).

β-diketonų šeimos molekulės pasižymi tokiu vandenilinio ryšio tipu [51, 52]. Šios molekulės gali egzistuoti kaip du tautomerai – *enol* ir *keto*. *Keto* forma yra labiau polinė, todėl dažniausiai stebima poliniuose tirpaluose [53-56]. Kitose aplinkose *enol* forma pastebima dažniau, nes ją stabilizuoja vidiniais vandenilinis ryšys. Kita molekulių klasė su vidiniais vandeniliniais ryšiais ir dar paprastesne struktūra yra aldehidai [48]. Šios gana paprastos sistemos gali būti naudojamos tiriant protonų tuneliavimą tarp dviejų deguonies atomų. Protonų tuneliavimas, arba pernaša, nulemia sudėtingas sąveikas molekuliniame lygmenyje, o jos savo ruožtu daro įtaką makroskopinio pasaulio procesams. Viena iš svarbiausių reakcijų, susijusių su tokia krūvių pernaša, yra fotosintezė. Labai svarbu suprasti, kaip šie procesai vyksta ir kokių sąlygų reikia jiems palaikyti. Tačiau iš prigimties šie

procesai yra labai greiti, todėl juos sunku stebėti [57–60]. Idealiu atveju analizė būtų vykdoma tik su viena molekule, izoliuota inertiškoje aplinkoje.

Dialdehidų ir diketonų šeimos molekulės gali būti naudojamos kaip modelinės sistemos protono pernašai ir vandenilinio ryšio stipriui tirti, tačiau jos ir pačios yra svarbios biologinėse sistemose. Malondialdehidas yra dažnai naudojamas kaip oksidacinio streso žymeklis. Ši molekulė gaunama lipidus peroksiduojant polinesočiosiomis riebalų rūgštimis, ir lengvai sąveikauja su proteinų, lipoproteinų, DNR ir RNR funkcinėmis grupėmis. Malondialdehidas yra reaktyvi ir potencialiai mutageninė medžiaga [61, 62]. Acetilacetono molekulė nėra tokia svarbi biologinėse sistemose, tačiau ji buvo naudota kaip tarpinė medžiaga sintetinant heterociklines medžiagas biologiškai aktyviems junginiams bei vaistus. Acetilacetonas taip pat naudojamas valant nuotekų vandenį nuo metalų priemaišų ir apsaugant medžiagas nuo korozijos [63, 64].

Struktūrinė informacija dažnai gaunama tiriant molekulinius virpesius infraraudonosios spinduliuotės sugerties spektroskopijos metodu [66, 67]. Tačiau kambario temperatūros bandinių spektrams yra būdingos plačios, nespecifinės juostos. Tokie spektrai neteikia informacijos apie labai nedidelius pokyčius ar greitus procesus – tokius kaip kaip protonų pernaša ar vienos funkcinės grupės pasisukimas molekulėje. Infraraudonosios sugerties spektroskopinis metodas suteikia geresnių rezultatų, kai yra derinamas su žemos temperatūros matricine izoliacija, ir gali būti naudojamas tiek gilesnei žinomų medžiagų analizei, tiek naujų junginių charakterizavimui [68-77]. Tiriamos molekulės yra izoliuojamos kietoje inertinių dujų matricoje, kur jos nesąveikauja nei tarpusavyje, nei su aplinka. Šis tarpmolekulinių sąveikų susilpninimas ir žemos temperatūros aplinka užtikrina, kad užregistruotus spektrus yra gana lengva analizuoti. Be to, matricoje izoliavus molekules, ir jas paveikus spinduliuote, galima stebėti molekulių fotoizomerizaciją, išvengiant jų disociacijos. Žemos temperatūros matricinės izoliacijos metodas buvo naudojamas atliekant platų spektrą eksperimentų, taip pat ir analizuojant acetilacetono, malondialdehido, jų darinių molekules ir konformacinę įvairovę [78-83]. Pagrindinis reikalavimas matricos dujoms yra silpna mėginio ir matricos molekulių sąveika. Inertinės dujos puikiai išpildo tokį reikalavimą, tačiau siauriausiomis spektrinėmis juostomis ir mažiausia sąveika su bandiniu pasižymi paravandenilio matrica. Vis dėl to, eksperimentai su šia matrica sunaudoja daugiau resursų dėl sudėtingo paravandenilio paruošimo [56, 67, 68, 84-86].

DARBO TIKSLAS IR UŽDUOTYS

Siekiant geriau suprasti sudėtingų biologinių molekulių struktūrą bei jose vykstančius procesus, reikia atlikti išsamią modelinių sistemų analizę. Šiame darbe modelinės molekulės buvo naudojamos vidiniui bei tarpmolekuliniui vandeniliniam ryšiui bei su juo susijusiai protono pernašai bei fotoizomerizacijai tirti. Išsikeltas šio baigiamojo darbo tikslas buvo žemos temperatūros matricinės izoliacijos ir virpesinės spektroskopijos metodų taikymas analizuojant molekules, turinčias vidinį vandenilinį ryšį – malondialdehido ir acetilacetono darinius, taip pat acetilsalicilo ir salicilo rūgštis. Šiam tikslui pasiekti buvo suformuluotos konkrečios užduotys:

1. Užregistruoti chloromalondialdehido molekulių, izoliuotų žemos temperatūros matricos aplinkoje, virpesinius spektrus, ir iš virpesinių juostų struktūros padaryti išvadas apie protono tuneliavimą molekulėje.

2. Stabilizuoti atvirus chloromalondialdehido *enol* izomerus, paveikus molekulę lazerine spinduliuote.

3. Fluoruotų acetilacetono darinių tyrimui pritaikius žemos temperatūros virpesinės spektroskopijos metodus, gauti informaciją apie vidinio ir tarpmolekulinio vandenilinio ryšio, susidariusio asociatuose su vandeniu, stiprumą.

4. Užregistruoti asimetrinio acetilacetono darinio – trifluoracetilacetono – virpesinius spektrus skirtingose matricinėse aplinkose, siekiant ištirti didesnės energijos izomero AcAcF3(OH) koncentraciją jose.

5. Taikant žemos temperatūros virpesinės spektroskopijos metodus žemo sočiųjų garų slėgio acetilsalicilo rūgšties ir salicilo rūgšties bandiniams, ištirti jų konformacines savybes.

GINAMIEJI TEIGINIAI

1. Protono tuneliavimas buvo pirmą kartą stebimas chloromalondialdehido molekulėje, izoliuotoje paravandenilio matricoje esant labai žemai temperatūrai (3 K).

2. Keturi iš aštuonių teoriškai apskaičiuotų chloromalondialdehido izomerų gali būti selektyviai sukuriami žemos temperatūros matricose, paveikiant molekules specifinio bangos ilgio lazerine spinduliuote.

3. Eksperimentiškai stebint kompleksus tarp vandens ir acetilacetono molekulių bei įvertinus jų energijas, galima patvirtinti, kad tarpmolekulinis vandenilinis ryšys turi mažai įtakos acetilacetono molekulių vidinio vandenilinio ryšio stiprumui.

4. Visose tirtose matricose (neono, argono, paravandenilio, ksenono, azoto, anglies monoksido) patvirtintas dviejų trifluoracetilacetono izomerų egzistavimas. Izomerų koncentracijų santykis priklauso nuo matricos aplinkos.

5. Nustatyta optimali temperatūra ASA ir SA mėginiams kaitinti (50 °C), kuriai esant matricinės izoliacijos bandinyje beveik nėra šiluminės disociacijos produktų. Žemos temperatūros argono matricoje stebimas vienas salicilo rūgšties ir du acetilsalicilo rūgšties izomerai.

6. Žemos temperatūros matricos aplinkoje galima stabilizuoti tik vieną salicilo rūgšties ir vandens komplekso struktūrą.

PUBLIKACIJŲ DOKTORANTŪROS TEMA SĄRAŠAS

1. Justinas Čeponkus, Rasa Platakytė, Valdas Šablinskas, Alejandro Gutiérrez-Quintanilla, FTIR study of acetylacetone, D2-acetylacetone and hexafluoroacetylacetone - water complexes in argon and nitrogen matrices, Chemija, 29(1), p. 1–16, 2018.

2. Alejandro Gutiérrez-Quintanilla, Michèle Chevalier, Rasa Platakytė, Justinas Čeponkus, Germán A. Rojas-Lorenzo, Claudine Crépin, 2-Chloromalonaldehyde, a Model System of Resonance-Assisted Hydrogen Bonding: Vibrational Investigation, Physical Chemistry Chemical Physics, 20(18), p. 12888 – 12897, 2018.

3. Alejandro Gutiérrez-Quintanilla, Michèle Chevalier, Rasa Platakytė, Justinas Čeponkus, Claudine Crépin, Selective photoisomerisation of 2-chloromalonaldehyde, Journal of Chemical Physics, 150(3), 034305, p. 1 – 11, 2019.

4. Rasa Platakytė, Alejandro Gutiérrez-Quintanilla, Valdas Šablinskas, Justinas Čeponkus, Influence of environment and association with water to internal structure of trifluoroacetylacetone. Matrix isolation FTIR study, Low Temperature Physics, 45(6), p. 722-735, 2019.

5. Alejandro Gutiérrez-Quintanilla, Michèle Chevalier, Rasa Platakytė, Justinas Čeponkus, Claudine Crépin, Intramolecular hydrogen tunneling in 2-chloromalondialdehyde trapped in solid para-hydrogen, Physical Chemistry Chemical Physics, 22(11), p. 6115-6121, 2020.

6. Alejandro Gutiérrez-Quintanilla, Rasa Platakytė, Michèle Chevalier, Claudine Crépin, Justinas Čeponkus, Hidden Isomer of Trifluoroacetylacetone Revealed by Matrix Isolation Infrared and Raman Spectroscopy, The Journal of Physical Chemistry A, 125(11), p. 2249-2266, 2021.

PUBLIKACIJŲ NE DISERTACIJOS TEMA SĄRAŠAS

1. Yevhenii Vaskivskyi, Yelyzaveta Chernolevska, Antonina Vasylieva, Valeriy Pogorelov, Rasa Platakyte, Joana Stocka, Iryna Doroshenkoa, 1-Hexanol isomers in a nitrogen matrix: FTIR study and high-level abinitio calculations, Journal of Molecular Liquids, 278, p. 356 – 362, 2019.

2. Vilma Jonauskė, Rimantas Ramanauskas, Rasa Platakytė, Gediminas Niaura, Lina Mikoliūnaitė, Kunio Ishikawa, Aivaras Kareiva, Formation of 2D calcium hydroxyapatite on stainless steel modified with a TiN sublayer, Mendeleev Communications, 30-4, p. 512-515, 2020.

3. Thomas M. C. McFadden, Rasa Platakytė, Joanna Stocka, Justinas Čeponkus, Valdemaras Aleksa, T. Carrigan-Broda, Valdas Šablinskas, Paweł Rodziewicz, Gamil A. Guirgis, Experimental (Raman and IR) and computational (DFT, MP2) studies of conformational diversity of 1-chloromethyl-1- fluorosilacyclohexane, Journal of Molecular Structure, 1221, p. 1-10, 2020.

4. Joanna Stocka, Rasa Platakytė, Thomas M. C. McFadden, Justinas Čeponkus, Valdemaras Aleksa, A. G. Hanna, Valdas Šablinskas, Paweł Rodziewiczc, Gamil A. Guirgis, Conformational diversity of 1-chloro-1-chloromethylsilacyclohexane with experimental (Raman and IR) and computational (DFT, MP2) methods, Journal of Molecular Structure, 1249, 2022.

PRANEŠIMAI KONFERENCIJOSE

1. Justinas Čeponkus, Rasa Platakytė, Claudine Crepin-Gilbert, Alejandro Gutierrez, Michèle Chevalier, Valdas Šablinskas, Vandens ir acetilacetono asociatų struktūros tyrimas matricinės izoliacijos infraraudonosios sugerties spektriniu metodu, LNFK, Vilnius, 2015.

2. Rasa Platakytė, Justinas Čeponkus, Valdas Šablinskas, Study of water-acetylacetone complexes by the means of matrix isolation infrared spectroscopy, Chemistry and Physics at low temperatures, Biarritz, Prancūzija, 2016.

3. Joanna Lach, Rasa Platakytė, Justinas Čeponkus, Valdas Šablinskas, Conformational analysis of tetrahydrofurean by means of FT-IR matrix isolation spectra - hot nozzle experiment, Open Readings, Vilnius, 2016.

4. Rasa Platakytė, Joanna Lach, Justinas Čeponkus, Claudine Crepin-Gilbert, Alejandro Gutierrez, Michele Chevalier, Valdas Šablinskas, Study of water-acetylacetone complexes by the means of matrix isolation infrared absorption spectroscopy, Open Readings, Vilnius, 2016.

5. Rasa Platakytė, Justinas Čeponkus, Claudine Crepin-Gilbert, Valdas Šablinskas, Fluoruotų acetilacetono darinių struktūros ir sąveikos su vandens molekulėmis tyrimas, LNFK, Vilnius, 2017.

6. Rasa Platakytė, Justinas Čeponkus, Study of Acetylsalicylic Acid by the Means of Matrix Isolation, EUCMOS, Coimbra, Portugalija, 2018.

7. Rasa Platakytė, Justinas Čeponkus, Valdas Šablinskas, Study of 3-methyl-acetylacetone structure and interaction with water, Open Readings, Vilnius, Lietuva, 2018.

8. Rimantė Bandzevičiūtė, Rasa Platakytė, Sonata Adomavičiūtė, Martynas Velička, Justinas Čeponkus, Vidita Urbonienė, Feliksas Jankevičius, Valdas Šablinskas, Optical fiber based spectroscopic device for in vivo detection of pathological tissue areas, Life Science Baltics, Vilnius, Lietuva, 2018.

9. Rasa Platakytė, Justinas Čeponkus, Conformational analysis of butanol and its complexes with water in low temperatures, Horizons in Hydrogen Bond Research, Amsterdamas, Nyderlandai, 2019.

10. Rasa Platakytė, Justinas Čeponkus, Valdas Šablinskas, Gamil A. Guirgis, Conformational analysis of 1-fluoro-1-chlormethylsilacyclohexane by vibrational spectroscopy, LNFK, Kaunas, 2019.

11. Morta Stadulytė, Rasa Platakytė, Justinas Čeponkus, Vaidas Pudžaitis, Library of red pigment Raman spectra and pigment identification in painted works of art, Open Readings, 2021.

12. Joanna Stocka, Rasa Platakytė, Justinas Čeponkus, Valdas Šablinskas, Gamil A. Guirgis, Paweł Rodziewiczc, Computational and experimental vibrational study of 1-chloromethyl-1-fluorosilacyclohexane conformations and its rearrangements, Open Readings, 2021.

13. Rasa Platakytė, Justinas Čeponkus, Claudine Crepin-Gilbert, Wutharath Chin, Julien Berthomier, Structural analysis of acetylsalicylic acid and its thermal dissociation products by low-temperature vibrational spectroscopy, LNFK, Vilnius 2021.

DARBO NAUJUMAS

Šiame darbe chloromalondialdehido molekulė buvo pirmą kartą analizuota eksperimentiniais – matricinės izoliacijos virpesinės spektroskopijos – metodais. Eksperimentiniai rezultatai įrodė, kad protono tuneliavimas

chloromalondialdehido molekulėje gali vykti žemos temperatūros matricos aplinkoje. Ištirta chloromalondialdehido konformacinė įvairovė, įrodant, kad chloromalondialdehidas yra pirmasis β-aldehidų ir β-diketonų šeimų narys, kurio vienas iš aukštesnės energijos *enol* izomerų egzistuoja kambario temperatūroje. Taip pat buvo nustatyta kuriuos izomerus galima sukurti fotoizomerizacijos eksperimentų metu, bandinį apšviečiant ultravioletine spinduliuote.

Trifluoroacetilacetono molekulė, turinti asimetrinį dvigubo minimumo potencialą, buvo ištirta žemos temperatūros IR ir Ramano spektroskopiniais metodais ir pirmą kartą buvo įrodyta, kad matricoje egzistuoja didesnės energijos AcAcF3(OH) izomeras. Kiekybiškai įvertinta jo koncentracijos priklausomybė nuo aplinkos.

Acetilsalicilo rūgštis pirmą kartą buvo izoliuota žemos temperatūros matricose, o jos konformacinė įvairovė ištirta infraraudonosios sugerties spektroskopijos ir fotoizomerizacijos eksperimentų metu. Sujungus žemos temperatūros matricos izoliaciją ir Ramano sklaidos spektroskopiją, buvo sukurtas naujas analizės metodas. Ramano sklaidos spektroskopijos matavimai yra daug sudėtingesni nei IR, nes bandinys turi būti daug labiau koncentruotas, kad užregistruoti spektrai turėtų pakankamą signalo ir triukšmo santykį. Metodas buvo pritaikytas acetilacetono ir salicilo rūgšties analizei.

DISERTACIJOS SANDARA

Disertaciją sudaro įvadas, trys pagrindiniai skyriai, literatūros sąrašas ir priedai. Pirmajame skyriuje apžvelgiamas rezonanso stiprinamas vandenilinis ryšys, ir būdai nustatyti jo stiprį tiriamųjų molekulių kontekste. Taip pat aprašomi tyrimai, iki šiol atlikti su malondialdehido, chloromalondialdehido, acetilacetono ir jo darinių bei acetilsalicilo ir salicilo rūgšties molekulėmis, daugiausia dėmesio kreipiant į matricinės izoliacijos metodo taikymą šių molekulių struktūriniuose tyrimuose. Antrajame skyriuje daugiau dėmesio skiriama matricinės izoliacijos technikai, jos privalumams bei trūkumams, dažniausiai naudojamoms matricinėms dujoms. Iš jų smulkiau aprašomas paravandenilio matricos paruošimas. Taip pat glaustai aptariami teorinių skaičiavimų metodai – *ab initio* bei tankio funkcionalo teorija, skaičiavimuose naudojamos bazinės funkcijos. Trečiojo skyriaus pradžioje aprašoma tyrimų metodika, tada trijuose skyreliuose pateikiami tyrimų rezultatai. Pirmajame iš jų aprašoma chloromalondialdehido molekulė, daugiausia dėmesio skiriant

protono tuneliavimo procesui, taip pat pateikiama informacija apie molekulės konformacinę įvairovę bei ji palyginama su malondialdehido molekule. Antrajame aprašomos acetilacetono ir jo darinių vidinio vandenilinio ryšio stiprio tendencijos, asociatai tarp acetilacetono ir vandens molekulių, taip pat daugiau dėmesio skiriama nesimetriškai trifluoroacetilacetono molekulei. Galiausiai pristatomi acetilsalicilo ir salicilo rūgščių molekulių tyrimų rezultatai, jų konformacinė įvairovė bei matricose susiformuojantys kompleksai su vandeniu.

TYRIMŲ METODIKA

Acetilacetonas (99%), trifluoroacetilacetonas (98%) ir heksafluoroacetilacetonas (99%) iš Sigma-Aldrich bei chloromalondialdehidas iš Acros, (95%) buvo naudojami be tolimesnio gryninimo, tik išvalant juos vakuuminėje sistemoje. Tai buvo atliekama šiuos skystus bandinius užšaldant panaudojus skystą azotą, tada išsiurbiant priemaišas – juose ištirpusias dujas – ir vėl iki galo atšildant bandinį. Malondialdehidas, kaip nestabili molekulė, buvo sintetinamas prieš pat matavimus pagal metodą aprašytą [183] šaltinyje. Vanduo buvo filtruojamas ir distiliuojamas naudojant EASYpure RoDi (Thermo Fisher Scientific) vandens valymo sistemą ir išvalomas nuo priemaišų tokiu pačiu principu, kaip ir aukščiau paminėtos medžiagos. Azoto (99,999 %), argono (99,999 %), ksenono, neono ir anglies monoksido dujos iš Elme Messer Gaas buvo naudojamos be papildomo apdorojimo. Dvigubai deuteruotas acetilacetonas buvo paruoštas naudojant metodą, aprašytą [83] šaltinyje. Salicilo rūgštis (Sigma–Aldrich, 99 %) ir acetilsalicilo rūgštis (Alfa Aesar, 99 %) buvo naudojamos miltelių pavidalu, ir todėl turėjo būti kaitinamos, kad galėtų būti sumaišytas dujinės fazės matricinis bandinys.

Eksperimentuose buvo naudojamos kelios skirtingos sistemos. Pirmojoje (esančioje Vilniuje, Lietuvoje) vakuuminėje sistemoje bandinys ir matricinės dujos buvo sumaišomas, įvertinant jų koncentracijas pagal dalinį dujų slėgį. Įprasto eksperimento metu buvo sumaišoma 1 mbar bandinio molekulės ir 500 mbar matricos dujų. Eksperimentuose su dvejomis bandinio medžiagomis (acetilacetonu ir vandeniu), šių molekulių santykis buvo įvairus (1 mbar acetilacetono ir 0,5–5 mbar vandens). Įprasto eksperimento metu maždaug 20 mmol dujų mišinio per 90 minučių buvo nusodinama ant spektrinio langelio (cezio jodido), laikomo 10 K temperatūroje uždaro ciklo He kriostate (Leybold-Heraeus RW2). Naujausiuose eksperimentuose su salicilo rūgštimi

ir acetilsalicilo rūgštimi, naudotas JANIS kriostatas, kuris gali pasiekti 3 K temperatūrą.

Infraraudonųjų spindulių sugerties spektrai buvo registruojami 500-4000 cm^{-1} srityje, naudojant Bruker IFS 113 spektrometrą su 1 cm^{-1} skyra. Fono spektrai ir bandinio spektrai buvo registruojami tomis pačiomis sąlygomis, suvidurkinant 256 spektrus. Siekiant pamatyti komplekso susidarymą matricoje, buvo atlikti atkaitinimo eksperimentai, temperatūrą keliant iki 30 K ir paskui vėl nuleidžiant iki 10 K. Ramano sklaidos eksperimentų metu buvo atlikta panaši procedūra. Įprasto eksperimento mišinio santykis buvo 1:100 analizuojamos medžiagos (šiuo atveju trifluoracetilacetono) molekulės ir matricos dujų, kad būtų gautas geresnis Ramano sklaidos signalo intensyvumas. Spektrai buvo registruojami 50-5000 cm^{-1} diapazone Bruker FT-Raman spektrometru su 4 cm^{-1} ir 1 cm^{-1} skyra. Nusodinimas (šiuo atveju ant kriostato viduje esančio veidrodžio, o ne spektrinio langelio) truko maždaug 2–3 val. Salicilo rūgšties ir acetilsalicilo rūgšties bandinių nusodinimo procedūra buvo šiek tiek kitokia ir bus aprašyta toliau.

IR tyrimams Orsay mieste, Prancūzijoje, buvo naudojamos dvi skirtingos matricinės izoliacijos sistemos. Pirmoje bandiniai buvo izoliuojami argono ir neono dujų matricose. Kita sistema buvo naudojama paravandenilio matricai, nes prieš kiekvieną eksperimentą turėjo būti atliekama orto/para konversija. Šiuo atveju bandinio ir matricos dujų maišymas vyko kartu su nusodinimu. Eksperimento metu buvo naudojami du uždaro ciklo helio kriostatai, sujungti nerūdijančio plieno vamzdeliu. Pirmasis kriostatas buvo naudojamas orto/para-vandenilio konversijos procesui (Air Products, Displex DE202) su Fe$_2$O$_3$ miltelių (Sigma-Aldrich 99 %) katalizatoriumi, o kitas – bandinio nusodinimui (ICE: Innovative Cryogenic Engineering, RDK 415D, He kompresorius: Sumitomo F-50). Orto/para konversijai reikalinga temperatūra yra ne aukštesnė nei 18 K, nes paskui pradeda didėti orto priemaišų koncentracija. Po konversijos pH$_2$ buvo paleidžiamas vamzdeliu, prie kurio buvo pritvirtintas mažas rezervuaras su bandiniu. Du Swagelok mikrovožtuvai leido valdyti dujų srautą (pH$_2$) ir garų kiekį iš bandinio. Dujų mišinys buvo nusodinamas ant deimantinio langelio (2,8 K) kriostate. Vakuumas šiame kriostate buvo palaikomas turbomolekuliniu siurbliu (Oerlikon, Leybold vakuuminis, Turbovac 600C, siurbimo greitis H2: 570 ls^{-1}), kuris leido pasiekti žemesnį nei 10^{-6} mbar slėgį. Paravandenilio konversijos sistema buvo pumpuojama difuziniu siurbliu (CIT Alcatel). Molekulėms, turinčioms aukštą garų slėgį, garavimui kontroliuoti buvo naudojamos vėsinančios ledo ir druskos vonios.

Spektrai buvo matuojami naudojant FTIR spektrometrą (Nicolet Nixus 670/680) su SiC (silicio karbido) šaltiniu ir MCT (HgCdTe – gyvsidabrio kadmio telūrido) detektoriumi, aušinamu skystu azotu. Suvidurkinamų spektrų skaičius įprastiniame eksperimente buvo 1024 (nors kartais buvo jų vidurkinama ir mažiau – 256 arba 512), spektrinis diapazonas buvo tarp 4000 cm^{-1} ir 500 cm^{-1}, tipinė skyros vertė 0,5 cm^{-1}. Fono spektrai buvo registruojami prieš kiekvieną eksperimentą tomis pačiomis sąlygomis. Spektrometras buvo valdomas naudojant Omnic 7.3 programinę įrangą, tačiau analizė dažniausiai buvo atliekama naudojant OPUS programinį paketą.

Salicilo ir acetilsalicilo rūgšties molekulės turi žemą garų slėgį, todėl šias medžiagas reikia kaitinti, norint gauti matricinį bandinį. Tokiu atveju neįmanoma tiksliai nustatyti susimaišiusių medžiagų koncentracijos. Miltelių pavidalo mėginiai buvo dedami į talpą, esančią ant vamzdelio, per kurį matricos dujos patenka į kriostatą. Pirmųjų eksperimentų metu talpa su salicilo arba acetilsalicilo rūgšties milteliais buvo šildoma varžiniu kaitinimo elementu, o temperatūra reguliuojama pagal maitinimo įtampą. Vėliau geresni rezultatai buvo pasiekti, kai talpa buvo kaitinama karšto oro srove. Ši sistema buvo įrengta taip, kad termoelementas, prijungtas prie bandinio talpos, rodytų 50 ºC temperatūrą. Matricos dujoms einant per vamzdelį, jos tuo pačiu metu „paimdavo" bandinio molekules taip, kad galutinis mišinys nusėstų ant kriostato spektrinio langelio (arba veidrodžio, jei tai buvo Ramano sklaidos eksperimentai). Infraraudonųjų spindulių sugerties eksperimentuose Vilniuje kaip matricos dujos dažniausiai buvo naudojamas argonas, o nusodinimas (kaitinant karšto oro srautu) užtrukdavo iki valandos. Ramano sklaidos eksperimentų metu nusodinimas užtruko apie keturias valandas, čia dažniausiai buvo naudojamos azoto dujos. Nusodinimo metu abiejose sistemose buvo palaikoma pastovi 17 K temperatūra. Orsay mieste, Prancūzijoje, taip pat buvo atlikti eksperimentai su salicilo ir acetilsalicilo rūgšties molekulėmis, daugiausia paravandenilio matricose. Kaitinimo temperatūra buvo nustatyta maždaug tokia pati (40-50 ºC), kad būtų gauta pakankama bandinio koncentracija geram signalo ir triukšmo santykiui spektre, bet būtų sumažinta terminės disociacijos produktų koncentracija.

Fotochemijos eksperimentai buvo atlikti tik Orsay mieste, Prancūzijoje. Jie buvo atliekami panaudojant optinį parametrinį osciliatorių iš Continuum, kuris buvo kaupinamas Nd:Yag (neodimiu legiruoto itrio aliuminio granato) lazeriu. Bandinio veikimo spinduliuote laikas svyravo nuo 10 minučių iki maždaug 40 minučių. Paprastai ilgas švitinimas tuo pačiu bangos ilgiu buvo

atliekamas smulkesniais žingsniais, tarp jų registruojant infraraudonosios sugerties spektrus.

Tankio funkcionalo teorija (DFT) B3LYP/6-311++G(3df,3dp) lygiu buvo naudojama analizuojamų molekulių, jų izomerų ir kompleksų su vandeniu geometrijoms optimizuoti ir apskaičiuoti harmoniniams virpesiniams dažniams. Visos molekulės buvo sumodeliuotos Gaussview 5.08, o skaičiavimai atlikti naudojant Gaussian 09 programos paketą [180] Vilniaus universiteto Fizikos fakulteto didelio našumo skaičiavimo centre „HPC Saulėtekis". Tipiškai skaičiavimų metu buvo naudojamas *nosymm* raktinis žodis, siekiant užtikrinti, kad skaičiavimo programa nebandytų pasiekti neteisingos molekulių simetrijos. Nustatyta, kad tai labai svarbu skaičiuojant acetilacetono molekules, nes potencinė duobė CH_3 grupių sukimosi modai yra labai negili. Apskaičiuoti bangų skaičiai lentelėse ir paveiksluose pateikti nepadauginus jų iš jokio koeficiento, nebent lentelių ir paveikslėlių pavadinime būtų nurodyta kitaip. Kai kurie skaičiavimai buvo atlikti MP2 metodu, bendradarbiaujant su Alejandro Gutiérrez-Quintanilla ISMO, Prancūzijoje.

PAGRINDINIAI REZULTATAI

Protono tuneliavimas chloromalondialdehido molekulėje

Chloromalondialdehido molekulė gaunama iš malondialdehido, pakeičiant vieną vandenilį chloro atomu (1 pav.). Chloromalondialdehidas, kaip ir malondialdehidas, turi rezonansu stiprinamą vidinį vandenilinį ryšį, kuris stabilizuoja jo *enol* formą. Chloro atomas, kuris yra didesnis ir elektroneigiamesnis už vandenilį, pakeičia molekulės geometriją. Vidinio vandenilinio ryšio stipris ir protono tuneliavimo procesas labai priklauso nuo tokių pasikeitimų. Dauguma tyrimų su malondialdehido ir chloromalondialdehido molekulėmis yra skirti šio proceso tyrinėjimui teoriniais metodais ir, tik MA atveju, eksperimentiniais metodais [48, 118–120].

Šiame darbe buvo atlikti eksperimentai su chloromalondialdehido molekule izoliuota argono, neono ir paravandenilio matricose. Gauti rezultatai leidžia suprasti protonų tuneliavimo procesą šiose molekulėse. Dėl molekulinės struktūros pokyčių taip pat skiriasi ir molekulių izomerų energijos pasiskirstymas. Norint gauti keturis iš aštuonių galimų atvirų *enol*

izomerų, fotoizomerizacijos eksperimentai buvo atlikti veikiant chloromalondialdehido bandinius skirtingo bangos ilgio spinduliuote.
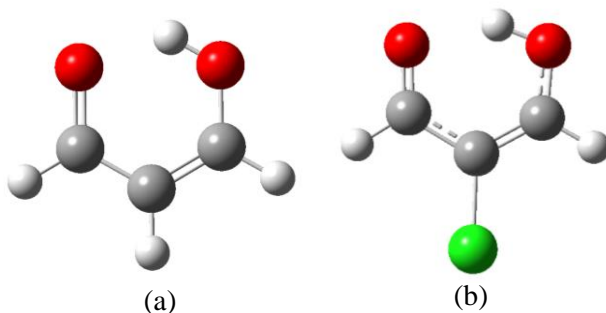
1 pav. Mažiausios energijos (a) malondialdehido ir (b) chloromalondialdehido *enol* tautomerai.

Molekulėje vykstant protono tuneliavimui, virpesiniai lygmenys skyla, dėl jo ir eksperimentiniuose spektruose stebimas virpesinių juostų suskilimas. Spektruose turėtų būti matomos juostos, atitinkančios šuolius iš pagrindinio lygmens į suskilusį sužadintą lygmenį g1-e1 ir g1-e2 (2 pav.), o jei tarpas tarp lygmenų pakankamai mažas, taip pat ir juostos, atitinkančios šuolius g2-e1 ir g2-e2. Pagal teorinius skaičiavimus [120], chloromalondialdehido pagrindinio virpesinio lygmens suskilimas yra lygus 12 cm^{-1}. Tai reikštų, kad temperatūroje, kurioje nusodinamas paravandenilis (3 K), tik 0.3 % molekulių yra aukštesnės energijos (pagrindiniame) lygmenyje.

Chloromalondialdehidas buvo izoliuotas paravandenilio, argono bei neono matricose – virpesinių juostų suskilimas stebimas pirmose dviejose aplinkose. Įvairios kitos priežastys, tokios kaip matricos narvelio efektas, kombinacinės juostos ar izotopinis efektas buvo įvertintos ir atmestos kaip nepaaiškinančios tokio juostų suskilimo. Atkaitinimo eksperimentai paravandenilio matricoje leido geriau priskirti virpesinius šuolius spektrinėms juostoms. Chloromalondialdehido, izoliuoto paravandenilio matricoje prie 3 K ir 5 K temperatūrų, spektrai ir šių dviejų spektrų skirtumai, parodyti 2 pav.
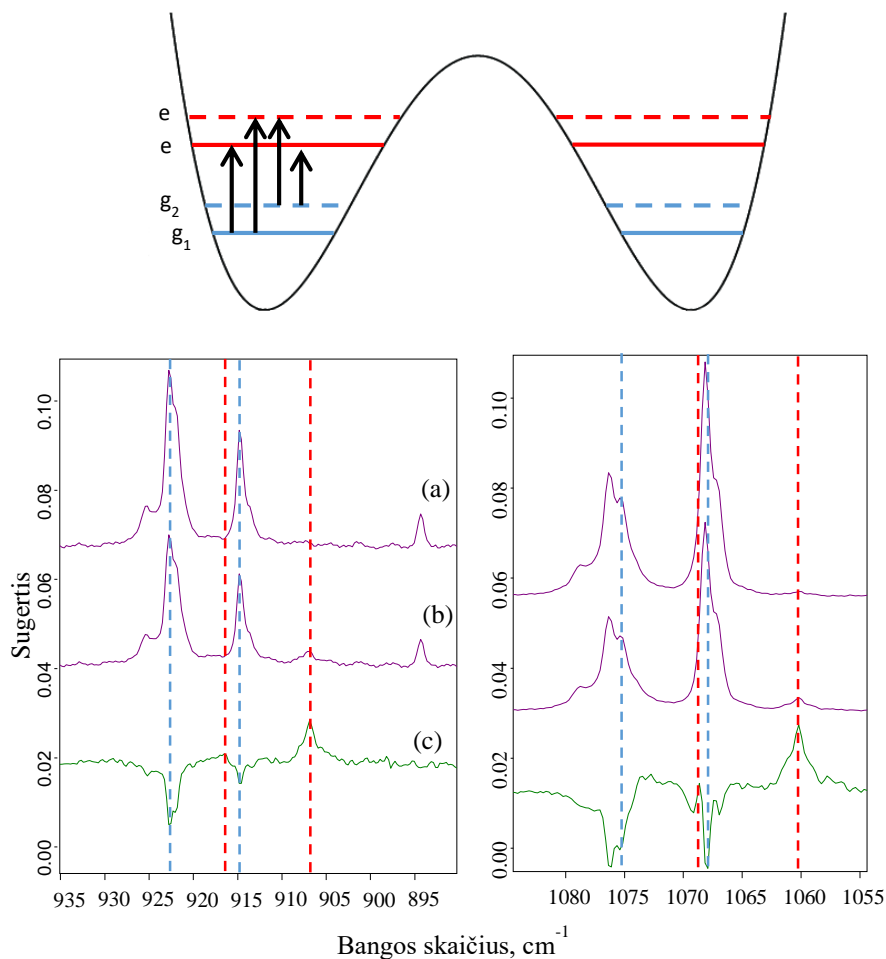
2 pav. Supaprastinta chloromalondialdehido lygmenų diagrama (viršuje). Chloromalondialdehido, izoliuoto paravandenilio matricoje (a) 3 K, (b) 5 K temperatūroje, bei (c) skirtuminis (b)-(a) infraraudonosios sugerties spektrai.

Skirtuminis spektras geriausiai parodo pokyčius ir patvirtina, kad juosta ties 1068 cm^{-1} atitinka g1-e1, o juosta ties 1076 cm^{-1} – g1-e2 šuolius. Palyginimas su teoriniais spektrais leidžia priskirti šias juostas žiedo CH plokštuminiams deformaciniams virpesiams. Juostos ties 915 cm^{-1} ir 923 cm^{-1} atitinka tuos pačius perėjimus mažesnės energijos virpesinei modai (žiedo bei OH grupės plokštuminiai deformaciniai virpesiai). Šios deformacijos yra simetriškos pereinamosios būsenos atžvilgiu, o simetrinės virpesinės modos, susijusios su protonų pernaša, yra linkusios padidinti tunelinį suskilimą. Tokiu
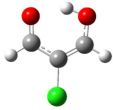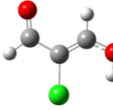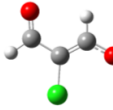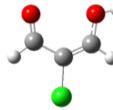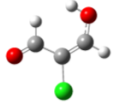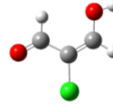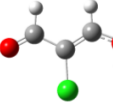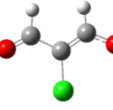
atveju, eksperimentiškai nustatomas suskilimas tarp lygmenų yra lygus 8 cm^{-1}, o tai atitiktų 2 % aukštesnio lygmens užpildą 3 K temperatūroje ir 9 % – 5 K temperatūroje.

Ties 907 cm^{-1} ir 1060 cm^{-1} skirtuminiame spektre matomas intensyvumo padidėjimas, ir todėl šios juostos gali būti priskirtos g2-e1 šuoliui. Taip pat stebimas nedidelis intensyvumo padidėjimas ties 916 cm^{-1} ir 1068 cm^{-1}, o atitinkami skirtumai tarp šių pozicijų gana gerai atitinka 8 cm^{-1} vertę. Taigi galima daryti išvadą, kad paravandenilio matricoje stebimas pagrindinio ir sužadinto chloromalondialdehido molekulės lygių skilimas dėl protono tuneliavimo.

Aukštesnės energijos chloromalondialdehido izomerai

Spektrai, užregistruoti iškart po bandinio nusodinimo, turi daugiau juostų, nei būtų galima priskirti vienam izomerui. Remiantis daugiausia OH valentinių virpesių sritimi, kurioje CCC izomerai neturi jokių spektrinių juostų, kitas iškart po nusodinimo stebimas izomeras identifikuojamas kaip TTC. Kiti atviri *enol* izomerai buvo gauti paveikus bandinius UV spinduliuote, jų struktūra ir pagrindiniai parametrai aprašyti 1 lentelėje.

1 lentelė. Chloromalondialdehido izomerų parametrai.

	CCC	CTC	CTT	CCT
ΔE, kJ/mol	0	14.4	27.2	47.1
dO-H, Å	1.00	0.97	0.96	0.96
	TCC	TCT	TTC	TTT
ΔE	41.0	39.5	10.1	27.3
dO-H, Å	0.96	0.96	0.97	0.96

Izomerų juostų evoliucijos santrauka pavaizduota 3 paveiksle. Visų pirma, infraraudonosios sugerties spektras buvo užregistruotas iškart po bandinio nusodinimo. Šiame spektre buvo stebimas CCC izomeras kartu su antrosios izomerų grupės (TTC izomero) pėdsakais. Pirmasis fotoizomerizacijos etapas buvo vykdomas su $\lambda_1 = 290$ nm bangos ilgio spinduliuote (2 taškas 3 paveiksle). Taip buvo sukurta pirmoji izomerų grupė, turinti CTC ir TCT izomerus. Be to, taip pat buvo pastebėtas greitas CCC koncentracijos mažėjimas ir lėtesnis TTC koncentracijos augimas. Su $\lambda_2 = 270$ nm (3 paveikslo 3 taškas) spinduliuotės poveikiu, pradėjo mažėti pirmosios izomerų grupės kiekis, todėl greitai susidarė TTC bei šiek tiek CCC izomerų. Švitinimas ties $\lambda_4 = 235$ nm paskatino antrąją izomerų grupę virsti atgal į CCC. Taip pat buvo pastebėtas nedidelis pirmosios izomerų grupės koncentracijos padidėjimas. Vėl padidinus veikiančios spinduliuotės bangos ilgį, pradėjo labiau didėti pirmosios grupės izomerų koncentracija.
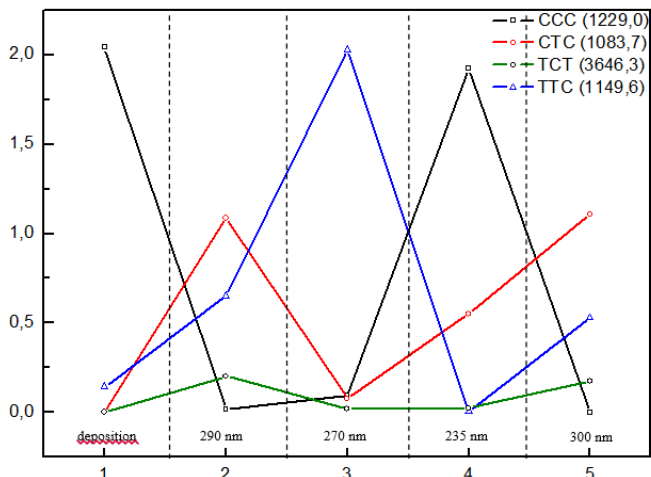
3 pav. Spektrinių juostų intensyvumo kitimas, vykdant fotoizomerizacijos eksperimentus: (1) iškart po nusodinimo, po (2) 290 nm spinduliuotės poveikio, (3) po 270 nm spinduliuotės poveikio, (4) po 235 nm spinduliuotės poveikio ir (5) po 300 nm spinduliuotės poveikio.

Vandenilinio ryšio stipris acetilacetono darinių molekulėse

Acetilacetonas yra β-diketonų klasės molekulė, malondialdehido dimetilo darinys, kuris taip pat turi vidinį vandenilinį ryšį, stabilizuojantį jo *enol* formą ir pasižymi π elektronų delokalizacija. Šiame darbe vidinio vandenilinio ryšio

stiprumas skirtingoms molekulėms buvo įvertintas pagal teoriškai apskaičiuotus geometrinius ir virpesinius parametrus bei eksperimentiškai stebint su OH jungtimi susijusių virpesinių juostų pozicijas. Kiti optimizuotų struktūrų geometriniai parametrai buvo svarbūs nustatant π elektronų delokalizacijos lygį.

Bendra vidinio vandenilinio ryšio stiprio tendencija, gauta įvertinus geometrinius parametrus yra tokia (CO ir OH prie AcAcF3 ir AcAcF2Cl molekulių nurodo, kurioje pusėje yra F₃ ar F₂Cl grupė): AcAcCH3 > AcAcCl > AcAc > AcAcF3(OH) > AcAcF3(CO) > AcAcF2Cl(OH) > AcAcF2Cl(CO) > AcAcF4 > AcAcF6.
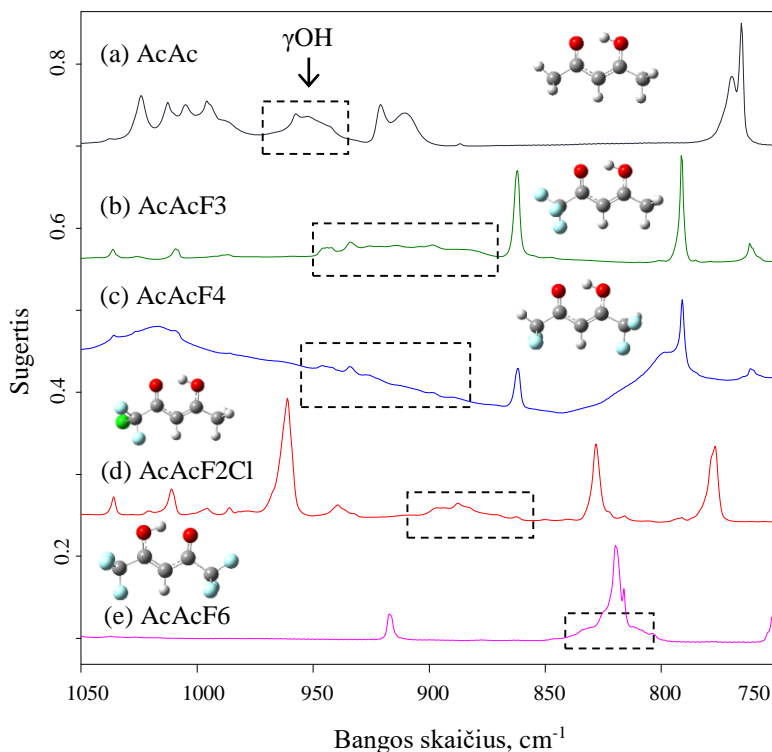
4 pav. (a) AcAc, (b) AcAcF3, (c) AcAcF4, (d) AcAcF2Cl ir (e) AcAcF6 izoliuotų argono matricoje (17 K) infraraudonosios sugerties spektrai 1050 cm⁻¹ – 750 cm⁻¹ srityje, bei stabiliausios struktūros molekulės.

Elektrostatinis efektas (elektroneigiamų fluoro atomų poveikis molekulės elektronų pasiskirstymui) paaiškina, kodėl vidinio vandenilinio ryšio stipris

134

mažėja su kiekvienu pridėtu fluoro atomu ir kodėl ryšys yra stipresnis (OH), o ne (CO) asimetrinių molekulių AcAcF3 ir AcAcF2Cl izomeruose.

Dėl vidinio vandenilinio ryšio, visų su OH grupe susijusių virpesinių modų spektrinės juostos bus labai išplitusios (4 pav.). Paveikslėlyje parodyta γOH virpesių sritis, kurių padėtis gali būti naudojama vidinio vandenilinio ryšio stipriui įvertinti. Šio virpesio spektrinė juosta pasirenkama, nes νOH virpesio juosta yra per plati ir per žemo intensyvumo, kad būtų stebima, o δOH virpesiai yra surišti su kitais molekulės virpesiais. Neplokštuminio OH virpesio (γOH) moda yra delokalizuota, taip pat ir AcAcF6 molekulėje, kur vidinis vandenilinis ryšys turėtų būti silpniausias. Tačiau net jei ir neįmanoma nustatyti tikslios γOH juostos pozicijos, galima patvirtinti, kad vidinio vandenilinio ryšio stipris atitinka numatytą teorinę tendenciją. Kuo stipresnis vandenilinis ryšys, tuo didesnė bangos skaičiaus vertė atitinką tos pačios su OH grupe susijusios virpesinės modos juostą. Ryšys yra stipriausias molekulėms, kuriose pakeista tik viena metilo grupė, silpnesnis tetrafluoracetilacetonui ir silpniausias heksafluoracetilacetonui.

Trifluoroacetilacetonas: asimetrinė sistema

Dėl asimetrinė AcAcF3 molekulės struktūros yra labiau tikėtina, jog vandenilis bus lokalizuotas šalia vieno iš deguonies atomų. Visi teoriniai ir eksperimentiniai trifluoracetilacetono tyrimai teigia, kad AcAcF3(CO) izomeras, kuriame vandenilis yra toje pačioje pusėje kaip CH_3, o ne CF_3 grupė, yra stabilesnis.

(a) (b)
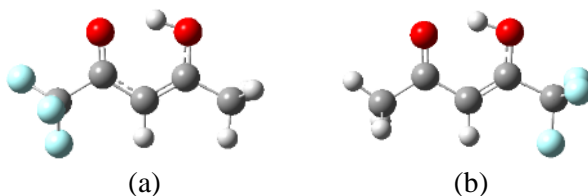
5 pav. Trifluoroacetilacetono (a) AcAcF3(CO) ir (b) AcAcF3(OH) izomerai.

AcAcF3(OH) struktūra atitinka vietinį minimumą, o apskaičiuotas energijos skirtumas tarp šių dviejų izomerų labai priklauso nuo pasirinkto skaičiavimo metodo [119]. Remiantis B3LYP 6-311++G(3df, 3pd) skaičiavimais, šis skirtumas yra 4.3 kJ/mol, o tai atitinka 85% AcAcF3(CO) ir 15% AcAcF3(OH) mišinį kambario temperatūroje pagal Boltzmann'o paskirstymą.
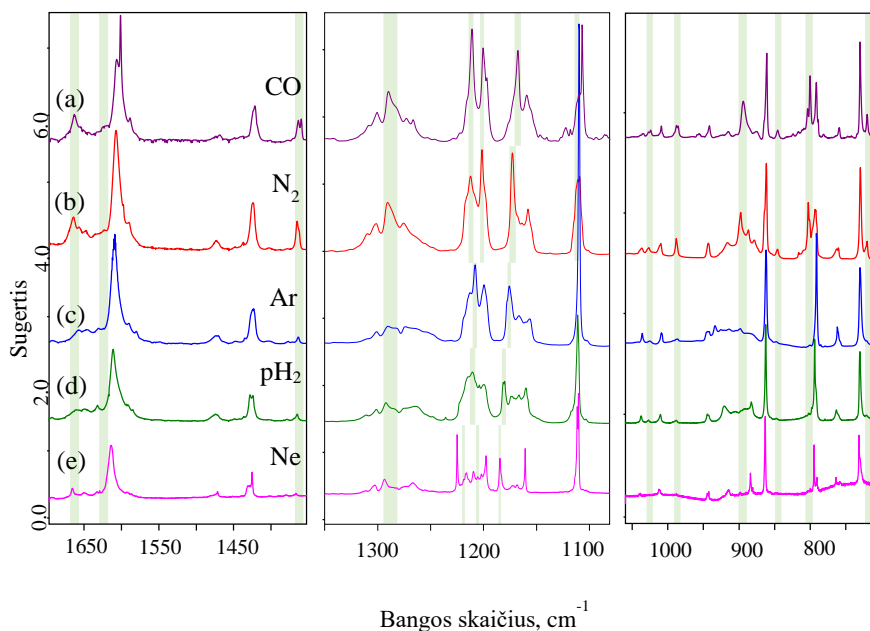
6 pav. AcAcF3 izoliuoto (a) CO, (b) N$_2$, (c) Ar, (d) pH$_2$ ir (e) Ne matricose
(T=3-12 K), infraraudonosios sugerties spektrai. Žalia spalva pažymėtos
AcAcF3(OH) juostos.

Geriausia sritis AcAcF3(OH) kiekiui skirtingose aplinkose nustatyti yra
nuo 900 cm^{-1} iki 700 cm^{-1}. γCH juosta (pagal teorinius skaičiavimus esanti ties
813 cm^{-1} AcAcF3(CO) izomerui ir ties 835 cm^{-1} AcAcF3(OH) izomerui) gali
būti aiškiai stebima N$_2$ ir CO matricose, atitinkamai maždaug ties 792 cm^{-1} ir
802 cm^{-1}. Santykinis šios juostos intensyvumas gali padėti priskirti kitas
AcAcF3(OH) izomerui priklausančias juostas, taip pat ir γOH juostą.
Teoriniai skaičiavimai numato, kad γOH virpesių juosta yra ties 962 cm^{-1}
AcAcF3(CO) ir ties 972 cm^{-1} AcAcF3(OH) izomero atveju. Tačiau, kaip buvo
aptarta anksčiau, ši eksperimentinė juosta yra labai plati ir šiuo atveju jos
struktūra priklauso nuo matricos aplinkos. Vienintelė juosta, kuri atrodo
labiau lokalizuota ir gali būti priskirta AcAcF3(OH) dėl savo intensyvumo,
yra ties 898 cm^{-1} N$_2$ ir 894 cm^{-1} CO matricų spektruose. Tokiu atveju
AcAcF3(CO) izomerui gali būti priskiriama plati juosta nuo 930 cm^{-1} iki 875
cm^{-1}. Neono matricoje galima identifikuoti dar dvi juostas – ties 884 cm^{-1} ir
915 cm^{-1} (stebimas ties 883 cm^{-1} ir 921 cm^{-1} pH$_2$ aplinkoje), kurios gali
priklausyti γOH virpesiui AcAcF3 molekulėje.

Ramano sklaidos eksperimentų rezultatai patvirtina AcAcF3(OH) izomerų egzistavimą, ir jų koncentracijos priklausomybę nuo matricos aplinkos. Taip pat buvo atlikti atkaitinimo ir fotoizomerizacijos eksperimentai, norint įvertinti temperatūros ir spinduliuotės poveikį izomerų koncentracijoms.
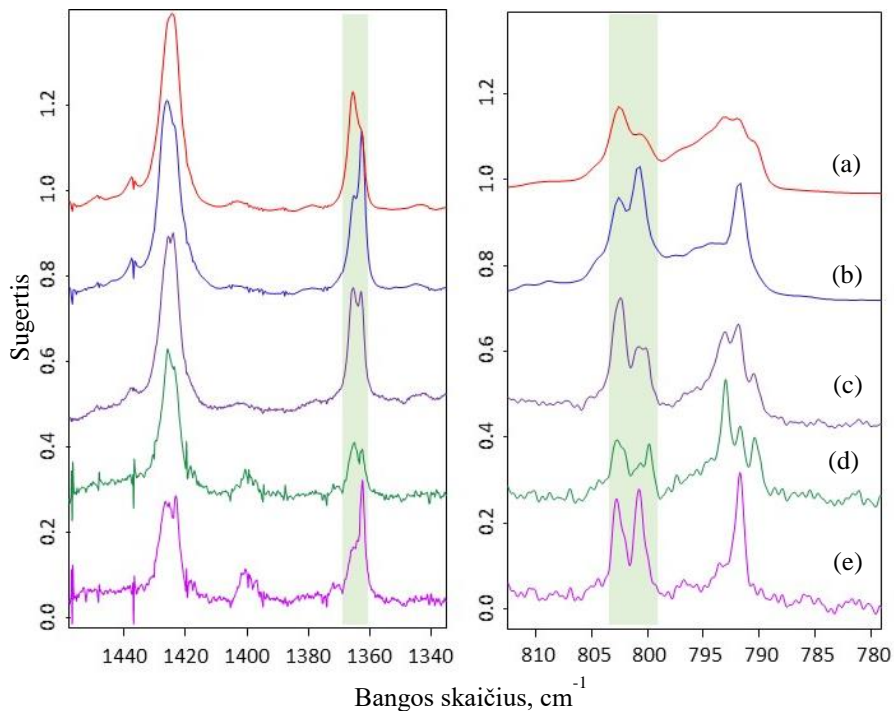
7 pav. AcAcF3, izoliuoto N_2 matricoje, spektrai: pirmasis bandinys (a) prieš ir (b) po atkaitinimo, antrasis bandinys (c) prieš, (b) po poveikio UV spindliuote, (e) po atkaitinimo ir poveikio UV spinduliuote. Žalia spalva pažymėtos AcAcF3(OH) juostos.

Atkaitinimo ir UV spinduliuotės poveikis virpesiniam spektrui pavaizduotas 6 paveiksle. Švitinimas buvo atliktas ne tik N_2, bet ir kitose matricose (pH_2, Ne, Ar), siekiant gauti atvirus *enol* izomerus. Tačiau čia parodytas tik poveikis AcAcF3(OH)/AcAcF3(CO) santykiui. Atkaitinimas padidina šį santykį, o švitinimas jį sumažina (lentelė 2).

Lentelėje parodyti skaičiavimai buvo atlikti pagal infraraudonosios sugerties spektro juostas (793 cm^{-1} AcAcF3(CO) ir 803 cm^{-1} AcAcF3(OH) izomerui), priklausančias γCH virpesinei modai. Izomerų santykis buvo

apskaičiuotas turint omeny teorinį juostų intensyvumų santykį (1.68 pagal M06-2X skaičiavimus).
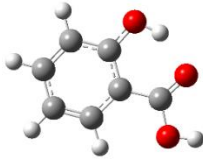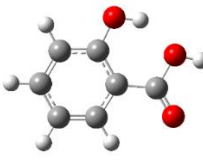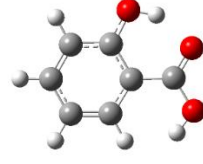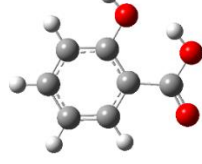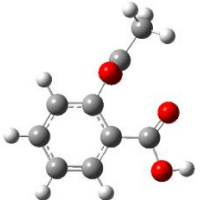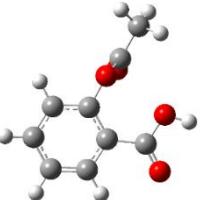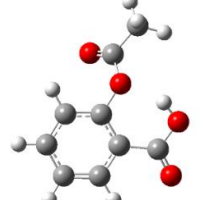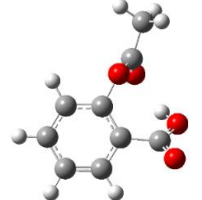
2 lentelė. AcAcF3(OH)/AcAcF3(CO) koncentracijų santykis, įvertintas pagal virpesinių spektrų juostų integralinius plotus.

Matrica	Santykis nusodintame bandinyje	Santykis po atkaitinimo	Santykis po UV spinduliuotės poveikio
Ne	>0.007		-
Ar	>0.01	>0.01	
pH$_2$	>0.08		
N$_2$	0.42±0.08	1.2±0.3	0.35±0.01
CO	0.8±0.2	1.5±0.3	-

Acetilsalicilo rūgštis ir salicilo rūgštis

Acetilsalicilo rūgštis (ASA, plačiau žinomas kaip aspirinas) yra nesteroidinis priešuždegiminis vaistas, plačiai naudojamas daugiau nei 100 metų, skiriamas norint išvengti krešėjimo ir sumažinti karščiavimą, uždegimą ir skausmą. Pati molekulė yra aromatinis junginys, kurio orto padėtyse yra karboksi ir esterio grupės. ASA sintetinamas iš salicilo rūgšties ($C_7H_6O_3$) ir acto anhidrido pertekliaus ($C_4H_6O_3$), dalyvaujant rūgštiniam katalizatoriui. Reakcijos metu salicilo rūgšties hidroksilo grupė pakeičiama esterio grupe ir gaunama acto rūgštis. Tiek salicilo, tiek acetilsalicilo rūgšties molekulinė struktūra buvo ištirta teoriniais metodais, o eksperimentiniai tyrimai daugiausia buvo susiję su jų kristalinėmis formomis. Tik vienas tyrimas buvo atliktas su salicilo rūgštimi, izoliuota žemos temperatūros matricose [141].

3 lentelė. Salicilo rūgšties ir acetilsalicilo rūgšties izomerai.

SA			
E	R	O	H
$\Delta E = 0$ kJ/mol	15.7 kJ/mol	22.0 kJ/mol	38.2 kJ/mol
ASA			
1a	2a	4a	5a
$\Delta E = 0$ kJ/mol	3.8 kJ/mol	11.8 kJ/mol	13.8 kJ/mol

Šių matricinės izoliacijos eksperimentų metu SA ir ASA bandiniai prieš nusodinimą buvo kaitinami. Spektrai dažnai yra sudėtingi dėl priemaišų ir šiluminės disociacijos produktų. Dėl skirtingos salicilo rūgšties ir acetilsalicilo rūgšties geometrijos, skiriasi ir jų izomerų pasiskirstymas. Salicilo rūgščiai stabiliausias izomeras pavadintas E, kitų izomerų pastebėti eksperimentiniuose spektruose beveik neįmanoma (artimiausio izomero R energija yra 15.7 kJ/mol didesnė). Du stabiliausi ASA izomerai, 1a ir 2a skiriasi mažiau – 3.8 kJ/mol. Šis energijos skirtumas reiškia, kad kambario temperatūros bandiniuose turėtų būti stebima maždaug 17 % didesnės energijos izomero koncentracija. Izomerui 4a, kuris yra trečias pagal stabilumą, ši vertė yra apie 0.8 %, todėl vėlgi labai mažai tikėtina, kad jis bus pastebėtas eksperimentiniuose spektruose. Pirmieji du izomerai (1a ir 2a) buvo stebimi eksperimentiniuose spektruose (8 pav.).
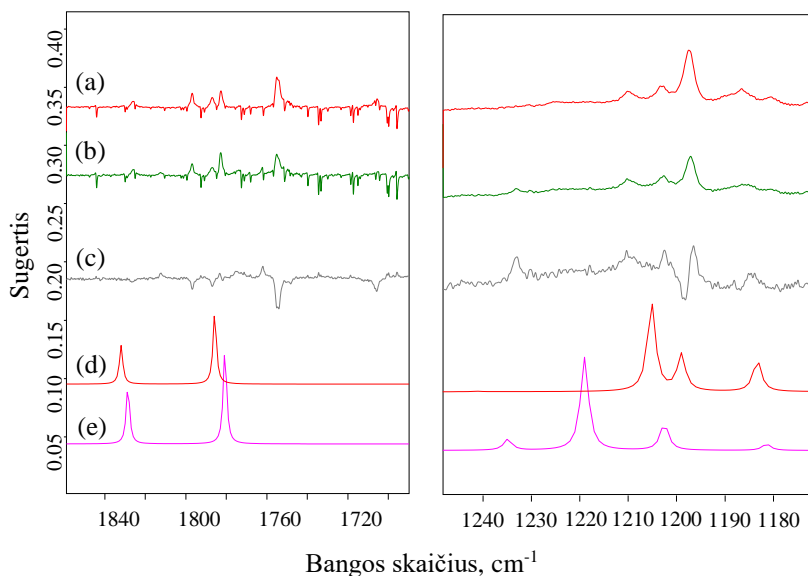
8 pav. Acetilsalicilo rūgšties, izoliuotos paravandenilio matricoje, infraraudonosios sugerties spektrai: (a) po nusodinimo, (b) po bandinio paveikimo 270 nm spinduliuote (40 min), (c) skirtuminis (b)-(a) spektras; (d) 1a ir (e) 2a teoriniai spektrai.

Srityje nuo 1860 cm^{-1} iki 1700 cm^{-1} (νC=O ir νC=C virpesinės juostos) matomas nedidelis poslinkis tarp apskaičiuotų izomerų virpesinių juostų. Iš tiesų, abiejuose eksperimentiniuose spektruose (ASA bandinio, kaitinto iki 50 ºC ir 55 ºC) yra keletas juostų, kurios gali būti priskirtos skirtingiems izomerams. Visų pirma, reikėtų atmesti priemaišų juostas: ties 1705 cm^{-1} yra juosta, priklausanti salicilo rūgščiai. Palyginus su apskaičiuotais ir grynų medžiagų spektrais bei santykinio intensyvumo reikšmėmis, acto rūgščiai galima priskirti 1782 cm^{-1} juostą. Kadangi ASA 2a izomero bandinyje turėtų būti mažiau, jam priskirtų spektrinių juostų intensyvumas taip pat turėtų būti daug mažesnis. Šiuo atveju, jei 1752 cm^{-1} juosta priskiriama ASA 1a izomerui, žemo intensyvumo juosta jos papėdėje (ties 1749 cm^{-1}) galima būtų priskirti ASA 2a izomerui. Dažnio poslinkis būtų panašus į apskaičiuotąjį. Kitose juostų porose, taip pat ir spektrinėje srityje nuo 1240 cm^{-1} iki 1180 cm^{-1} galima kai kurias silpnas spektrines juostas priskirti 2a izomerui (pavyzdžiui, 1210 cm^{-1}). Taigi, galima daryti išvadą, kad aukštesnės energijos izomeras yra ir ką tik nusodintuose bandiniuose. Tolesnė fotoizomerizacija neabejotinai

sumažina stabiliausio izomero kiekį, greičiausiai tuo pačiu padidindama kito izomero koncentraciją.

Kita vertus, pagal teorinius skaičiavimus 99.8 % SA bandinio turėtų sudaryti vienas, E, izomeras. Eksperimentiniame spektre nepastebėta jokių tokiai išvadai prieštaraujančių spektrinių juostų. Didesnės energijos izomerai gali būti gaunami tik fotoizomerizacijos eksperimentų metu. Tačiau bandiniuose, kuriuose yra pakankamai vandens, buvo stebimi matricoje besiformuojantys SA-vandens kompleksai (9 pav.).
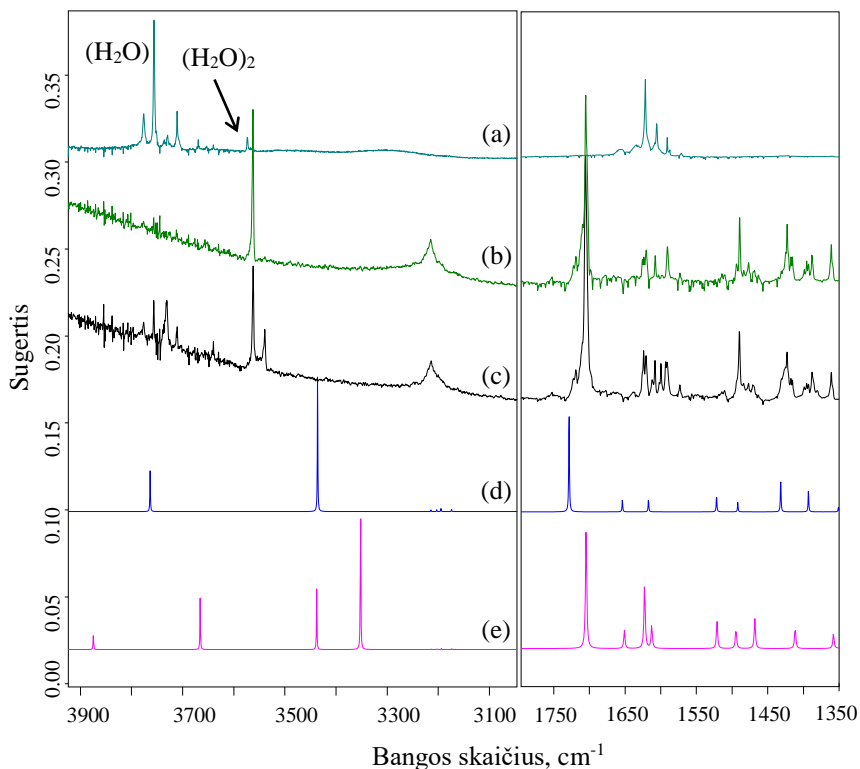
9 pav. Vandens (a), salicilo rūgšties (b) ir salicilo rūgšties su vandeniu (c), izoliuotų argono matricoje (17 K) infraraudonosios sugerties spektrai bei (d) SA ir (e) SA+H_2O teoriniai spektrai.

Šiame paveiksle galima aiškiai stebėti naują juostą, augančią kartu su vandens koncentracija (3540 cm^{-1}). Palyginus eksperimentinius spektrus su teoriniais, galima nustatyti, kad vandens molekulė sudaro ryšį su COOH grupe salicilo molekulėje. Todėl iš vienos salicilo molekulės apskaičiuotų νOH virpesių, esantis ties 3436 cm^{-1} (COH) prisijungus vandeniui nepakeičia

141

padėties, o esantis ties 3764 cm^{-1} (COOH), pasislenka per maždaug 300 cm^{-1}. Salicilo rūgšties spektre yra stebimos dvi juostas, kurias galima priskirti šiems virpesiams. Tada salicilo rūgšties ir vandens spektre juostą ties 3540 cm^{-1} galima priskirti vandens molekulės, sudariusios kompleksą, OH valentiniam virpesiui, o juostą, besiformuojančią 3200 cm^{-1} juostos šlaite, SA molekulės, sudariusios kompleksą, COOH grupės νOH virpesiui.

IŠVADOS

1. Įrodyta, kad 2-chloromalondialdehido molekulėse protono tuneliavimas gali būti stebimas esant labai žemai temperatūrai argone (7 K) ir paravandenilyje (3 K), bet ne neono matricoje. Eksperimentiniai rezultatai gana gerai atitinka teoriškai apskaičiuotą tuneliavimo suskilimo 12 cm^{-1} vertę.

2. Du iš aštuonių teorinių skaičiavimų numatomų chloromalondialdehido *enol* izomerų yra stebimi žemos temperatūros matricose – CCC ir TTC. Iš XYC ir XYT porų vienas izomeras gali būti selektyviai stabilizuojamas apšvitinant bandinius tam tikru bangos ilgiu 230 nm –300 nm diapazone.

3. Eksperimentiniai ir teoriniai rezultatai rodo, kad acetilacetono dariniuose stipriausias vidinis vandenilinis ryšys yra acetilacetone, silpniausias – heksafluoroacetilacetone, tarpe yra trifluoroacetilacetono molekulė. Tarpmolekulinio vandenilinio ryšio, susidariusio tarp molekulių ir vandens, stipris taip pat pasižymi tokia pačia tendencija ir turi mažai įtakos vidinio vandenilinio ryšio stiprumui.

4. Trifluoracetilacetono izomeras (AcAcF3(CO)) stabilizuojamas dėl π elektronų delokalizacijos. Tačiau abu izomerai buvo stebimi esant žemai temperatūrai skirtingose matricos aplinkose (neono, argono, paravandenilio, ksenono, azoto, anglies monoksido). Didesnės AcAc(OH) koncentracijos užfiksuotos azoto ir anglies monoksido matricose, taip pat bandiniuose su daugiau vandens priemaišų.

5. Salicilo ir acetilsalicilo rūgšties molekulės gali būti izoliuojamos žemos temperatūros matricose, jei bandiniai kaitinami 50 ⁰C temperatūroje. Kaitinant bandinius aukštesnėje temperatūroje, buvo stebimi terminės disociacijos produktai.

6. Žemos temperatūros matricos aplinkoje egzistuoja vienas SA izomeras ir du ASA izomerai. Parodyta, kad matricos aplinkoje formuojasi vienos salicilo rūgšties ir vienos vandens molekulės asociatai, kuriuose vandens molekulė yra prisijungusi prie SA COOH grupės.

BIBLIOGRAPHY

[1] M. W. Latimer, W. H. Rodebush, Polarity and ionization from the standpoint of the Lewis theory of valence, Journal of the American Chemical Society, 42, 7, p. 1419 —1433, 1920.

[2] G. C. Pimentel, A. L. McClellan, The Hydrogen Bond, W. H. Freeman and Company, San Francisco, 1960.

[3] G. A. Jeffrey, W. Saenger, Hydrogen Bonding in Biological Structures, Springer, Berlin, 1991.

[4] E. Arunan, G. R. Desiraju, R. A. Klein, J. Sadlej, S. Scheiner, I. Alkorta, D. C. Clary, R. H. Crabtree, J. J. Dannenberg, P. Hobza, H. G. Kjaergaard, A. C. Legon, B. Mennucci, D. J. Nesbitt, Defining the hydrogen bond: An account (IUPAC Technical Report), Pure Applied Chemistry, 83, 8, p. 1637 —1641, 2011.

[5] S. J. Grabowski, Hydrogen Bond – Definitions, Criteria of Existence and Various Types, in *Understanding Hydrogen Bonds: Theoretical and Experimental Views*, Royal Society of Chemistry, London, p. 1-40, 2020.

[6] S. J. Kerber, J. J. Bruckner, K. Wozniak, S. Seal, S. Hardcastle, T. L. Barr, The nature of hydrogen in x-ray photoelectron spectroscopy: General patterns from hydroxides to hydrogen bonding, Journal of Vacuum Science & Technology A, 14, 3, p. 1314-1320, 1996.

[7] S. J. Grabowski, Ab Initio Calculations on Conventional and Unconventional Hydrogen Bonds – Study of the Hydrogen Bond Strength, Journal of Physical Chemistry A, 105, 47, p. 10739–10746, 2001.

[8] P. Gilli, V. Bertolasi, V. Ferretti, G. Gilli, Evidence for resonance-assisted hydrogen bonding. 4. Covalent nature of the strong homonuclear hydrogen bond. Study of the O-H--O system by crystal structure correlation methods, Journal of the American Chemical Society, 116, 3, p. 909–915, 1994.

[9] A. K. Samanta, G. Czako, Y. Wang, J. S. Mancini, J. M. Bowman, Hanna Reisler, Experimental and Theoretical Investigations of Energy Transfer and Hydrogen-Bond Breaking in Small Water and HCl Clusters, Accounts of Chemical Research, 47, 8, p. 2700–2709, 2014.

[10] A. K. Samanta, L. C. Ch'ng, H. Reisler, Imaging Bond Breaking and Vibrational Energy Transfer in Small Water Containing Clusters, Chemical Physics Letters, 575, p. 1−11, 2013.

[11] A. Luzar, D. Chandler, Effect of Environment on Hydrogen Bond Dynamics in Liquid Water, Physical Review Letters, 76, 928, 1996.

[12] J. B. Asbury, T. Steinel, M. D. Fayer, Hydrogen Bond Networks: Structure and Evolution after Hydrogen Bond Breaking, Journal of Physical Chemistry B, 108, 21, p. 6544–6554, 2004.

[13] A. Mentes, A. M. Florescu, E. Brunk, J. Wereszczynski, M. Joyeux, I. Andricioaei, Free-Energy Landscape and Characteristic Forces for the Initiation of DNA Unzipping, Biophysical Journal, 108, 7, p. 1727-1738, 2015.

[14] M. W. Feyereisen, D. Feller, D. A. Dixon, Hydrogen Bond Energy of the Water Dimer, Journal of Physical Chemistry, 100, 8, p. 2993–2997, 1996.

[15] L. C. Ch'ng, A. K. Samanta, G. Czakó, J. M. Bowman, H. Reisler, Experimental and Theoretical Investigations of Energy Transfer and Hydrogen-Bond Breaking in the Water Dimer, Journal of the American Chemical Society, 134, 37, p. 15430–15435, 2012.

[16] M. Chaplin, Water's Hydrogen Bond Strength, Soft Condensed Matter, p. 87-104, 2007.

[17] J. Nochebuena, C. Cuautli, J. Ireta, Origin of cooperativity in hydrogen bonding, Physical Chemistry Chemical Physics, 19, 23, 2017.

[18] B. W. Gung, Z. Zhu, B. Everingham, Elucidation of Hydrogen-Bonding Cooperativity at the Molecular Level, Journal of Organic Chemistry, 62, 11, p. 3436-3437, 1997.

[19] S. Iwata, D. Akase, M. Aidab, S. S. Xantheas, Electronic origin of the dependence of hydrogen bond strengths on nearest-neighbor and next-nearest-neighbor hydrogen bonds in polyhedral water clusters $(H_2O)_n$, n = 8, 20 and 24, Physical Chemistry Chemical Physics, 18, 29, p. 19746-19756, 2016.

[20] J. M. Guevara-Vela, E. Romero-Montalvo, V. Arturo Mora Gomez, R. Chavez-Calvillo, M. Garcıa-Revilla, E. Francisco, A. M. Pendas, T. Rocha-Rinza, Hydrogen bond cooperativity and anticooperativity within the water hexamer, Physical Chemistry Chemical Physics, 18, 29, p. 19557-19566, 2016.

[21] I. Bakó, A. Lábas, K. Hermansson, A. Bencsura, J. Oláh, How can we detect hydrogen bond local cooperativity in liquid water: A simulation study, Journal of Molecular Liquids, 245, p. 140–146, 2017.

[22] N. Dominelli-Whiteley, J. J. Brown, K. B. Muchowska, I. K. Mati, C. Adam, T. A. Hubbard, A. Elmi, A. J. Brown, I. A. W. Bell, S. L. Cockroft, Strong Short-Range Cooperativity in Hydrogen-Bond Chains, Angewandte Chemie International Edition, 56, 26, p. 7658 –7662, 2017.

[23] M. Masella, J. P. Flament, Influence of Cooperativity on Hydrogen Bond Networks, Molecular Simulation, 24, 1-3, p. 131-156, 2000.

[24] K. Stokely, M. G. Mazza, H. E. Stanley, G. Franzese, Effect of hydrogen bond cooperativity on the behavior of water, Proceedings of the National Academy of Sciences of the United States of America, 107, 4, p. 1301-1306, 2010.

[25] V. M. Castor-Villegas, J. M. Guevara-Vela, W. E. Vallejo Narváez, A. M. Pendás, T. Rocha-Rinza, A. Fernández-Alarcón, On the strength of hydrogen bonding within water clusters on the coordination limit, Journal of Computational Chemistry, 41, 26, p. 2266-2277, 2020.

[26] M. Huš, T. Urbic, Strength of hydrogen bonds of water depends on local environment, Journal of Chemical Physics, 136, 14, 144305, 2012.

[27] S. Iwata, Analysis of hydrogen bond energies and hydrogen bonded networks in water clusters $(H2O)_{20}$ and $(H2O)_{25}$ using the charge-transfer and dispersion terms, Physical Chemistry Chemical Physics, 16, 23, p. 11310-11317, 2014.

[28] Y. Shi, W. Jiang, Z. Zhang, Z. Wang, Cooperative vibrational properties of hydrogen bonds in Watson–Crick DNA base pairs, New J. Chem., 41, 20, p. 12104-12109, 2017.

[29] N. Kobko, L. Paraskevas, E. del Rio, J. J. Dannenberg, Cooperativity in Amide Hydrogen Bonding Chains: Implications for Protein-Folding Models, Journal of the American Chemical Society, 123, 18, p. 4348-4349, 2001.

[30] Y. Zhou, G. Deng, Y. Z. Zheng, J. Xu, H. Ashraf, Z. W. Yu, Evidences for Cooperative Resonance-Assisted Hydrogen Bonds in Protein Secondary Structure Analogs, Scientific Reports, 6, 36932, 2016.

[31] I. T. Rakipov, A. A. Petrov, A. A. Akhmadiyarov, A. A. Khachatrian, M. A. Varfolomeev, B. N. Solomonov, Thermochemistry of hydrogen bonding

of proton acceptors in the media of linear and cyclic amides. Cooperativity effects in multi-particle complexes of amides, Thermochimica Acta, 657, p. 20-25, 2017.

[32] J. S. Lomasa, L. Joubert, On the importance of intramolecular hydrogen bond cooperativity in D-glucose – an NMR and QTAIM approach, Magnetic Resonance Chemistry, 55, 10, p. 893–901, 2017.

[33] R. Montis, M. Arca, M. C. Aragoni, A. Bauzá, F. Demartin, A. Frontera, F. Isaiaa, V. Lippolis, Hydrogen- and halogen-bond cooperativity in determining the crystal packing of dihalogen charge-transfer adducts: a study case from heterocyclic pentatomic chalcogenone donors, CrystEngComm, 19, 30, p. 4401-4412, 2017.

[34] H. Muta, M. Miwa, M. Satoh, Ion-specific swelling of hydrophilic polymer gels, Polymer, 42, 14, p. 6313-6316, 2001.

[35] H. Muta, S. Kawauchi, M. Satoh, Ion effects on hydrogen-bonding hydration of polymer an approach by 'induced force model', Journal of Molecular Structure: Theochem, 620, 1, p. 65-76, 2003.

[36] G. Gilli, F. Bellucci, V. Ferretti, V. Bertolasi, Evidence for resonance-assisted hydrogen bonding from crystal-structure correlations on the enol form of the beta-diketone fragment, Journal of the American Chemical Society, 111, 3, p. 1023–1028, 1989.

[37] V. Bertolasi, P. Gilli, V. Ferretti, G. Gilli, Evidence for resonance-assisted hydrogen bonding. 2. Intercorrelation between crystal structure and spectroscopic parameters in eight intramolecularly hydrogen bonded 1,3-diaryl-1,3-propanedione enols, Journal of the American Chemical Society, 113, 13, p. 4917-4925, 1991.

[38] G. Gilli, V. Bertolasi, V. Ferretti, P. Gilli, Resonance-assisted hydrogen bonding. III. Formation of intermolecular hydrogen-bonded chains in crystals of [beta]-diketone enols and its relevance to molecular association, Acta Crystallographica B, 49, p. 564-576, 1993.

[39] P. Gilli, V. Bertolasi, V. Ferretti, G. Gilli, Evidence for resonance-assisted hydrogen bonding. 4. Covalent nature of the strong homonuclear hydrogen bond. Study of the O-H--O system by crystal structure correlation methods, Journal of the American Chemical Society, 116, 3, p. 909-915, 1994.

[40] V. Bertolasi, L. Pretto, G. Gilli, P. Gilli, Pi-Bond cooperativity and anticooperativity effects in resonance-assisted hydrogen bonds (RAHBs), Acta Crystallographica B, 62, p. 850-863, 2006.

[41] R. W. Góra, M. Maja, S. J. Grabowski, Resonance-assisted hydrogen bonds revisited. Resonance stabilization vs. charge delocalization, Physical Chemistry Chemical Physics, 15, 7, p. 2514-2522, 2013.

[42] J. M. Guevara-Vela, E. Romero-Montalvo, A. Costales, Á. M. Pendás, T. Rocha-Rinza, The nature of resonance-assisted hydrogen bonds: a quantum chemical topology perspective, Physical Chemistry Chemical Physics, 18, 38, p. 26383-26390, 2016.

[43] G. Baranović, Intramolecular resonance-assisted hydrogen bonds: a theoretical description by means of atomic charges and charge fluxes, Spectrochimica Acta Part A: Molecular and Biomolecular Spectroscopy, 117, p. 465-472, 2014.

[44] K. T. Mahmudov, A. J. L. Pombeiro, Resonance-Assisted Hydrogen Bonding as a Driving Force in Synthesis and a Synthon in the Design of Materials, Chemistry – A European Journal, 22, 46, p. 16356-16398, 2016.

[45] T. M. Krygowski, J. E. Zachara-Horeglad, Resonance-assisted hydrogen bonding in terms of substituent effect, Tetrahedron, 65, 10, p. 2010-2014, 2009.

[46] A. V. Gurbanov, M. L. Kuznetsov, S. D. Demukhamedova, I. N. Alieva, N. M. Godjaev, F. I. Zubkov, K. T. Mahmudov, A. J. L. Pombeiro, Role of substituents on resonance assisted hydrogen bonding vs. intermolecular hydrogen bonding, CrystEngComm, 22, 4, p. 628-633, 2020.

[47] M. Palusiak, S. Simon, M. Solà, Interplay between Intramolecular Resonance-Assisted Hydrogen Bonding and Aromaticity in o-Hydroxyaryl Aldehydes, Journal of Organic Chemistry, 71, 14, p. 5241–5248, 2006.

[48] J. N. Woodford, Density Functional Theory and Atoms-in-Molecules Investigation of Intramolecular Hydrogen Bonding in Derivatives of Malondialdehyde and Implications for Resonance-Assisted Hydrogen Bonding, Journal of Physical Chemistry A, 111, 34, p. 8519–8530, 2007.

[49] L. O. Johannissen, T. Irebo, M. Sjödin, O. Johansson, L. Hammarström, The Kinetic Effect of Internal Hydrogen Bonds on Proton-Coupled Electron Transfer from Phenols: A Theoretical Analysis with Modeling of

Experimental Data, Journal of Physical Chemistry B, 113, 50, p. 16214–16225, 2009.

[50] S. Shetty, S. Pal, D. Kanhere, A. Goursot, A quantitative and a qualitative study of the resonance assisted double proton transfer in formic acid dimer, Indian Journal of Chemistry - Section A Inorganic, Physical, Theoretical and Analytical Chemistry, 45, 2005.

[51] P. Sanz, O. Mó, M. Yáñez, J. Elguero, Resonance-Assisted Hydrogen Bonds: A Critical Examination. Structure and Stability of the Enols of β-Diketones and β-Enaminones, Journal of Physical Chemistry A, 111, 18, p. 3585–3591, 2007.

[52] J. J. Dannenberg, R. Rios, Theoretical study of the enolic forms of acetylacetone. How strong is the H-bond?, Journal of Physical Chemistry, 98, 1994.

[53] J. L. Burdett, M. T. Rogers, Keto-Enol Tautomerism in β-Dicarbonyls Studied by Nuclear Magnetic Resonance Spectroscopy.1 I. Proton Chemical Shifts and Equilibrium Constants of Pure Compounds, Journal of the American Chemical Society, 86, 11, p. 2105–2109, 1964.

[54] M. M. Folkendt, B. E. Weiss-Lopez, J. P. Chauvel Jr., N. S. True, Gas-phase proton NMR studies of keto-enol tautomerism of acetylacetone, methyl acetoacetate, and ethyl cetoacetate, Journal of Physical Chemistry, 89, 15, p. 3347–3352, 1985.

[55] J. C. Sloop, C. L. Bumgardner, G. Washingtonl, W. D. Loehle, S. S. Sankar, A. B. Lewis, Keto–enol and enol–enol tautomerism in trifluoromethyl-β-diketones, Journal of Fluorine Chemistry, 127, 6, p. 780-786, 2006.

[56] R. R. Lozada-Garcia, J. Čeponkus, W. Chin, M. Chevalier, C. Crépin, Acetylacetone in hydrogen solids: IR signatures of the enol and keto tautomers and UV induced tautomerization, Chemical Physics Letters, 504, 4-6, p. 142-147, 2011.

[57] E. F. Caldin, V. Gold, Proton-Transfer Reactions, Springer, New York, 2013.

[58] A. J. Kresge, What makes proton transfer fast, Accounts of Chemical Research, 8, 10, p. 354–360, 1975.

[59] L. I. Krishtalik, The mechanism of the proton transfer: an outline, Biochimica et Biophysica Acta (BBA) – Bioenergetics, 1458, 1, p. 6-27, 2000.

[60] F. Dolati, S. Faramarz Tayyari, M. Vakili, Y. A. Wang, Proton transfer in acetylacetone and its α-halo derivatives, Physical Chemistry Chemical Physics, 18, 1, p. 344-350, 2016.

[61] P. E. Hartman, Putative mutagens and carcinogens in foods. IV. Malonaldehyde (malondialdehyde), Environmental and Molecular Mutagenesis, 5, 4, p. 603-607, 1983.

[62] G. Landau, V. K. Kodali, J. D. Malhotra, R. J. Kaufman, Detection of Oxidative Damage in Response to Protein Misfolding in the Endoplasmic Reticulum, Part A in *Methods in Enzymology*, Academic Press, Cambridge, p. 231-250, 2013.

[63] H. Siegel, M. Eggersdorfer, Ketones in *Ullmann's Encyclopedia of Industrial Chemistry (7th ed.),* John Wiley & Sons, New York, 2011.

[64] J. Pradhan, A. Goyal, β-diketones: Important Intermediates for Drug Synthesis, International Journal of Pharmaceutical Research & Allied Sciences, 4, 2, p. 1-18, 2015.

[65] M. Parolini, Toxicity of the Non-Steroidal Anti-Inflammatory Drugs (NSAIDs) acetylsalicylic acid, paracetamol, diclofenac, ibuprofen and naproxen towards freshwater invertebrates: A review, Science of The Total Environment, 740, 140043, 2020.

[66] J. M. Hollas, Modern Spectroscopy, John Wiley & Sons, Ltd, West Sussex, 2004.

[67] G. Gaulitz, T. Vo-Dinh, Handbook of Spectroscopy, Wiley-VCH, Weinheim, 2003.

[68] T. Bally, Matrix Isolation in *Reactive Intermediate Chemistry,* eds. R. A. Moss, M. S. Platz, M. Jones Jr., John Wiley & Sons, Inc., Fribourg, 2004.

[69] Z. Yan Ying, Z. Ming Fei, Are matrix isolated species really "isolated"? Infrared spectroscopic and theoretical studies of noble gas-transition metal oxide complexes, Science China, 53, 2, p. 327-336, 2009.

[70] A. Barnes, W. J. Orville-Thomas, R. Gaufrès, A. Müller, Matrix Isolation Spectroscopy, Springer Science & Business Media, New York, 2012.

[71] S. Cradock, A. J. Hinchcliffe, Matrix Isolation: A Technique for the Study of Reactive Inorganic Species, Cambridge University Press, Cambridge, 1975.

[72] J. Čeponkus, A. Engdahl, P. Uvdal, B. Nelander, Structure and dynamics of small water clusters, trapped in inert matrices, Chemical Physics Letters, 581, p. 1-9, 2013.

[73] L. Khriachtchev, Matrix-Isolation Studies of Noncovalent Interactions: More Sophisticated Approaches, Journal of Physical Chemistry A, 119, 12, p. 2735–2746, 2015.

[74] A. Schrivera, L. Schriver-Mazzuolia, A. A. Vigasin, Matrix isolation spectra of the carbon dioxide monomer and dimer revisited, Vibrational Spectroscopy, 23, 1, p. 83-94, 2000.

[75] K. Szczepaniak, M. M. Szczesniak, W. B. Person, Raman and Infrared Spectra of Thymine. A Matrix Isolation and DFT Study, Journal of Physical Chemistry A, 104, 16, p. 3852–3863, 2000.

[76] G. Bazsó, G. Tarczay, G. Fogarasi, P. G. Szalay, Tautomers of cytosine and their excited electronic states: a matrix isolation spectroscopic and quantum chemical study, Physical Chemistry Chemical Physics, 13, 15, p. 6799-6807, 2011.

[77] L. George, W. Sander, Matrix isolation infrared and ab initio study of the hydrogen bonding between formic acid and water, Spectrochimica Acta A: Molecular and Biomolecular Spectroscopy, 60, 13, p. 3225-3232, 2004.

[78] N. Nagashima, S. Kudoh, M. Nakata, IR and UV-visible absorption spectra of hexafluoroacetylacetone in a low-temperature argon matrix, II. Detection of the nπ* transition by monitoring IR spectral changes due to photoisomerization, Chemical Physics Letters, 374, 1, p. 67-73, 2003.

[79] N. Nagashima, S. Kudoh, M. Takayangi, M. Nakata, UV-induced photoisomerisation of acetylacetone and identification of less-stable isomers by low-temperature matrix-isolation infrared spectroscopy and density functional theory calculation, Journal of Physical Chemistry, 105, 48, p. 10832-10838, 2001.

[80] S. F. Tayyari, M. Zahedi-Tabrizi, R. Afzali, S. Laleh, H. A. Mirshashi, Y. A. Wang, Structure and vibrational assignement of the enol form of 3-

chloro-pentane-2,4-dione, Journal of Molecular Structure, 873, 1-3, p. 79-88, 2008.

[81] A. Trivella, S. Coussan, T. Chiavassa, P. Theule, C. Manca, P. Roubin, Comparative study of structure and photoinduced ractivity of malondialdehyde and acetylacetone isolated in nitrogen matrices, Fizika Nizkikh Temperatur, 32, 11, p. 1042-1049, 2006.

[82] R. Lozada-Garcia. Dynamics and photodynamics of acetylacetone in para-hydrogen matrices, Université Paris Sud - Paris XI, Orsay, France, 2012.

[83] A. Gutierrez Quintanilla, Molecules and complexes with hydrogen bond: solvation and photoreactivity in cryogenic matrices, Université Paris Sud - Paris XI, Orsay, France, 2017.

[84] M. Takamasa, S. Tadamasa, Matrix-Isolation Spectroscopy Using Solid Parahydrogen as the Matrix: Application to High-Resolution Spectroscopy, Photochemistry, and Cryochemistry, Bulletin of the Chemical Society of Japan, 71, 1, p. 1-15, 1998.

[85] M. E. Fajardo, S. Tam, M. E. DeRose, Matrix isolation spectroscopy of H_2O, D_2O, and HDO in solid parahydrogen, Journal of Molecular Structure, 695–696, p. 111-127, 2004.

[86] T. Masashi, T. Chih-Yu, L. Yuan-Pern, Spectroscopy of prospective interstellar ions and radicals isolated in para-hydrogen matrices, Phys. Chem. Chem. Phys., 20, 8, p. 5344-5358, 2018.

[87] H. D. Lutz, Structure and strength of hydrogen bonds in inorganic solids, Journal of Molecular Structure, 646, 1-3, p. 227-236, 2003.

[88] M. C. Etter, Encoding and decoding hydrogen-bond patterns of organic compounds, Accounts of Chemical Research, 23, 4, p. 120–126, 1990.

[89] O. Takahashi, Y. Kohno, M. Nishio, Relevance of Weak Hydrogen Bonds in the Conformation of Organic Compounds and Bioconjugates: Evidence from Recent Experimental Data and High-Level ab Initio MO Calculations, Chemical Reviews, 110, 10, p. 6049–6076, 2010.

[90] S. J. Park, M. K. Seo, Solid-Solid Interfaces in *Interface Science and Technology*, Academic Press, Cambridge, p. 253-331, 2011.

[91] J. Emsley, Very strong hydrogen bonding, Chemical Society Reviews, 9, 1, p. 91-124, 1980.

[92] P. R. Rablen, J. W. Lockman, W. L. Jorgensen, Ab Initio Study of Hydrogen-Bonded Complexes of Small Organic Molecules with Water, Journal of Physics Chemistry A, 102, 21, p. 3782–3797, 1998.

[93] R. Iwamoto, T. Matsuda, T. Sasaki, H. Kusanagi, Basic Interactions of Water with Organic Compounds, Journal of Physical Chemistry B, 107, 31, p. 7976–7980, 2003.

[94] G. Zeng, J. Gao, S. Chen, H. Chen, Z. Wang, X. Zhang, Combining Hydrogen-Bonding Complexation in Solution and Hydrogen-Bonding-Directed Layer-by-Layer Assembly for the Controlled Loading of a Small Organic Molecule into Multilayer Films, Langmuir, 23, 23, p. 11631–11636, 2007.

[95] S. F. Tayyari, F. Milani-Nejad, H. Rahemi, Structure and vibrational spectra of the enol form of hexafluoro-acetylacetone. A density functional theoretical study, Spectrochimica Acta Part A: Molecular and Biomolecular Spectroscopy, 58, 8, p. 1669-1679, 2002.

[96] V. V. Sliznev, S. B. Lapshina, G. V. Girichev, Ab Initio Structure Investigation of the Enol Forms of β-Diketones $RCOCH_2COR$ (R = H, CH_3, CF_3), Journal of Structural Chemistry, 43, 1, p. 47–55, 2002.

[97] C. Castro, W. L. Karney, Heavy-Atom Tunneling in Organic Reactions, Angewandte Chemie, 59, 22, p. 8355-8366, 2020.

[98] W. Siebrand, Z. Smedarchina, A. Fernández-Ramos, Communication: selection rules for tunneling splitting of vibrationally excited levels, J. Chem. Phys., 139, 2, p. 1-4, 2013.

[99] J. B. Brubach, Signatures of the hydrogen bonding in the infrared bands of water, J. Chem. Phys., 122, 18, 184509, 2005.

[100] S. F. Tayyari, M. Z. Tabrizi, F. Tayyari, F. Milani-Nejad, A two-dimensional double minimum potential function for bent hydrogen bonded systems. I-malondialdehyde, Journal of Molecular Structure: Theochem., 637, p. 171–181, 2003.

[101] D. P. Tew, N. C. Handy, S. Carter, A reaction surface Hamiltonian study of malonaldehyde, Journal of Chemical Physics, 125, 8, 084313, 2006.

[102] P. Lenain, M. Mandado, R. A. Mosquera, P. Bultinck, Interplay between Hydrogen-Bond Formation and Multicenter π-Electron Delocalization:

Intramolecular Hydrogen Bonds, Journal of Physical Chemistry, 112, 42, p. 10689–10696, 2008.

[103] N. V. Belova, V. V. Sliznev, H. Oberhammer, G. V. Girichev, Tautomeric and conformational properties of b-diketones, Journal of Molecular Structure, 978, 1, p. 282–293, 2010.

[104] Y. Arasaki, K. Yamazaki, M. T. do N. Varella, K. Takatsuka, Real-time observation of ground state proton transfer: a model study, Chemical Physics 311, 3, p. 255–268, 2005.

[105] M. T. do N. Varella, Y. Arasaki, H. Ushiyama, V. McKoy, K. Takatsuka, Time-resolved photoelectron spectroscopy of proton transfer in the ground state of chloromalonaldehyde: Wave-packet dynamics on effective potential surfaces of reduced dimensionality, Journal of Chemical Physics, 124, 15, 154302, 2006.

[106] S. Scheiner, Relationship Between Strength of Hydrogen Bond and Barrier to Proton-Transfer, Journal of Molecular Structure: Theochem, 113, p. 65-71, 1993.

[107] S. L. Baughcum, R. W. Duerst, W. F. Rowe, Z. Smith, E. Bright Wilson, Microwave spectroscopic study of malondialdehyde (3-hydroxy-2-propenal). 2. Structure, dipole moment, and tunneling, Journal of the American Chemical Society, 103, 21, p. 6296–6303, 1981.

[108] C. Duan, D. Luckhaus, High resolution IR-diode laser jet spectroscopy of malonaldehyde, Chemical Physics Letters, 391, 1-3, p. 129–133, 2004.

[109] C. J. Seliskar, R. E. Hoffmann, On the Infrared Spectrum of Malondialdehyde, A Tunneling Hydrogen-Bonded Molecule, Journal of Molecular Spectroscopy, 96, 1, p. 146–155, 1982.

[110] T. N. Wassermann, D. Luckhaus, S. Coussan, M. A. Suhm, Proton tunneling estimates for malondialdehyde vibrations from supersonic jet and matrix quenching experiments, Physical Chemistry Chemical Physics, 8, 20, p. 2344–2348, 2006.

[111] N. O. B. Lüttschwager, T. N. Wassermann, S. Coussan, M. A. Suhm, Periodic bond breaking and making in the electronic ground state on a sub-picosecond timescale: OH bending spectroscopy of malonaldehyde in the frequency domain at low temperature, Physical Chemistry Chemical Physics, 12, 29, 2010.

[112] N. O. B. Lüttschwager, T. N. Wassermann, S. Coussan, M. A. Suhm, Vibrational tuning of the hydrogen transfer in malonaldehyde – a combined FTIR and Raman jet study, Molecular Physics, 111, 14-15, p. 2211–2227, 2013.

[113] V. A. Benderskii, E. V. Vetoshkin, I. S. Irgibaeva, Hans P. Trommsdorff, Tunneling splittings in vibrational spectra of non-rigid molecules: IX. Malonaldehyde and its isotopomers as a test case for fully coupled multidimensional tunneling dynamics, Chemical Physics, 262, 2, p. 393–422, 2000.

[114] T. Hammer, M. D. Coutinho-Neto, A. Viel, U. Manthe, Multiconfigurational time-dependent Hartree calculations for tunneling splittings of vibrational states: theoretical considerations and application to malonaldehyde, Journal of Chemical Physics, 131, 22, 224109, 2009.

[115] F. Wu, Y. Ren, W. Bian, The hydrogen tunneling splitting in malonaldehyde: a full-dimensional time-independent quantum mechanical method, Journal of Chemical Physics, 145, 7, 074309, 2016.

[116] D. W. Firth, P. F. Barbara, H. P. Trommsdorff, Matrix induced localization of proton tunneling in malonaldehyde, Chemical Physics, 136, 2, p. 349–360, 1989.

[117] T. Chiavassa, P. Verlaque, L. Pizzala, A. Allouche, P. Roubin, Experimental and theoretical studies of the photoisomerization of malonaldehyde isolated in rare gas matrixes, Journal of Physical Chemistry, 96, 26, p. 5917–5925, 1993.

[118] E. Nakhaei, A. Nowroozi, On the performance of resonance assisted hydrogen bond theory in malonaldehyde derivatives, Computational and Theoretical Chemistry, 1096, p. 27–32, 2016.

[119] A. Nowroozi, H. Raissi, H. Hajiabadi, P. M. Jahani, Reinvestigation of Intramolecular Hydrogen Bond in Malonaldehyde Derivatives: An Ab initio, AIM and NBO Study, International Journal of Quantum Chemistry, 111, 12, p. 3040–3047, 2011.

[120] M. A. Rios, J. Rodriguez, Analysis of the effect of substitution on the intramolecular hydrogen bond of MA by ab initio calculations at the 3-21G level, Journal of Molecular Structure, 228, 1, p. 149–158, 1991.

[121] A. Trivella, P. Roubin, P. Theule, M. Rajzmann, S. Coussan, C. Manca, UV and IR Photoisomerization of Acetylacetone Trapped in a Nitrogen Matrix, Journal of Physical Chemistry A, 111, 16, p. 3074-3081, 2007.

[122] A. Trivella, T. N. Wassermann, J. M. Mestdagh, C. M. Tanner, F. Marinelli, P. Roubin, S. Coussan, New insights into the photodynamics of acetylacetone: isomerization and fragmentation in low-temperature matrixes, Physical Chemistry Chemical Physics, 29, 12, p. 8300-8310, 2010.

[123] S. F. Tayyari, F. Milani-Nejad, Vibrational assignment of acetylacetone, Spectrochimica Acta Part A: Molecular and Biomolecular Spectroscopy, 56, 14, p. 2679-2691, 2000.

[124] B. Czarnik-Matusewicz, M. Matusiak-Kucharska, J. P. Hawranek, Principal Components Analysis of Infrared Spectra of Liquid Acetylacetone, Polish Journal of Chemistry, 83, 5, p. 999-1011, 2009.

[125] R. R. Lozada-Garcia, J. Čeponkus, M. Chevalier, W. Chin, J. M. Mestdagh, C. Crépin, Nuclear Spin Conversion to Probe the Methyl Rotation Effect on Hydrogen-Bond and Vibrational Dynamics, Angewandte Chemie International Edition, 51, 28, p. 6947-6950, 2012.

[126] N. Nagashima, S. Kudoh, M. Nakata, Infrared and UV–visible absorption spectra of hexafluoroacetylacetone in a low-temperature argon matrix. I. Structure of a non-chelated enol-type isomer, Chemical Physics Letters, 374, 1-2, p. 59-66, 2003.

[127] Y. Minoura, N. Nagashima, S. Kudoh, M. Nakata, Mechanism of UV-Induced Conformational Changes among Enol-Type Isomers of (Trifluoroacetyl)acetone Studied by Low-Temperature Matrix-Isolation Infrared Spectroscopy and Density Functional Theory Calculation, Journal of Physical Chemistry A, 108, 12, p. 2353-2362, 2004.

[128] A. Nowroozi, H. Roohi, M. S. S. Ghoogheri, M. Sheibaninia, The competition between the intramolecular hydrogen bond and π-electron delocalization in trifluoroacetylacetone – A theoretical study, International Journal of Quantum Chemistry, 111, 3, p. 578-585, 2011.

[129] H. Raissi, A. Nowroozi, M. Roozbeh, F. Farzad, Molecular structure and vibrational assignment of (trifluoroacetyl)acetone: A density functional study, Journal of Molecular Structure, 787, 1-3, p. 148-162, 2006.

[130] M. Zahedi-Tabrizi, F. Tayyari, Z. Moosavi-Tekyeh, A. Jalali, S. F. Tayyari, Structure and vibrational assignment of the enol form of 1,1,1-trifluoro-2,4-pentanedione, Spectrochimica Acta Part A: Molecular and Biomolecular Spectroscopy, 65, 2, p. 387-396, 2006.

[131] A. L. Andreassen, S. H. Bauer, The structures of acetylacetone, trifluoroacetylacetone and trifluoroacetone, Journal of Molecular Structure, 12, 3, 1972.

[132] K. I. Lazaar, S. H. Bauer, Intramolecular unsymmetrical oxygen-hydrogen-oxygen (OHO) bonds. Thermochemistry, Journal of Physical Chemistry, 87, 13, p. 2411-2416, 1983.

[133] L. B. Favero, L. Evangelisti, B. Velino, W. Caminati, Morphing the Internal Dynamics of Acetylacetone by CH3 → CF3 Substitutions. The Rotational Spectrum of Trifluoroacetylacetone, Journal of Physical Chemistry A, 118, 24, p. 4243−4248, 2014.

[134] M. Takano, T. Takahashi, K. Iijima, Y. Yamada, The acetylacetone-water complex in a low-temperature solid argon matrix, Journal of Molecular Spectroscopy, 333, p. 27-35, 2017.

[135] I. Raskin, Role of salicylic acid in plants, Annual Review of Plant Biology, 43, 1, p. 439-463, 1992.

[136] G. A. Green, Understanding NSAIDs: From aspirin to COX-2, Clinical Cornerstone, 3, 5, p. 50-59, 2001.

[137] J. N. Cashman, The Mechanisms of Action of NSAIDs in Analgesia, Drugs, 52, p. 13–23, 1996.

[138] T. Yahagi, A. Fujii, T. Ebata, N. Mikami, Infrared Spectroscopy of the OH Stretching Vibrations of Jet-Cooled Salicylic Acid and Its Dimer in S0 and S1, Journal of Physical Chemistry A, 105, 47, p. 10673-10680, 2001.

[139] E. Abd El-Hakam, A. El-Nasr, A. Fujii, T. Ebata, N. Mikami, Substitution effects on the excited-state intramolecular proton transfer of salicylic acid: an infrared spectroscopic study on the OH stretching vibrations of jet-cooled 5-methoxysalicylic acid, Chemical Physics Letters, 376, 5-6, p. 788–793, 2003.

[140] A. L. Sobolewski, W. Domcke, Intramolecular Hydrogen Bonding in the S1(ππ*) Excited State of Anthranilic Acid and Salicylic Acid: TDDFT

Calculation of Excited-State Geometries and Infrared Spectra, Journal of Physical Chemistry A, 108, 49, p. 10917-10922, 2004.

[141] M. Miyagawa, N. Akai, M. Nakata, UV-induced photoreaction pathways of salicylic acid: Identification of the fourth stable isomer and ketoketene–water complex, Chemical Physics Letters, p. 52-57, 2014.

[142] R. Szostak, S. Mazurek, Quantitative determination of acetylsalicylic acid and acetaminophen in tablets by FT-Raman spectroscopy, Analyst, 127, 1, p. 144–148, 2002.

[143] S. H. Frasson Scafi, C. Pasquini, Identification of counterfeit drugs using near-infrared spectroscopy, Analyst, 126, 12, p. 2218–2224, 2001.

[144] A. B. Moreira, I. L.T. Dias, G. Oliveira Neto, E. A. G. Zagatto, L. T. Kubota, Solid-phase fluorescence spectroscopy for the determination of acetylsalicylic acid in powdered pharmaceutical samples, Analytica Chimica Acta, 523, p. 49–52, 2004.

[145] P. Vishweshwar, J. A. McMahon, M. Oliveira, M. L. Peterson, M. J. Zaworotko, The Predictably Elusive Form II of Aspirin, Journal of the American Chemical Society, 127, 48, p. 16802-16803, 2005.

[146] J. Cruz, M. Bautista, J. M. Amigo, M. Blanco, NIR-chemical imaging study of acetylsalicylic acid in commercial tablets, Talanta, 80, 2, p. 473–478, 2009.

[147] L. F. Sallum, F. L. F. Soares, J. A. Ardila, R. L. Carneiro, Determination of acetylsalicylic acid in commercial tablets by SERS using silver nanoparticle-coated filter paper, Spectrochimica Acta Part A: Molecular and Biomolecular Spectroscopy, 133, p. 107-111, 2014.

[148] J. Schneider, C. Zheng, K. Reuter, Thermodynamics of surface defects at the aspirin/water interface, Journal of Chemical Physics, 141, 12, 124702, 2014.

[149] J. P. Li, J. M. Guo, E. X. Shang, Z. H. Zhu, Y. Liu, B. C. Zhao, J. Zhao, Z. S. Tang, J. A. Duan, Quantitative determination of five metabolites of aspirin by UHPLC–MS/MS coupled with enzymatic reaction and its application to evaluate the effects of aspirin dosage on the metabolic profile, Journal of Pharmaceutical and Biomedical Analysis, 138, p. 109-117, 2017.

[150] Y. A. Ribeiro, A. C. F. Caires, N. Boralle, M. Ionashiro, Thermal decomposition of acetylsalicylic acid (aspirin), Termochimica Acta, 279, p. 177-181, 1996.

[151] R. Glaser, Aspirin. An ab Initio Quantum-Mechanical Study of Conformational Preferences and of Neighboring Group Interactions, Journal of Organic Chemistry, 66, 3, p. 771-779, 2001.

[152] C. Cabezas, J. L. Alonso, J. C. Lopez, S. Mata, Unveiling the Shape of Aspirin in the Gas Phase, Angewandte Chemie International Edition, 51, 6, p. 1375 –1378, 2012.

[153] E. D. Becker, G. C. Pimentel, Spectroscopic Studies of Reactive Molecules by the Matrix Isolation Method, Journal of Chemical Physics, 25, 2, 224, 1956.

[154] E. D. Becker, G. C. Pimentel, Mathias Van Thiel, Matrix Isolation Studies: Infrared Spectra of Intermediate Species in the Photolysis of Hydrazoic Acid, Journal of Chemical Physics, 26, 145, 1957.

[155] L. Khriachtchev, Physics and Chemistry at Low Temperatures, Pan Stanford, Singapore, 2011.

[156] V. E. Bondybey, A. M. Smith, J. Agreiter, New Developments in Matrix Isolation Spectroscopy, Chemical Reviews, 96, 6, p. 2113−2134, 1996.

[157] C. M. Nunes, I. Reva, R. Fausto, Direct Observation of Tunnelling Reactions by Matrix Isolation Spectroscopy in *Tunnelling in Molecules: Nuclear Quantum Effects from Bio to Physical Chemistry*, Royal Society of Chemistry, London, p. 1-60, 2020.

[158] I. R. Dunkin, Matrix Isolation Techniques: A Practical Approach, Oxford University Press, Oxford, 1998.

[159] M. Winter, K. Seranski, U. Schurath, Site effects in spectra of matrix-isolated diatomic molecules: a modeling approach, Chemical Physics, 159, 2, p. 235–246, 1992.

[160] A. J. Barnes, Z. Mielke, Matrix effects on hydrogen-bonded complexes trapped in low-temperature matrices, Journal of Molecular Structure, 1023, p. 216-221, 2012.

[161] M. Okuruma, M. C. Chan, T. Oka, High resolution infrared spectroscopy of solid hydrogen: The tetrahexacontapole-induced Delta J=6 transitions, Physical Reviews Letters, 62, 1, p. 32-35, 1989.

[162] S. Tam, M. E. Fajardo, Ortho/para hydrogen converter for rapid deposition matrix isolation spectroscopy, Review of Scientific Instruments, 70, 4, 1926, 1999.

[163] M. E. Fajardo, S. Tam, Rapid vapor deposition of millimeters thick optically transparent parahydrogen solids for matrix isolation spectroscopy, Journal of Chemical Physics, 108, 10, 4237, 1998.

[164] S. Tam, M. E. Fajardo, Single and Double Infrared Transitions in Rapid-Vapor-Deposited Parahydrogen Solids: Application to Sample Thickness Determination and Quantitative Infrared Absorption Spectroscopy, Applied Spectroscopy, 55, 12, p. 1634-1644, 2001.

[165] I. F. Silvera, The solid molecular hydrogens in the condensed phase: Fundamentals and static properties, Reviews of Modern Physics, 52, 393, 1980.

[166] F. Jensen, Introduction to Computational Chemistry, John Wiley & Sons, Inc., Fribourg, 2007.

[167] T. Tsuneda, Density Functional Theory in Quantum Chemistry, Springer, New York, 2014.

[168] J. Šulskus, Kompiuterinės chemijos įvadas (mokomoji knyga), Vilnius, 2006.

[169] D. R. Hartree, The Wave Mechanics of an Atom with a Non-Coulomb Central Field, Mathematical Proceedings of the Cambridge Philosophical Society, 24, 1, p. 89-110, 1928.

[170] J. C. Slater, Note on Hartree's Method, Physical Review, 35, 2, p. 210–211, 1930.

[171] K. Kim, K. D. Jordan, Comparison of Density Functional and MP2 Calculations on the Water Monomer and Dimer, Journal of Physical Chemistry, 98, 40, p. 10089–10094, 1994.

[172] D. S. Sholl, J. A. Steckel, Density functional theory: a practical introduction, Wiley, New Jersey, 2009.

[173] W. Kohn, L. J. Sham, Self-consistent equations including exchange and correlation effects, Physical Reviews, 140, A1133, 1965.

[174] A. D. Becke, Density-functional exchange-energy approximation with correct asymptotic behavior, Physical Reviews A, 38, 3098, p. 3098–3100, 1988.

[175] C. Lee, W. Yang, R. G. Parr, Development of the Colle-Salvetti correlation-energy formula into a functional of the electron density, Physical Reviews B, 37, 2, p. 785–789, 1988.

[176] A. D. Becke, Density-functional thermochemistry. III. The role of exact exchange., Journal of Chemical Physics 98, 7, p. 5648–5652, 1993.

[177] C. J. Cramer, Essentials of computational chemistry: theories and models, Wiley, New Jersey, 2004.

[178] P. M. W. Gill, Molecular integrals Over Gaussian Basis Functions, Advances in Quantum Chemistry, 25, p. 141-205, 1994.

[179] H. Taketa, S. Huzinaga, K. O-ohata, Gaussian-Expansion Methods for Molecular Integrals, Journal of the Physical Society of Japan, 21, 11, p. 2313–2324, 1966.

[180] T. H. Dunning Jr., Gaussian Basis Functions for Use in Molecular Calculations. I. Contraction of (9s5p) Atomic Basis Sets for the First-Row Atoms, Journal of Chemical Physics, 53, 7, 2823, 1970.

[181] S. Huzinaga, Gaussian-Type Functions for Polyatomic Systems. I, Journal of Chemical Physics, 42, 4, 1293, 1965.

[182] T. H. Dunning Jr., Gaussian basis sets for use in correlated molecular calculations. I. The atoms boron through neon and hydrogen, Journal of Chemical Physics, 90, 2, 1007, 1990.

[183] A. Trivella, S. Coussan, T. Chiavassa, Malonaldehyde synthesis, Synthetic Communications, 38, 19, p. 3285–3290, 2008.

[184] Gaussian 16, Revision C.01, M. J. Frisch, G. W. Trucks, H. B. Schlegel, G. E. Scuseria, M. A. Robb, J. R. Cheeseman, G. Scalmani, V. Barone, G. A. Petersson, H. Nakatsuji, X. Li, M. Caricato, A. V. Marenich, J. Bloino, B. G. Janesko, R. Gomperts, B. Mennucci, H. P. Hratchian, J. V. Ortiz, A. F. Izmaylov, J. L. Sonnenberg, D. Williams-Young, F. Ding, F. Lipparini, F. Egidi, J. Goings, B. Peng, A. Petrone, T. Henderson, D. Ranasinghe, V. G.

Zakrzewski, J. Gao, N. Rega, G. Zheng, W. Liang, M. Hada, M. Ehara, K. Toyota, R. Fukuda, J. Hasegawa, M. Ishida, T. Nakajima, Y. Honda, O. Kitao, H. Nakai, T. Vreven, K. Throssell, J. A. Montgomery, Jr., J. E. Peralta, F. Ogliaro, M. J. Bearpark, J. J. Heyd, E. N. Brothers, K. N. Kudin, V. N. Staroverov, T. A. Keith, R. Kobayashi, J. Normand, K. Raghavachari, A. P. Rendell, J. C. Burant, S. S. Iyengar, J. Tomasi, M. Cossi, J. M. Millam, M. Klene, C. Adamo, R. Cammi, J. W. Ochterski, R. L. Martin, K. Morokuma, O. Farkas, J. B. Foresman, and D. J. Fox, Gaussian, Inc., Wallingford CT, 2016.

[185] A. H. Lowrey, C. George, P. D'Antonio, J. Karle, Structure of acetylacetone by electron diffraction, Journal of the American Chemical Society, 93, 24, p. 6399–6403, 1971.

[186] M. R. Johnson, Structure and dynamics of the keto and enol forms of acetylacetone in the solid state, Journal of Chemical Physics, 116, 13, 5694, 2002.

[187] W. Caminati, J. U. Grabow, The C_{2v} Structure of Enolic Acetylacetone, Journal of the American Chemical Society, 128, 3, p. 854-857, 2005.

[188] I. Matanović, N. Došlić, Z. Mihalić, Exploring the potential energy surface for proton transfer in acetylacetone, Chemical Physics, 306, 1-3, p. 201-207, 2004.

[189] K. Hinsen, B. Roux, Potential of mean force and reaction rates for proton transfer in acetylacetone, Journal of Chemical Physics, 106, 9, 3567, 1997.

[190] E. D. Raczyńska, W. Kosińska, B. Ośmiałowski, R. Gawinecki, Tautomeric Equilibria in Relation to Pi-Electron Delocalization, Chemical Reviews, 105, 10, p. 3561-3612, 2005.

[191] S. A. Broadbent, L. A. Burns, C. Chatterjee, P. H. Vaccaro, Investigation of electronic structure and proton transfer in ground state acetylacetone, Chemical Physics Letters, 434, 1, p. 31-37, 2007.

[192] S. Coussan, C. Manc, Y. Ferro, P. Roubin, UV and IR photoisomerizations of an intramolecularly H-bonded molecule: acetylacetone trapped in nitrogen matrix, Chemical Physics Letters, 370, 1-2, p. 118-125, 2003.

[193] P. K. Verma, F. Koch, A. Steinbacher, P. Nuernberger, T. Brixner, Ultrafast UV-Induced Photoisomerization of Intramolecularly H-Bonded Symmetric β-Diketones, Journal of the American Chemical Society, 136, 42, p. 14981–14989, 2014.

[194] V. B. Delchev, H. Mikosch, G. St. Nikolov, The Keto-Enol Equilibrium of Pentane-2,4-dione Studied by ab initio Methods, Chemical Monthly, 132, p. 339–348, 2001.

[195] X. Z. Li, B. Walker, A. Michaelides, Quantum nature of the hydrogen bond, Proceedings of the National Academy of Sciences of the United States of America, 108, 16, p. 6369-6373, 2011.

[196] J. Čeponkus, B. Nelander, Water Dimer in Solid Neon. Far-Infrared Spectrum. Journal of Physical Chemistry A, 108, 31, p. 6499-6502, 2004.

Table AI-1. Vibrational assignments of CCC isomer of ClMA molecule.

experimental				calculations		
Ne	pH$_2$	Ar		vibrational mode	CCC	
$\tilde{\nu}$, cm^{-1}	$\tilde{\nu}$, cm^{-1}	$\tilde{\nu}$, cm^{-1}	int, cm^{-1}		$\tilde{\nu}$, cm^{-1}	int, rel. un.
				νOH	3314.0	43
	2909.8	2977.1	0.08	νOH, νCH (OH)	3168.4	49
2875.1	2876.7	2885.8	0.3	νCH (CO)	3001.9	21
1670.2	1665.8	1664.7	0.8	νC=O + νC=C + δCH	1700.7	65
1600.0	1608.8	1601.5	0.1	δOH + δCH (OH) + νCO + νC=C (s)	1613.3	100
1586.7	1563.0	1579.3	0.1			
1573.5						
1396.2	1387.0	1396.2	0.1	δCH (CO) + δCH (OH)	1421.6	11
1381.3		1382.9	0.03			
1347.7	1346.4			δCH (CO) + δCH (OH)	1383.2	43
1343.0		1343.4	0.5	δOH + δCH (OH)	1371.4	27
1233.6	1232.3	1229.0	2.1	δOH + δCH (OH)	1272.0	84
1070.6	1076.4	1070.0	0.4	νC-Cl + δCCC	1080.2	34
	1068.1	1066.1				
				γCH (CO) + γCH (OH)	1034.6	3
953.7	952.8	952.7	0.04	γCH (CO) + γCH (OH) (s) + γOH	997.2	17
		950.8	0.05			
916.5	922.5	918.2	0.1	Δ	926.1	15
	914.7	913.4				
830.8	829.3	823.5	0.5	γOH	909.5	22

Table AI-2. Vibrational assignments of CTC and TCT isomers of ClMA molecule.

experimental				calculations				
Ne	pH$_2$	Ar		vibrational mode	CTC		TCT	
$\tilde{\nu}$, cm^{-1}	$\tilde{\nu}$, cm^{-1}	$\tilde{\nu}$, cm^{-1}	int, cm^{-1}		$\tilde{\nu}$, cm^{-1}	int, rel. un.	$\tilde{\nu}$, cm^{-1}	int, rel. un.
		3646.3	0.4	νOH			3852.0	61
3534.7	3524.1	3524.9	0.05	νOH	3709.1	13		
		3521.6	0.2					
				νCH (OH)			3175.9	1
3085.4	3079.2			νCH (OH)	3211.9	1		
		2888.1	0.01	νCH (CO)			2953.0	14
		2877.9	0.01					
2858.5	2862.4	2871.4	0.01	νCH (CO)	2936.1	12		
2839.9	2844.4	2858.4	0.1					
		2748.4	2750.9	0.03				
1719.0	1715.9	1713.8	0.2	νC=O + νC=C + δCH (CO)	1770.6	20		
	1702.9	1700.8	0.1	νCO + δCH (CO)			1763.0	79
		1650.7	0.07	δOH + δCH (OH) + νC=C			1685.3	64
1621.3	1616.1	1613.7	1.3	δOH + νC=O + νC=C	1641.8	100		
		1612.1	0.1					
				δCH (CO)			1434.3	4
		1386.6	0.04	δCH (CO) + δCH (OH)	1421.9	2		
				δCH (CO) + δCH (OH)			1366.8	11
1336.5	1334.2	1334.4	0.03	δOH + δCH (OH)	1372.4	1		
				δOH + δCH (OH)			1286.0	52
1277.9	1275.7	1275.4	0.09	δCH (OH)	1299.8	5		

Ne	pH₂	Ar ṽ	Ar int	vibrational mode	calc ṽ	calc int	calc ṽ	calc int
1276.6								
1211.5	1210.2	1209.5	0.2	δOH + δCH (OH)	1236.2	16		
1209.7								
				δOH + δCH (OH)			1197.7	4
		1112.7	0.04	δOH + δCH (Δ)			1088.2	100
1088.6	1087.7	1083.7	1.0	δOH + δCH (Δ)	1096.2	35		
1087.1								
				γCH (CO)			1013.9	0.5
				γCH (CO)	1022.5	0.5		
				γCH (OH)			923.4	3
913.9	916.3			γCH (OH)	951.3	3		
762.5	760.4			Δ	765.8	19		
761.7		759.6	0.4					
		706.8	0.05	Δ			713.3	21

Table AI-3. Vibrational assignments of TTC isomer of ClMA molecule.

experimental				calculations		
Ne	pH₂	Ar		vibrational mode	TTC	
ṽ, cm⁻¹	ṽ, cm⁻¹	ṽ, cm⁻¹	int, cm⁻¹		ṽ, cm⁻¹	int, rel. un.
3512.9	3525.1	3512.2	0.03	νOH	3698.1	17
		3508.4	0.3			
	3085.4			νCH(OH)	3201.7	0.5
2840.2	2826.4	2838.5	0.01	νCH(CO)	2892.1	18
		2777.6	0.03			
1719.7	1715.6	1714.7	1.2	νC=O + δCH(CO)	1771.0	54
1650.5	1646.2	1645.0	0.3	νC=C + δCH(OH)	1667.8	100
1642.7	1637.0	1635.2	1.3			
				δCH(CO) + δCH(OH) + δOH	1429.4	1
		1297.9	0.03	δCH(CO) + δCH(OH) + δOH	1372.7	1
		1264.6	0.02	δCH(OH) + δOH	1306.9	2
1195.7	1194.3	1194.9	0.1		1220.8	14

1194.1				νC-C + δCH(CO) + δOH		
1154.3	1152.8	1149.6	1.6	δOH + νC-C + δCH(CO) + δCH(OH)	1162.2	73
1153.5						
		1115.8	0.2			
	981.9			γCH(CO)	1005.6	0.5
893.5	894.2	895.0	0.07	γCH(OH)	919.7	4

Table AI-4. Vibrational assignments of relevant modes in AcAc, dAcAc, ACAcF6 and their associates with water.

experimental			calculations			
ACETYLACETONE						
AcAc + H_2O (Ar)	AcAc (Ar)	vibrational mode	AcAc + H_2O (C=O)	Int	AcAc	Int.
3776.7		ν_{as}OH (H_2O)				
3755.7		ν_{as}OH (H_2O)				
3711.5		ν_{as}OH (H_2O)				
3705.9		νOH (free, H_2O+AcAc)	3885.2			15
		ν_sOH (H_2O)				
3573.7		νOH (H_2O)$_2$				
3514.1		νOH (H_2O)$_3$				
3512.1		νOH (bound, H_2O+AcAc)	3640.8			100
3495.1		νOH (bound, H_2O+AcAc)				
1635.4	1637.5	νC=O + νC=C-OH + δOH	1668.1		1676.5	81
1624.1		νC=O + νC=C-OH + δOH				

1617.3	1616.5	νC=O + νC=C-OH +δOH (AcAc)	1624.7		1644.9	48
1590.0		δOH (bound, H_2O+AcAc)	1657.8		-	1
937.0	960.3	γOH (AcAc)	987.4		1010.0	11
DEUTERATED ACETYLACETONE						
D2-AcAc + H_2O (Ar)	D2-AcAc (Ar)		D2-AcAc + H_2O	D2-AcAc		
2740.6		νOD (free, D_2O+AcAc)	2835.2	17		
2569.1 2564.0		νOD (bound, D_2O+AcAc)	2638.2	57		
		νCD	2379.1	0.5	2373.9	0.5
		νOD (AcAc)	2243.2	58	2199.8	69
1621.9	1632.4	νC=O + νC=C-OD	1647.4	56	1662.8	70
1534.4	1535.4	νC=O + νC=C-OD + δOD (AcAc)	1551.2	100	1560.0	100
709.6	701.6	γOD	738.7	8	750.9	10
HEXAFLUOROACETYLACETONE						
6FAcAc (Ar)	6FAcAc + H_2O (Ar)		6FAcAc		6FAcAc + H_2O	
	3776.6	ν_{as}OH (H_2O)				
	3756.3					
	3730.1	ν_{as}OH (H_2O)				

	3711.3	ν_{as}OH (H$_2$O)+ νOH (free, H$_2$O+AcAc)			3895.2	15
	3670.2	ν_sOH (H$_2$O)				
	3639.8					
	3580.3*	νOH (H$_2$O)$_2$ + νOH (bound, H$_2$O+AcAc)			3779.4	19
	3516.3	νOH (H$_2$O)$_3$				
1696.0*	1696.0*	νC=O (CO) + νC=C + δOH	1722.7	27	1715.7	16
1639.2*	1639.2*	νC=C + δOH + δOH (H$_2$O	1650.1	49	1642.7	28
	1608.9					
	1592.1	δOH (H$_2$O, bound to AcAc)			1639.4	3
819.5*	819.5*	γOH	884.2	12	884.2	6

Table AI-5. Vibrational assignments (infrared absorption) of AcAcF3. Bands assigned to AcAcF3(OH) in bold. Calculation method M06-2X/6-311++G(3df,3pd).

Experimental					Calculated	
CO	N$_2$	Ar	Ne	pH$_2$		vibrational mode
3022	**3027**		**3032**	**3026**	**3186 vw**	**νCH$_3$(as)**
3014	3020	3019	3021	3016	3183 vw	νCH$_3$(as)
2980		2980	2980	2977	3138 vw	νCH$_3$(as)
2968				**2971**	**3132 vw**	**νCH$_3$(as)**
2932		2933	2933	2932	3074 vw	νCH$_3$(s)
1665 m	**1664 m**	**1658 w**	**1666 w**	**1661 w**	**1769.0 vs**	**[νCO + νC=C] oop**

1653 w	1654 w	1646 w	1650 w	1649 w	1774.5 s	[νCO + νC=C] oop
1623 w	**1623 w**	**1631 w**	**1633 vw**		**1695.8 s**	**[νCO + νC=C)] ip + δOH**
1607 s	1607 s	1609 s	1614 s	1611.5 s	1657.7 vvs	[νCO + νC=C)] ip + δOH
1470 vw	1473 w	1473 w	1471.5 w	1472 w	1508.9 w	δCH₃ (scissoring) + δC$_{sp2}$H
1422.5 w	1425 m	1424 m	1425.5 m 1429 m, sh	1424 w 1428.5 w	1465.1 s	δOH + δCH₃ (scissoring)
1360 w 1363.5	**1365.5 w 1363**	**1364 vw**	**1367 vvw**	**1365 vvw**	**1406.1 s**	**[δCH₃(umbrella) + δOH] oop**
1301 w 1284 br, struct	1301 1285 1275 br, struct	1301 1283 1273 1264 br, struct	1303 *1285 1274* 1267 br, struct	1301 *1288 1274* 1264 br, struct	1348.8 vs	ν(C-CF₃) + δOH
1290 m	**1304 1291 m, br**	**1290 w**	**1294 w**	**1292 m**	**1327.7 vvs**	**ν(C-CF₃) + ΔOH + δC$_{sp2}$H**
1216 sh	1217 sh	1213 s	1224.7 s	1223.5 s 1221.5 s	1279.0 s	νCF₃(as) + δC$_{sp2}$H
1211 s 1201 s	**1212 s 1201 s**	**1208 vs**	**1219 ᵈ m 1209 m**	**1210 s, br**	**1264.0 vs**	**νCF₃ (as)**

1204 m	1210 m, sh		1205 w	1204 w		
1197 m	1198 m	1199 m	1197.5 m	1198 m	1225.1 s	$\delta C_{sp2}H$
1168 vs	**1173 vs**	**1175 w**	**1184.5 m**	**1181 m**	**1239.3 vs**	**νCF_3 (as)**
	1164 w	1166 w		1173 w		
1160 m	1158 m	1156 w	1160.5 m	1160 m	1213.8 vs	νCF_3 (as)
1112	**1112 m**	**1110^b**	**1111.5 ^{b}**	**1111^b**	**1147.7 m**	**$\delta C_{sp2}H$**
1107.4 s	1109 m	1110 vs	1110.5 s 1111.5 s	1110 s	1137.6 s	$\delta C_{sp2}H$ + ν(CO-$C_{sp2}H$) + $\nu(CF_3)$
1034 vvvw	1036 vw	1036 vw	1039 vw	1037 vw	1063.7 vw	ρCH_3
1024 vw	**1027 vw**	**1024.4 vw**		**1027 vw**	**1052.0 vw**	**ρCH_3**
1009 vw	1010 vw	1009 vw	1012 vw	1010 vw	1033.1 vw	ρCH_3
986 vw	**988 vw**	**987 vvvw**	**988 vvvw**	**988 vw**	**1004.9 w**	**Δ + ρCH_3**
941.5 vw	943 vw	944 vw	942.5 vw 944.5 vw	942 vw 944.5 vw	967.5 vw	Δ
894 vw	**898 w**	**898 vw**	**898 vvw**	**895 vvw**	**921.2 m**	**γOH**
915 vw 875 vvw	916 vw 887 vw 878 vvw	934 vw 913 vw 898 vw	915 vw 884.0 vw	921 vw 905 vvw 882.5 vw	904.0 m	γOH

861 w	861 w	862.1 m	863 m	862.5 m	889.6 w	ν(CH₃-C) + ν(C- CF₃)
845 vw	**846 vw**				**872.7 vw**	**ν(CH₃-C) + ν(C- CF₃)**
803 vw **800.0 w**	**802.5 w** **800 vw**	**801 vvw**		**801.5 vw** **806.0 vw**	**833.7 m**	**γC_sp2H**
791 w	793 w 792 w	791 m	794.3 w 790.2 vw	793.5 m	813.7 w	γC_sp2H
759 vw	762 vw	761 vw	763.5 vw	763 w	775.0 w	Γ + γC_sp2H
730 w	729.5 w	729.5 w	731.3 m	730.5 w	749.4 m	δCF₃ (umbrella)
720 w	**720 w**	**720 vvw**			**736.1 w**	**δCF₃ (umbrella)**
	575 m				**584.7 m**	**δ(CH₃-C-O)**

Table AI-6. Vibrational assignments (Raman scattering) of AcAcF3. Bands assigned to AcAcF3(OH) in bold.
Calculation method M06-2X/6-311++G(3df,3pd).

Experimental				Calculated	
CO	N₂	Ar	Xe		vibrational mode
3126	3130 w	3130		3257	νC_sp2H
3017	3019 m	3020	3006	3183	νCH₃(as)
2977	2981 s	2979	2970	3138	νCH₃(as)
2932	2937 vs	2935	2926	3074	νCH₃(s)

1657	1657 wm	1654	1657	1775	[νCO + νC=C] oop
1627	**1628** m	**1628**	**1625**	**1696**	**[νCO + νC=C] ip + δOH**
1600	1608 s	1608	1608	1658	[νCO + νC=C] ip + δOH
1471	1471 w			1509	δ(CH$_3$) (scissoring) + δC$_{sp2}$H
1438	1438 sh	1436	1431	1475	δ(CH$_3$) (scissoring)
1423	1426 m	1425	1421	1465	δOH + δCH$_3$ (scissoring)
1391	**1390** vw, sh	**1390**		**1381**	
1381	1381 m	1379	1377	1395	[δ(CH$_3$) umbrella / δOH] ip
1346	1348 w	1345		1395	
1315	**1313** vw			**1381**	**[δCH$_3$(umbrella) + δOH] ip**
1302 1286 1275	1303 w 1286 vs 1275 vs	1303 1285 1272	1302 1286 1274	1349	ν(C-CF$_3$) + δOH
1210	1210 m, sh	1210	1210	1279	νCF$_3$(as) + δC$_{sp2}$H
1200	1200 m	1200	1200	1225	δC$_{sp2}$H
1114	**1113** w	**1112**	**1113**	**1148**	**δC$_{sp2}$H**
1108	1108 w			1138	δC$_{sp2}$H + ν(CO-C$_{sp2}$H) + ν(CF$_3$)
1039	1038 w	1037	1036	1064	ρCH$_3$
1014	1012 vw	1011	1011	1033	ρCH$_3$
990	**989** w	**989**		**1005**	**Δ + ρCH$_3$**
944	944 s	945	945	967	Δ
917	**917** w	**918**	**919**	**938**	**Δ + ρCH$_3$**
863	863 w	863	864	890	ν(CH$_3$-C) + ν(C-CF$_3$)
847	**847** vw			**873**	**ν(CH$_3$-C) + ν(C-CF$_3$)**
767	765 vvw	762	762	775	Γ + γC$_{sp2}$H

729	730 s	730	731	749	δCF_3 (umbrella)
720	**721** m	**721**	**722**	**736**	**δCF_3 (umbrella)**
590	593 m	591	589	598	Γ
575	**575** w	**576**		**585**	**$\delta(CH_3\text{-}C\text{-}O)$**
25	526 s	525	526	528	$\delta(C\text{-}C\text{-}OH)$
518	517 sh	519	518	524	δCF_3(scissoring)
440	441 w	439	440	444	$\delta(CF_3\text{-}C\text{-}C_{sp2})$ + δCF_3 (scissoring)
395	394 vw	393		395	Δ [$\delta(CH_3\text{-}C(OH)$ - CH)]
372	**371** vw			**366**	**Δ**
323	324 w	322	320	325	$\delta(CH_3\text{-}C(OH)$ -CH) + $\delta(F\text{-}C\text{-}C(CO))$
310	**314** w	**310**	**311**	**308**	**Δ**
300	**300** vvw			**302**	**Γ**
264	264 wm	263	264	252	Δ
190	192 w	186	185	178	Γ

Table AI-7. Salicylic acid (E form) assignments (with impurity bands identified as ASA – acetylsalicylic acid, AA – acetic acid, and H_2O).

experimental (cm^{-1})		calculations			
		vibrational mode		int., rel. un.	
3776.6	m				H_2O
3757.3	s				H_2O
3711.7	w				H_2O
3562.7	s	νOH (COOH)	3763.8	25	SA
3436.0	m, br	νOH (COH)	3214.6	1	SA
3215.7	w	$\nu_{as} CH$ (ring)	3100-2800		
1779.2	vw				AA
1752.3	w				ASA
1722.9	vw				
1718.9	w				ASA

1705.3	s	δOH (COOH, COH) + νC=O	1728.7	100	SA
1625.8	w	νC=C + δCH + δOH (COH)	1653.8	12	SA
1620.7	w				
1623.8	m				H$_2$O
1608.0	m				H$_2$O
1590.6	w	νC=C + δCH + δOH (COH)	1617.3	13	SA
1573.0	w				H$_2$O
1493.7	vw				
1489.5	m	δCH (ring) + δOH (COH)	1521.8	16	SA
1476.3	w	δCH (ring)	1491.9	9	SA
1422.8	m	δOH (COOH, COH) + δCH (ring)	1431.7	33	SA
1417.4	w				
1415.4	w				
1398.9	w				
1395.2	w				
1392.9	w				ASA
1387.6	m	δOH (COOH, COH) + δCH (ring)	1392.5	21	SA
1360.9	m				ASA
1319.9	w				ASA
1317.8	w	δOH (COOH, COH) + δCH (ring)	1350.8	5	SA
1289.4	vw				
1274.2	m	νC=O (COH)	1300.0	15	SA
1259.5	vw				
1223.9	w	δOH (COOH, COH) + δCH (ring)	1256.5	9	SA
1218.2	w				
1196.0	vw				

1186.8	m	δOH (COOH) + δCH (ring)	1205.6	42	SA
1175.6	m				ASA
1172.1	m				ASA
1153.1	vs	δOH (COOH) + δCH (ring)	1178.9	40	SA
1137.2 1135.1	m	δCH (ring)	1157.0	16	SA
1124.8	w				
1074.9	m	δCH (ring) + νC-O (COOH)	1090.7	16	SA
1033.7	w	δCH (ring)	1054.5	2	SA
865.2	vw	γCH (ring)	885.4	1	SA
851.6	w	γCH (ring)	861.7	3	SA
802.2	w	γCH (ring) ir γOH (COH)	826.8	9	SA
760.4	m	γOH (COH)	789.3	11	SA
758.5	m				
747.0	m	γCH (ring)	772.5	15	SA
722.8	vw				ASA
718.9	w				ASA
713.4 715.0	m				ASA
705.5	m	γOH (COOH) + δCH (ring)	709.8	6	SA
668.4	vw				
644.6	m	δCOOH (ring)	655.6	11	SA
563.4 560.5	m	γOH (COH)	582.9	18	SA

CURRICULUM VITAE

Name: Rasa
Surname: Platakytė
Date of birth: 1992-09-04
Place of birth: Vilnius, Lithuania
Email: rasa.platakyte@gmail.com

Education:

2017-2021	Vilnius University, Faculty of Physics *PhD studies*
2015-2017	Vilnius University, Faculty of Physics *Master's degree*
2011-2015	Vilnius University, Faculty of Physics *Bachelor's degree*
2007-2011	Vilnius lyceum
2008-2011	Young Physicists' School "Fotonas"
1999-2007	Vilnius Simonas Daukantas Secondary School

Work experience:

2017-now	Vilnius university, Faculty of Physics, Institute of Chemical Physics *Lecturer*
2015-2017	Vilnius university, Faculty of Physics, Institute of Chemical Physics *Laboratory technician*

PUBLICATIONS

1. Justinas Čeponkus, Rasa Platakytė, Valdas Šablinskas, Alejandro Gutiérrez-Quintanilla, FTIR study of acetylacetone, D2-acetylacetone and hexafluoroacetylacetone - water complexes in argon and nitrogen matrices, Chemija, 29(1), p. 1–16, 2018. (https://doi.org/10.6001/chemija.v29i1.3639)

2. Alejandro Gutiérrez-Quintanilla, Michèle Chevalier, Rasa Platakytė, Justinas Čeponkus, Germán A. Rojas-Lorenzo, Claudine Crépin, 2-Chloromalondialdehyde, a Model System of Resonance-Assisted Hydrogen Bonding: Vibrational Investigation, Physical Chemistry Chemical Physics, 20(18), p. 12888 – 12897, 2018. (https://doi.org/10.1039/C7CP06481K)

3. Alejandro Gutiérrez-Quintanilla, Michèle Chevalier, Rasa Platakytė, Justinas Čeponkus, Claudine Crépin, Selective photoisomerisation of 2-chloromalonaldehyde, Journal of Chemical Physics, 150(3), 034305, p. 1 – 11, 2019. (https://doi.org/10.1063/1.5082916)

4. Rasa Platakytė, Alejandro Gutiérrez-Quintanilla, Valdas Šablinskas, Justinas Čeponkus, Influence of environment and association with water to internal structure of trifluoroacetylacetone. Matrix isolation FTIR study, Low Temperature Physics, 45(6), p. 722-735, 2019. (https://doi.org/10.1063/1.5103254)

5. Alejandro Gutiérrez-Quintanilla, Michèle Chevalier, Rasa Platakytė, Justinas Čeponkus, Claudine Crépin, Intramolecular hydrogen tunneling in 2-chloromalonaldehyde trapped in solid para-hydrogen, Physical Chemistry Chemical Physics, 22(11), p. 6115-6121, 2020. (https://doi.org/10.1039/C9CP06866J)

6. Alejandro Gutiérrez-Quintanilla, Rasa Platakytė, Michèle Chevalier, Claudine Crépin, Justinas Čeponkus, Hidden Isomer of Trifluoroacetylacetone Revealed by Matrix Isolation Infrared and Raman Spectroscopy, The Journal of Physical Chemistry A, 125(11), p. 2249-2266, 2021. (https://doi.org/10.1021/acs.jpca.0c10945)

CONFERENCE LIST

1. Rasa Platakytė, Justinas Čeponkus, Claudine Crepin-Gilbert, Valdas Šablinskas, Fluoruotų acetilacetono darinių struktūros ir sąveikos su vandens molekulėmis tyrimas, LNFK, Vilnius, 2017.

2. Rasa Platakytė, Justinas Čeponkus, Study of Acetylsalicylic Acid by the Means of Matrix Isolation, EUCMOS, Coimbra, Portugalija, 2018.

3. Rasa Platakytė, Justinas Čeponkus, Valdas Šablinskas, Study of 3-methyl-acetylacetone structure and interaction with water, Open Readings, Vilnius, Lietuva, 2018.

4. Rasa Platakytė, Justinas Čeponkus, Conformational analysis of butanol and its complexes with water in low temperatures, Horizons in Hydrogen Bond Research, Amsterdamas, Nyderlandai, 2019.

5. Rasa Platakytė, Justinas Čeponkus, Valdas Šablinskas, Gamil A. Guirgis, Conformational analysis of 1-fluoro-1-chlormethylsilacyclohexane by vibrational spectroscopy, LNFK, Kaunas, 2019.

6. Joanna Stocka, Rasa Platakytė, Justinas Čeponkus, Valdas Šablinskas, Gamil A. Guirgis, Paweł Rodziewiczc, Computational and experimental vibrational study of 1-chloromethyl-1-fluorosilacyclohexane conformations and its rearrangements, Open Readings, 2021.

7. Rasa Platakytė, Justinas Čeponkus, Claudine Crepin-Gilbert, Wutharath Chin, Julien Berthomier, Structural analysis of acetylsalicylic acid and its thermal dissociation products by low-temperature vibrational spectroscopy, LNFK, Vilnius 2021.